JOURNAL OF THE AERONAUTICAL SCIENCES

VOLUME 21 JULY, 1954 NUMBER 7

Measurements of Turbulent Friction on a Smooth Flat Plate in Supersonic Flow*

DONALD COLES†

California Institute of Technology

SUMMARY

Direct measurements of supersonic local skin friction, using the floating-element technique, are presented for Mach Numbers from 2.0 to 4.5 and Reynolds Numbers from 3×10^6 to 9×10^6. Turbulent flow and transition are emphasized, although some measurements in the laminar regime are included. The observed effect of compressibility is to reduce the magnitude of turbulent skin friction by a factor of two at a Mach Number of 4.5 and a Reynolds Number of about 10^7.

The boundary-layer momentum-integral equation for constant pressure is verified within a few per cent by two experimental methods. Typical static pressure measurements are presented to show that transition can be detected by observing disturbances in pressure associated with changes in displacement thickness of the boundary layer.

It is found that the turbulent boundary layer cannot be defined experimentally for values of $u_1\theta/\nu_1$ less than about 2,000, where θ is the momentum thickness. For larger values of $u_1\theta/\nu_1$ there is a unique relationship between local friction coefficient and momentum-thickness Reynolds Number at a fixed Mach Number. The Appendix compares the present measurements at $M = 2.5$ with experimental data from other sources.

INTRODUCTION

THE FLOATING-ELEMENT TECHNIQUE, which attempts to measure directly the friction drag on a portion of a body in a fluid flow, was successfully used in 1929 by Kempf[1] and later by Schultz-Grunow.[2] An early but largely unproductive effort to apply the technique at supersonic speeds was that of Ginsburgh.[3] Beginning in 1948, H. W. Liepmann at GALCIT‡ undertook the development of a floating-element instrument for high-speed flow, and this work has been carried forward by Dhawan[4] and by Hakkinen.[5] The method has also been used, with variations, by Weiler and Hartwig[6] at the University of Texas, by Eimer[7] at GALCIT, by Bradfield, DeCoursin, and Blumer[8] at the University of Minnesota, and with conspicuous success by Chapman and Kester[9] at the Ames Aeronautical Laboratory of the NACA, the last two of these investigations being made with a body of revolution rather than with a flat-plate model.

The writer's research at JPL,** although inspired by the success of Liepmann and his group, is an independent attack on the flat-plate drag problem. During the research full advantage was taken of the size and range of the 20-in. supersonic wind tunnel at the Jet Propulsion Laboratory and of Liepmann's experience with the floating-element technique. Design of the flat-plate model and instrumentation was begun in early 1951, and the experiments discussed here were carried out in the spring of 1952. The present research has been briefly reported at the 1952 Annual Summer Meeting of the Institute of the Aeronautical Sciences in Los Angeles and at the Eighth International Congress on Theoretical and Applied Mechanics in Istanbul, and some preliminary data have been published in a short note.[10] A comprehensive discussion of the research can be found in the writer's thesis,[11] which has been published in three reports of the Jet Propulsion Laboratory.[12–14] Some introductory remarks in the thesis have also appeared as a survey paper.[15]

LIST OF SYMBOLS

C_f = local friction coefficient

C_F = mean friction coefficient

Received December 22, 1953.

* This paper presents the results of one phase of research carried out at the Jet Propulsion Laboratory, California Institute of Technology, under joint sponsorship of the Department of the Army, Ordnance Corps (under Contract No. DA-04-495-Ord 18), and the Department of the Air Force.

† Research Engineer, Jet Propulsion Laboratory; now Research Fellow.

‡ Guggenheim Aeronautical Laboratory, California Institute of Technology.

** Jet Propulsion Laboratory, California Institute of Technology.

M = free-stream Mach Number
p = pressure
q = free-stream dynamic pressure, $\rho_1 u_1^2/2$
R = ideal Reynolds Number
R' = Reynolds Number per unit length, u_1/ν_1
R_t = ideal Reynolds Number corresponding to point of observed maximum surface shearing stress
R_θ = momentum-thickness Reynolds Number, $u_1\theta/\nu_1$
T = temperature
u = velocity
x = distance from plate leading edge
y = distance from plate surface
γ = ratio of specific heats
δ = boundary-layer thickness
δ^* = boundary-layer displacement thickness
θ = boundary-layer momentum thickness
θ_0 = momentum-thickness increment of tripping device
μ = viscosity
ν = kinematic viscosity, μ/ρ
ρ = density
τ_w = wall shearing stress

Subscripts

0 = value at stagnation condition
1 = value in free stream
i = value for $M = 0$ at fixed R

Model and Instrumentation

(1) Flat Plate

Fig. 1 shows the flat-plate model installed in the test section of the 20-in. supersonic wind tunnel at the Jet Propulsion Laboratory. The plate completely spanned the tunnel in order to isolate the working surface from disturbances originating elsewhere on the model. Three floating-element instruments were mounted in the plate, on the tunnel plane of symmetry, at $x = 5.5$, 13.0, and 24.0 in. from the leading edge. Three small windows of $^1/_2$-in. plate glass were installed in each door, so that flow over the plate surface and leading edge could be observed using the tunnel schlieren system.

A series of static-pressure orifices was provided on the plate surface about 3 in. from the tunnel centerline. In addition, each of the floating-element instruments incorporated three orifices for static-pressure measurement; one of these orifices was the gap around the element itself. Three copper-constantan thermocouples were soldered to stainless-steel buttons buried in the plate surface near the floating-element stations, and the temperature was also measured in the element balance chambers and in the tunnel reservoir.

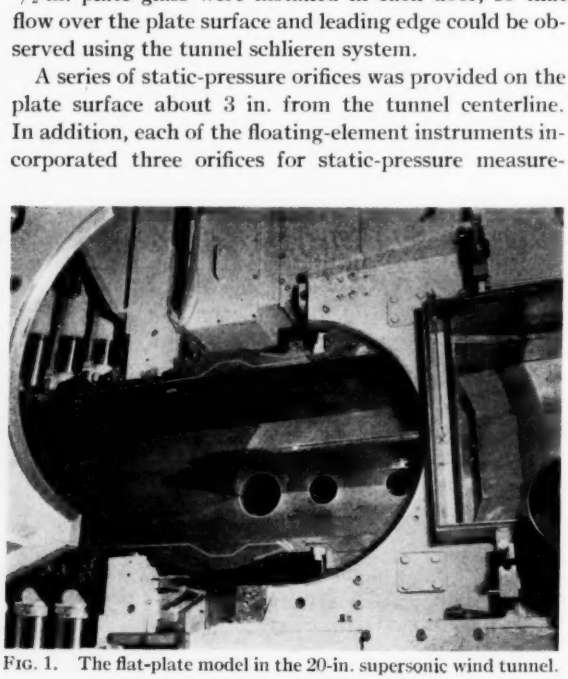

Fig. 1. The flat-plate model in the 20-in. supersonic wind tunnel.

All metal components exposed to the air stream on the working surface of the plate were fabricated of stainless steel. Particular attention was paid to working-surface finish and to the sharpness of the leading edge, which was a wedge of 15-deg. included angle. Various methods of estimating the leading-edge radius indicated that the value finally achieved was less than one half-thousandth of an inch.

(2) Floating Element

The skin-friction instrument used at JPL was similar in principle to the floating-element mechanism of Liepmann and Dhawan.[4] The most important difference, aside from size and range, was the use at JPL of a null technique in measuring applied forces.

The basic components of the instrument are shown in Figs. 2 and 3. The inner flexure system, consisting of the table, two flexlinks, and the ring, allowed a deflection of the element under an applied load. The deflection was measured indirectly as the displacement that must be given to the table in order to return the element to a standard null position with respect to the surrounding structure. Motion of the table was effected by means of a precision micrometer, acting through a piano-wire push rod clamped at both ends, and was constrained by the second or outer flexure system shown in the figures.

The null position of the floating element was detected by a Schaevitz variable-reluctance transformer[16] whose coil was fixed on the instrument structure and whose core was attached to the element ring. Two dashpots were provided for damping in the inner flexure system and were adjusted to give slightly less than critical damping. The choice of a rectangular surface element was made in order to approximate a local measurement, and the corresponding rectangular hole, $^1/_4$ by $1^1/_2$ in., was fabricated by a combination of milling, machine-filing, and broaching operations.

(3) Micrometer

The micrometer shown in Figs. 2 and 3 was designed around a standard commercial lead-screw of 0.025-in. pitch. The lead-screw was keyed to prevent rotation and was actuated by a rotating nut that was driven through a worm and worm gear. A counter and graduated dial on the micrometer input shaft indicated the position of the lead-screw in millionths of an inch.

Each of the micrometers was calibrated by direct comparison with a Pratt & Whitney standard measuring machine. It was found that the maximum micrometer position error did not exceed 0.5 per cent and so

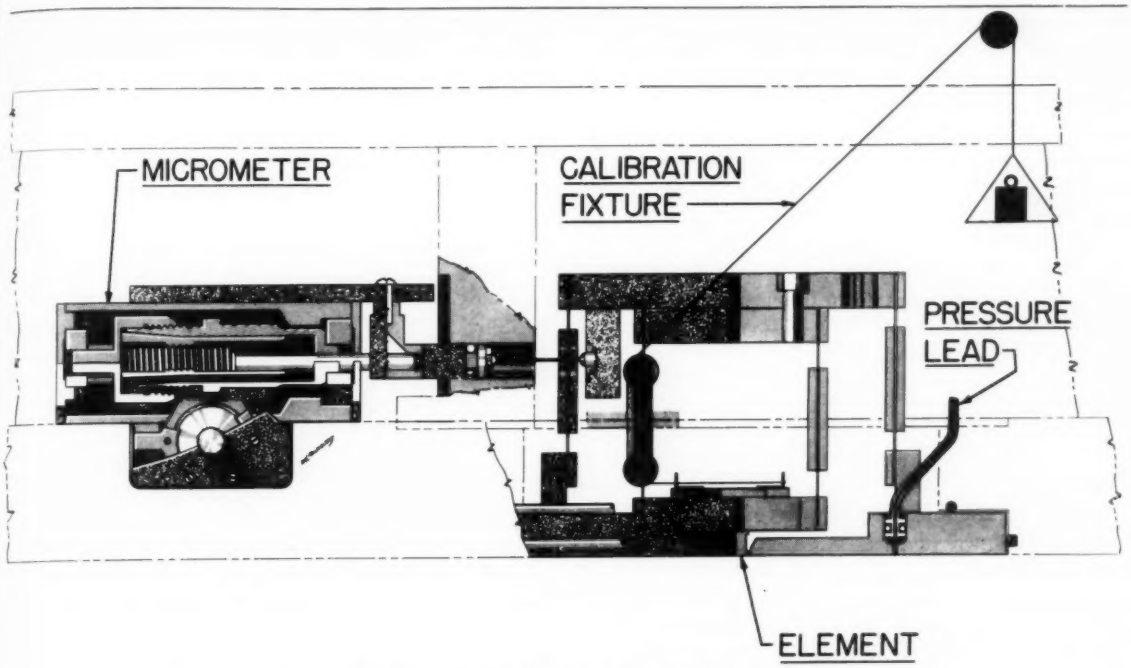

FIG. 2. The floating element and micrometer installed in the plate.

could be neglected in the present measurements. In general, under steady conditions, the null position as indicated by the Schaevitz gage could be repeated within one or two millionths of an inch using ordinary care to avoid backlash in the mechanism of the micrometer. Failure to obtain the sensitivity mentioned could usually be traced to the presence of foreign material in the clearance gaps. The spring constant for the inner flexure system was about 0.4 lb. per in., and deflections ranging from 0.0005 to 0.015 in. were encountered in the wind tunnel.

(4) *Tripping Devices*

During the JPL research, three different tripping devices were used to stimulate transition to turbulent flow. These were a sand strip, a leading-edge fence, and a row of airjets. The fence, consisting of a row of wire posts normal to the airflow and to the plate surface, was used in most of the measurements of turbulent friction. The sand strip was tested at $M = 4.5$, and the effect of air discharge on transition was investigated at Mach Numbers of 2.0 and 4.5. Fig. 4 shows the appearance of the boundary-layer flow at $M = 4.5$ with natural transition and with the various tripping devices.

The fence was found to have the virtue that the initial momentum loss at the wires could be computed from the known drag characteristics of cylinders in supersonic flow. However, there is some doubt as to whether true equilibrium was reached in the turbulent boundary layer far downstream, where the fence usually contributed from 10 to 20 per cent of the total momentum loss. The wires used were 0.014 in. in diameter, spaced $^1/_4$ in. apart, and projected about $^1/_{10}$ in. beyond the surface of the plate. For increasing Mach Number, there was a small but noticeable increase in the wire Reynolds Number needed to trip the boundary layer.

The device of discharging air from small holes in a surface was proposed by Fage and Sargent[17] as a method of stimulating transition to turbulent flow in the boundary layer. The most important property of such a tripping device, aside from the obvious advantage of control, is the small intrinsic drag of the jets. In the JPL tests, air was discharged from a row of holes 0.014 in. in diameter, spaced $^1/_4$ in. apart, and located $^3/_4$ in. from the leading edge. During some preliminary measurements at a Mach Number of 2.0, it was found

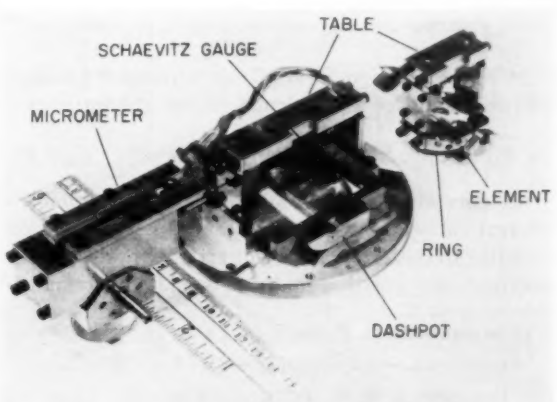

FIG. 3. Separated view of the floating element.

that there was a critical discharge rate, which did not appear to depend on tunnel pressure. For smaller rates than the critical value the airjets had a negligible effect on the distribution of surface friction, while for larger rates the effect was large and did not change appreciably with a further increase in the strength of the disturbance. At $M = 2.0$, the critical decrement in displacement-thickness Reynolds Number was about 10 for values of $u_1\delta^*/\nu_1$ between 700 and 2,000 at the station of the jets. At $M = 4.5$, the boundary-layer transition was less sensitive to discharge rate, and the critical decrement in $u_1\delta^*/\nu_1$ was about 25 for initial values between 3,000 and 5,000.

Friction Measurements

(1) *Local Friction*

The direct friction measurements of the present research are shown in Figs. 5–14. Both the ordinate τ_w/q and the abscissa u_1x/ν_1 have been deduced in an unambiguous way from measured physical quantities. In particular, the static pressure in the balance chambers was used in all cases to determine the local free-stream Mach Number, temperature, velocity, and density. For this calculation the fluid was assumed to be a perfect gas expanding isentropically from the tunnel reservoir with $\gamma = 1.400$, and the Sutherland equation† was used to relate temperature and viscosity.

Two corrections, always amounting together to less than 2 per cent in the shear, have been applied to the data of the figures. First, streamwise pressure forces, caused by small local pressure variations in the element gaps, have been compensated for on the basis of a channel calibration discussed in reference 13. Second, the turbulent friction data, which are relatively sensitive to variations in Mach Number, have been corrected to the nominal Mach Numbers of the figures by means of the approximate relationship

$$(\partial C_f/\partial M)_R = -m^2 C_f/M$$

where

$$m^2 = [(\gamma - 1)\, M^2/2]/[1 + (\gamma - 1)\, M^2/2]$$

That is, the function $C_f(M, R)$ at constant R has been approximated, for this calculation, by the quantity

$$\sqrt{T_1/T_0}\, C_f(0, R) = [1 + (\gamma - 1)M^2/2]^{-1/2} C_f(0, R)$$

Random error in the local turbulent friction coefficients is believed to be less than 2 per cent. Contributing to this error are the uncertainty in the element electrical zero position under dynamic conditions and the uncertainty in both the element static calibration and the micrometer calibration. In addition, the friction measurements at large Mach Numbers required the accurate measurement of tunnel static pressures of the order of 2 to 10 mm. Hg absolute. Both the pressure and the zero position are, of course, relatively more uncertain at low Reynolds Numbers. It was possible, during the profile surveys mentioned below, to repeat some of the shear measurements at the first and second stations. These data are shown as flagged points in Figs. 5–14, and in general indicate excellent reproducibility. The only systematic error that is believed to be important arises because flow over the clearance gaps may contribute to the force on the element; this error probably does not exceed 3 per cent.[13]

(2) *Mean Friction*

The execution of boundary-layer research with impact-probe instrumentation will not be discussed at greater length than is necessary to establish the approximations that are usual in an analysis of the data. It should be noted, however, that the experience of many investigators has shown that an impact probe in a boundary layer is an instrument subject to several sources of error. The presence of the probe may influence the development of the original boundary layer through upstream propagation of pressure disturbances, especially in the case of laminar flow. The existence of a velocity gradient and the proximity of a wall will lead to distortion of the flow pattern around the probe. On the other hand, the use of small probes, in an effort to minimize the problems already mentioned, may introduce new errors associated with viscous dissipation near the probe nose. Finally, the effect of velocity and density fluctuations on the pressure indicated by the probe may not be negligible.

In the present experiments the quantity sought is the momentum thickness, defined by

$$\theta = \int_0^\delta \frac{\rho}{\rho_1}\frac{u}{u_1}\left(1 - \frac{u}{u_1}\right) dy \qquad (1)$$

Fig. 15 shows the variation with y of the integrand in this expression for two typical boundary-layer profiles at a Mach Number of 4.5. The quantity directly measured was, of course, the impact pressure; the static pressure was assumed to correspond to isentropic expansion from the tunnel reservoir with $\gamma = 1.400$ and was taken to be constant through the boundary layer. The latter assumption was in each instance confirmed by measurement of surface pressure near the probe station. From these pressure data the local Mach Number in the boundary layer follows.

The stagnation temperature in the boundary layer has been assumed constant at the value in the tunnel reservoir. The local static temperature, density, velocity of sound, and fluid velocity were obtained from the

† The parameters C, T_r, and μ_r in

$$\mu/\mu_r = (T/T_r)^{3/2}[(T_r + C)/(T + C)]$$

have been taken as 192°R., 492°R., and 3.59×10^{-7} (slugs/ft.)-(ft./sec.)(ft.), respectively.

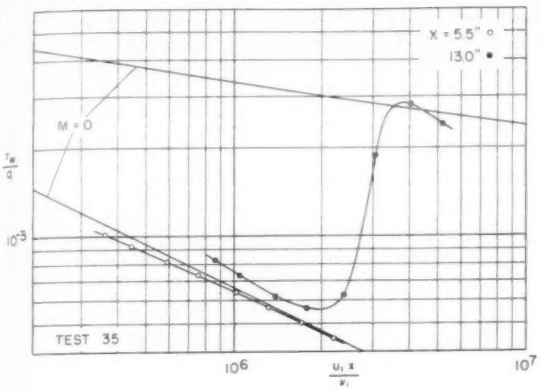

FIG. 5. Local friction, natural transition, $M = 1.97$.

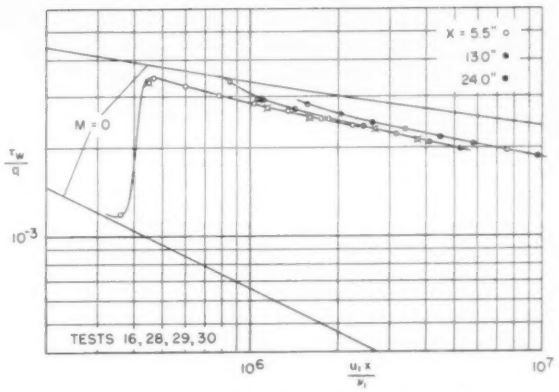

FIG. 6. Local friction, fence trip, $M = 1.97$.

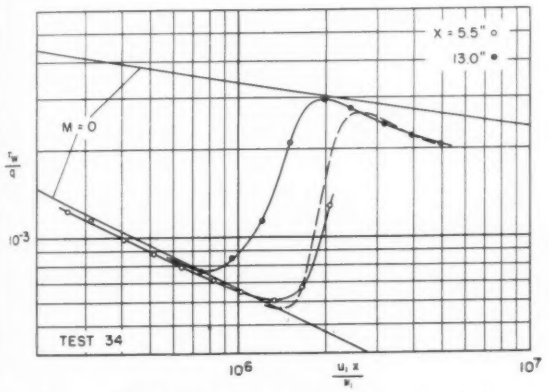

FIG. 7. Local friction, natural transition, $M = 2.57$.

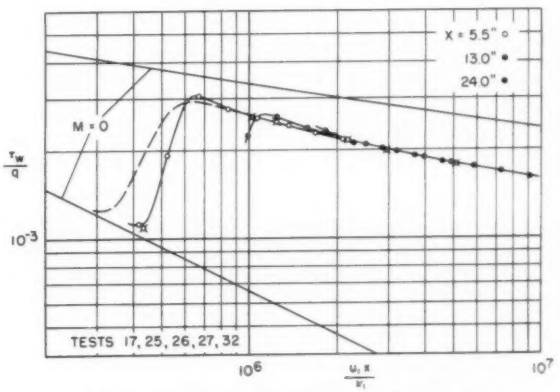

FIG. 8. Local friction, fence trip, $M = 2.57$.

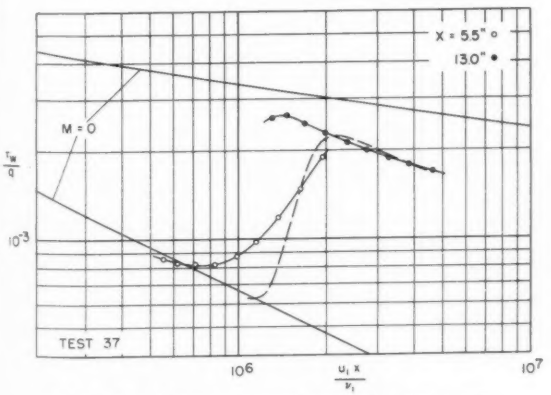

FIG. 9. Local friction, natural transition, $M = 3.70$.

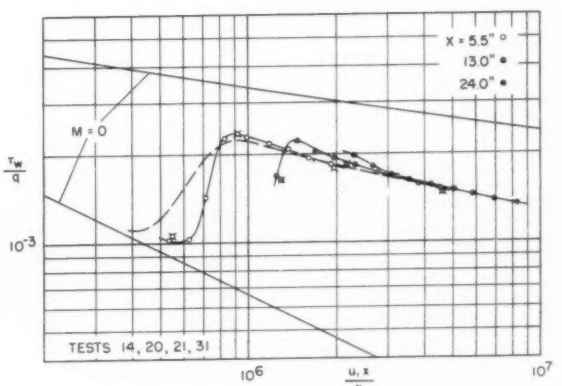

FIG. 10. Local friction, fence trip, $M = 3.70$.

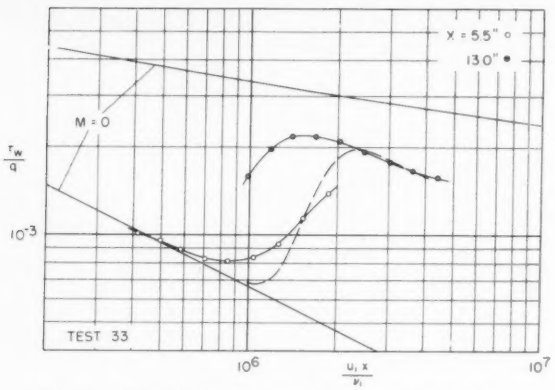

FIG. 11. Local friction, natural transition, $M = 4.54$.

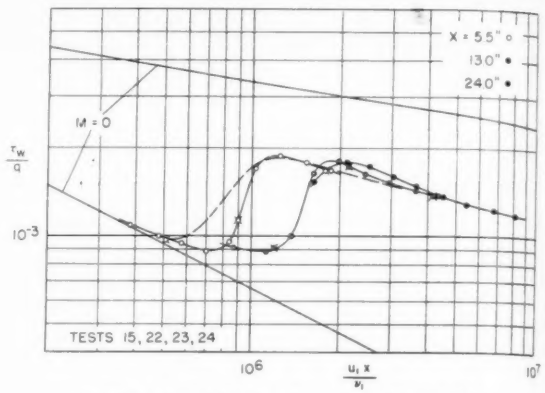

FIG. 12. Local friction, fence trip, $M = 4.54$.

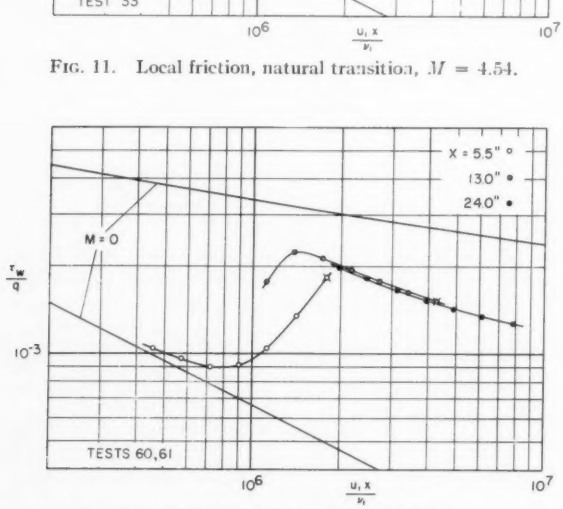

FIG. 13. Local friction, sand trip, $M = 4.54$.

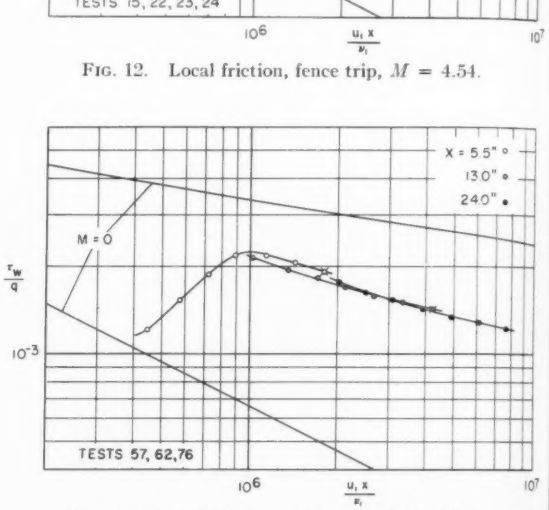

FIG. 14. Local friction, air-jet trip, $M = 4.54$.

usual equations of energy and state.† An inspection of the method of data analysis shows that errors in the velocity u and the momentum ρu will be, respectively, in the same and opposite direction as the error in the local stagnation temperature and will be of half the magnitude. Although the calculation of the integrand in Eq. (1) thus involves a cumulative error at a given point, it seems unlikely that the net error in θ from this source might be larger than the probable uncertainty of a few per cent in the stagnation temperature which is typical for most of the boundary layer.

(3) *Static Pressure*

Before discussing the friction measurements in detail, it is convenient to describe a second technique that was found useful in establishing the nature of the boundary-layer flow over the plate. During the present research, relatively large static-pressure disturbances were observed on the plate surface, especially in the region of transition from laminar to turbulent flow. These disturbances are believed to be connected with the apparent body shape which the boundary-layer displacement thickness presents to the airflow.

† The gas constant $\mathfrak{R}$ has been taken as 1,716 (lb./ft.²)/(slug/-ft.³)(°R.) in the state equation $p = \rho \mathfrak{R} T$.

Figs. 16 and 17 show typical pressure distributions observed during the friction measurements of Figs. 9 and 10 at a nominal Mach Number of 3.7. The expansion downstream of the leading edge and the compression in the transition region are conspicuous when the observed pressures are compared to the empty test-section pressure distribution.

(4) *Transition*

The region of transition from laminar to turbulent flow may be identified by a minimum and a maximum in the curve of local shearing stress plotted against Reynolds Number. The transition is not in general a unique function of the Reynolds Number for the experiments reported here, and this fact increases the difficulty in determining the shear distribution from observations at three points. However, the strong correlation observed between shear and pressure distributions is useful in interpolating between measured values of the friction coefficient at a given stagnation pressure.

Figs. 18–24 show, for the tests with natural transition and with the leading-edge fence, Reynolds Numbers of the minima and maxima in the shear and pressure distributions as obtained from Figs. 5–12 and from pressure measurements like those of Fig. 16. Some judgment has, of course, been exercised in estimating the

Reynolds Numbers for the pressure extrema, since the data are not always adequate to the demands imposed. Furthermore, for technical reasons the pressure measurements were made approximately 3 in. from the tunnel plane of symmetry, and it is not certain that the boundary-layer flow was accurately two-dimensional. In spite of these defects in the pressure data, it appears that the minimum in the static-pressure distribution corresponds closely in all cases to the position of maximum rate of change of the local friction coefficient. It should be remembered that both the friction and pressure measurements in the region of transition represent the response of a highly damped instrument to a quantity that is fluctuating rapidly with time and, therefore, that the present experience with transition may be peculiar to the particular wind tunnel and instrumentation involved.

Several other features of Figs. 18–24 are of special interest. The Reynolds Number per inch, R', is proportional to the tunnel stagnation pressure, and the movement of the natural transition toward smaller values of x but toward larger values of u_1x/ν_1 with increasing tunnel pressure is evident in the coordinate system of the figures. On the other hand, the fence tripping device apparently has the property at high stagnation pressures of causing transition to occur at a fixed Reynolds Number increment from the leading edge. It is therefore possible that the tendency of the corresponding local-friction measurements to define a single curve in the turbulent flow regime is not accidental (see, for example, Fig. 8, where the measurements are relatively insensitive to the presence of local pressure gradients).

At low values of tunnel stagnation pressure, however, the effect of the fence is entirely different. The large

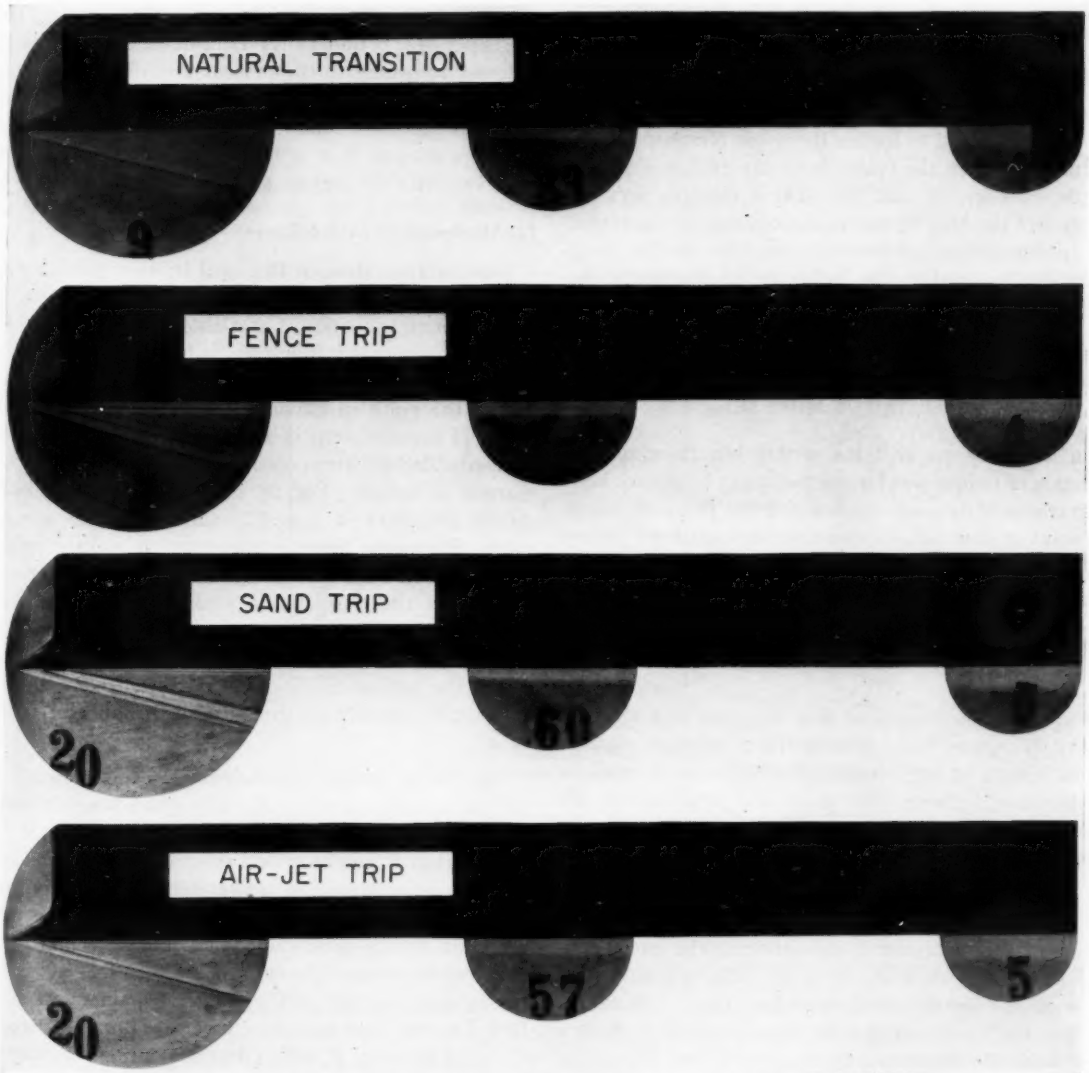

FIG. 4. Schlieren photographs of the boundary layer at $M = 4.5$, $R' = 130{,}000$ per in.

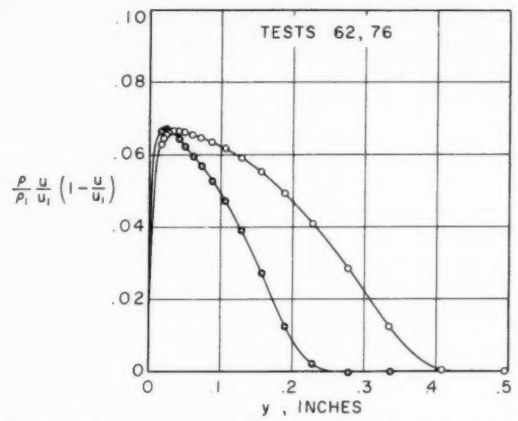

FIG. 15. Typical momentum-thickness determination, $M = 4.5$.

initial increment in θ caused by wire drag apparently does not strongly influence the slope of the velocity profile at the wall upstream of actual transition, as may be verified by a comparison of Figs. 11 and 12. Furthermore, at the lowest tunnel pressures, the transition may actually be moved to higher Reynolds Numbers by the disturbance from the fence, from the evidence, for example, of Figs. 23 and 24. These remarks serve to emphasize the lack of real understanding of the transition phenomenon and show the need for caution in attempting to predict the influence of upstream disturbances.

INTERPRETATION

(1) *Uniqueness*

In a survey paper,[15] the writer has discussed the question of uniqueness for the turbulent boundary layer with constant density, emphasizing the phenomenological point of view. Unfortunately, there exists at present no adequate basis for a generalization of this study to compressible flows. The present discussion will therefore depend entirely on experimental information in attempting to determine the properties of the ideal boundary layer.

Experience in low-speed flow suggests that the turbulent boundary layer with uniform pressure may be characterized as fully developed when there is a unique relationship between the slope and ordinate of the momentum-thickness distribution $\theta(x)$. That is, the assumption of uniqueness implies a function

$$C_f = 2(dR_\theta/dR) = g(R_\theta) \qquad (2)$$

which may be integrated, on satisfying the initial condition $R = 0$ when $R_\theta = 0$, to yield a relationship $R = G(R_\theta)$ for the ideal boundary layer. Since the surface friction is supposedly always positive, R_θ is a monotonically increasing function of R, and the initial condition $R = R_\theta = 0$ can always be satisfied.

However, the integration can be carried out, and an exact definition of R achieved, only if the function g of Eq. (2) is known for all positive values of R_θ. The function in question being defined experimentally, it is clear that any corresponding definition of R is not itself unique and can be valid only in an asymptotic sense. In other words, various experimental determinations of R become equivalent only when R_θ is large compared with values below which the turbulent boundary layer is not observed and is therefore undefined. It also follows, when considering various measurements of turbulent friction, that discrepancies in the final corrected data may not mean that one or another series of measurements is in error but only that they have been differently interpreted.

Fig. 25 shows the relationship between τ_w/q and $u_1\theta/\nu_1$ at various Mach Numbers, as determined experimentally at JPL, together with the corresponding curve for zero Mach Number from reference 15. It appears that the supersonic boundary layers in question are fully developed according to the present criterion, except perhaps for the points that are farthest to the left in the figure at the lower Mach Numbers. In particular, two of the profiles at $M = 4.5$ were obtained with the fence trip, two with the airjets, and one with the sand strip.

(2) *Maximum Shearing Stress*

One interpretation of the local friction data of Figs. 5–12 is suggested by the fact that relatively detailed information on transition is available in Figs. 18–24. For the measurements in question, it has been observed by the writer that the increment in Reynolds Number between the point of maximum shearing stress and the point of measurement is a well-defined function of the measured local friction coefficient, whether transition is natural or forced. Fig. 26 shows this relationship for Mach Numbers of 2.6, 3.7, and 4.5. The abscissa $(R - R_t)$ in the figure is the quantity $u_1\Delta x/\nu_1$, where Δx is measured between the point of maximum shearing stress and the downstream element station for each operating condition. Data at a Mach Number of 2.0 are omitted because small local pressure gradients affect the surface friction and simultaneously make it difficult to identify the pressure disturbance at transition.

The local friction coefficient is experimentally a unique function of $(R - R_t)$ at a given Mach Number and also by assumption a unique function of R. It follows that R_t can only be a function of R for constant M. However, since the measurements at different stations at a fixed value of tunnel pressure should be characterized by the same value of R_t, the latter must be a constant for each of the three curves of Fig. 26. This is to say that the end of the transition region, when referred to the ideal boundary layer, occurs at a value of C_f, or of R_θ, or of R, which depends only on M whether transition is stimulated or not.

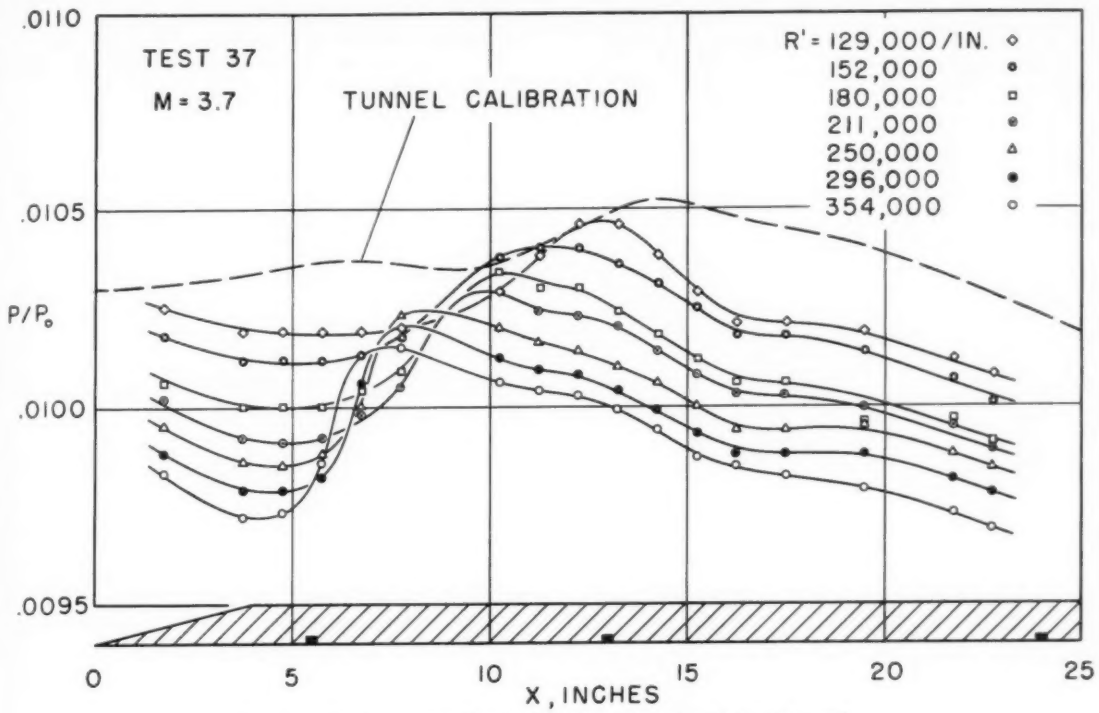

FIG. 16. Static pressure distribution with natural transition, $M = 3.7$.

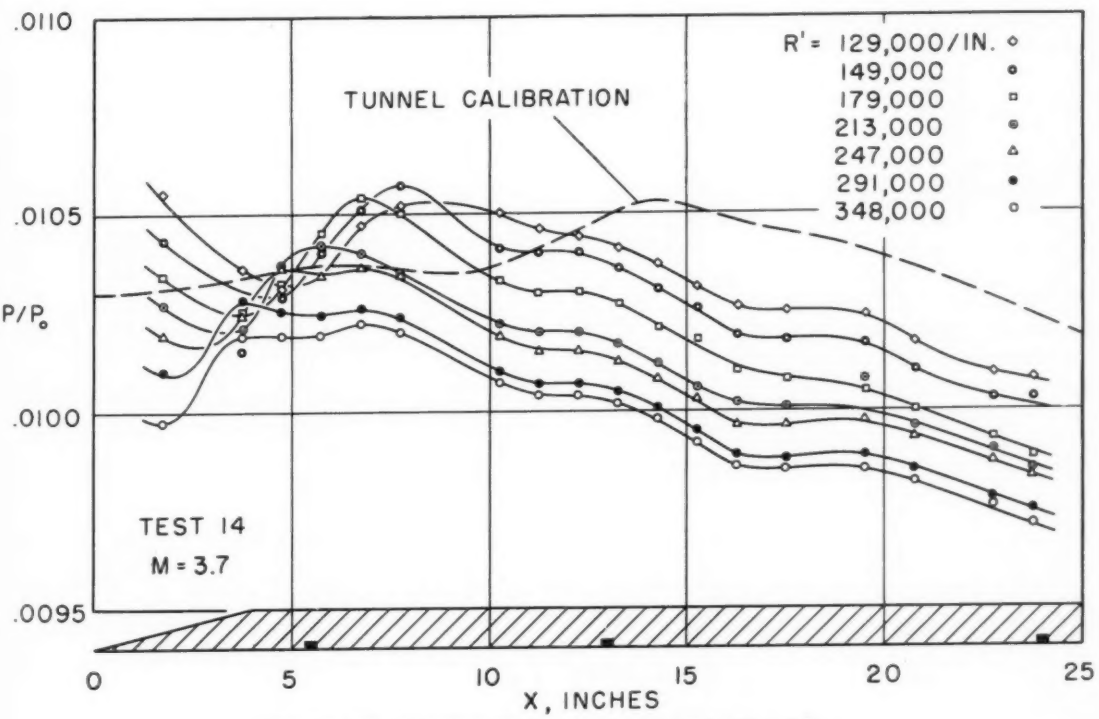

FIG. 17. Static pressure distribution with fence trip, $M = 3.7$.

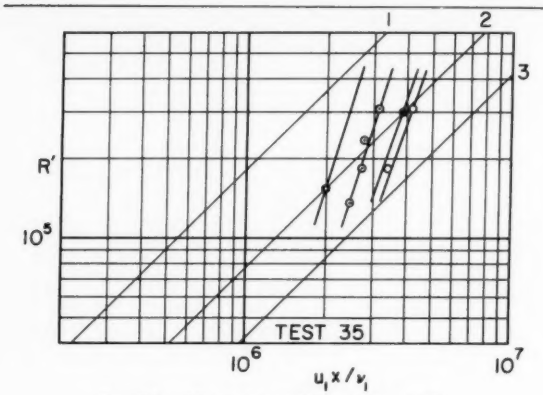

FIG. 18. Natural transition, $M = 1.97$.

- ● MINIMUM SHEARING STRESS
- ⊙ MINIMUM STATIC PRESSURE
- ● MAXIMUM SHEARING STRESS
- ○ MAXIMUM STATIC PRESSURE

FIGURES 18-24 OBSERVATIONS OF TRANSITION

ELEMENT STATIONS ARE DENOTED BY 1, 2, 3

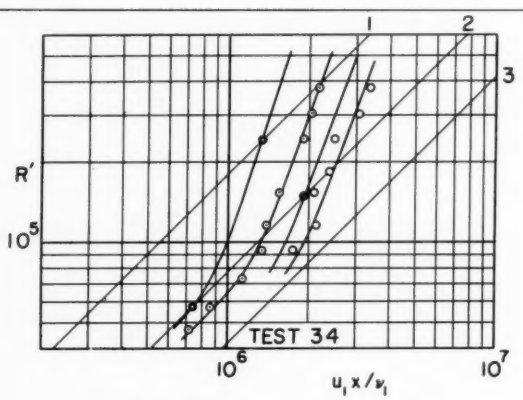

FIG. 19. Natural transition, $M = 2.57$.

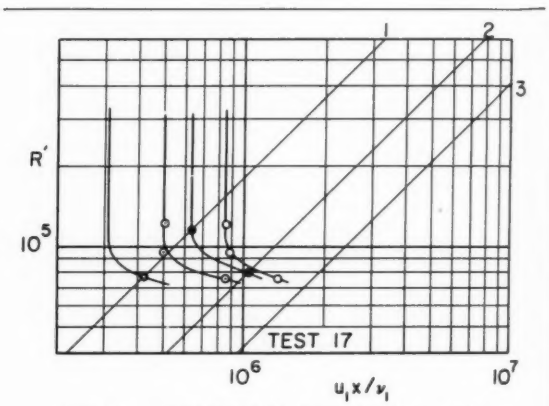

FIG. 20. Transition with fence trip, $M = 2.57$.

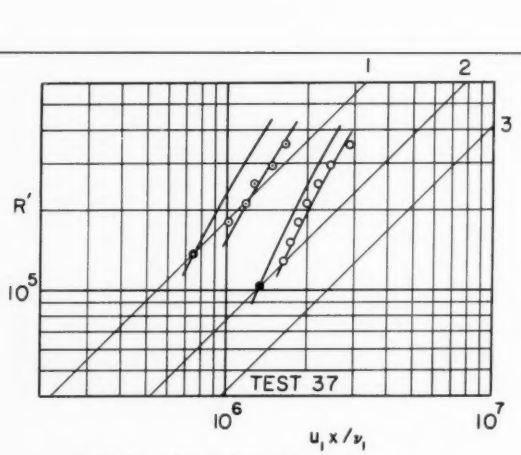

FIG. 21. Natural transition, $M = 3.70$.

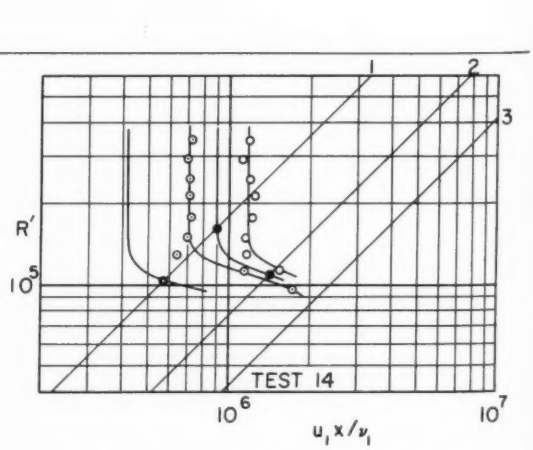

FIG. 22. Transition with fence trip, $M = 3.70$.

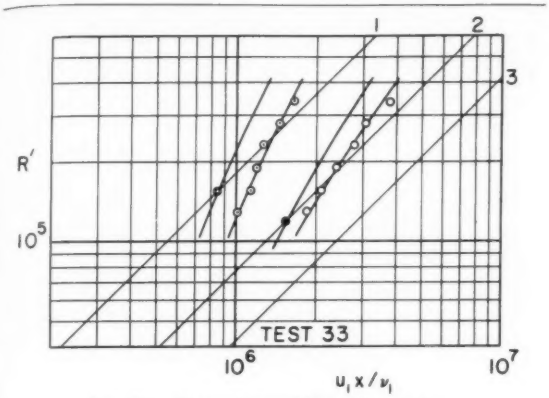

FIG. 23. Natural transition, $M = 4.54$.

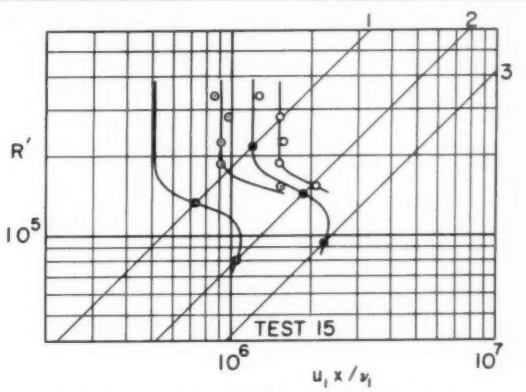

FIG. 24. Transition with fence trip, $M = 4.54$.

(3) Momentum Balance

The argument of the preceding section is clearly incomplete. Neither the question of uniqueness nor the question of momentum balance can be resolved experimentally without reference to momentum-thickness measurements, and these have not been cited in developing Fig. 26.

The momentum-integral equation for two-dimensional flow without pressure gradient is

$$C_f = \tau_w/q = 2(d\theta/dx) \tag{3}$$

where the measured quantities $2d\theta/dx$ and τ_w/q represent, respectively, the rate of momentum loss in the fluid and the drag force on the surface. For the experiments with the fence trip, Eq. (3) may be integrated in the form

$$\theta = \theta_0 + \int_0^x \frac{\tau_w}{2q}\,dx \tag{4}$$

where θ_0 is the contribution of the tripping device. For example, if the drag coefficient of a cylinder based on projected area is 1.2 for the range of M and R considered here, then[14] $\theta_0 = 0.0034$ in.

Multiplying Eq. (4) by the Reynolds Number per inch, R', there is obtained

$$R_\theta = R'\theta_0 + \int_0^{u_1x/\nu_1} \frac{\tau_w}{2q}\,dR'x \tag{5}$$

This expression is to be applied to measurements of R_θ with x fixed and R' variable. However, the behavior of the transition curves in Figs. 20, 22, and 24 implies that τ_w/q in the laminar, transition, and turbulent regimes is a function of u_1x/ν_1 only, at least for large R'. Thus Eq. (5) becomes

$$R_{\theta_2} - R_{\theta_1} = \int_{R'_1x}^{R'_2x} \left(\frac{\tau_w}{2q} + \frac{\theta_0}{x}\right) dR'x \tag{6}$$

It is evident at once that the measurements with the fence trip must violate the principle of uniqueness expressed by Eq. (2). If Eq. (6) is correct, it follows that R_θ cannot be a unique function of τ_w/q when R' is variable and θ_0 is different from zero. It also follows that Fig. 26 should be viewed with suspicion, since the evidence is against the proposition that a unique value of R_θ can be associated with each point in the figure.

Integration of Eq. (6) may be carried out conveniently in Fig. 26, on replacing the variable of integration $R'x$ by the equivalent quantity $(R - R_t)$. Table 1 lists some observed values of $(R_{\theta_2} - R_{\theta_1})$, together with the corresponding quantities computed from the right-hand side of Eq. (6) using $\theta_0 = 0.0034$ in. and $x = 21.5$ in. The general agreement in the table confirms the supposition that τ_w/q is a function of $(R_\theta - R'\theta_0)$ rather than of R_θ for the experiments with the fence tripping device. In other words, a residual disturbance from the fence is detectable, at least in part, as an additive increment in R_θ, and the hypothesis of uniqueness is therefore not supported by these data.

Whether this conclusion is important in the present context depends on whether the effect can be distinguished in Fig. 25. In particular, Eq. (6) may be considered merely as a formula for experimental continuation of the direct measurements of R_θ given in the figure, the continuation being consistent with momentum balance without assuming uniqueness. In this sense, Eq.

TABLE 1

Investigation of Momentum Balance

M	Tests	Trip	$(R_{\theta_2} - R_{\theta_1})$ Eq. (6)	$(R_{\theta_2} - R_{\theta_1})$ Eq. (5)	$(R_{\theta_2} - R_{\theta_1})$ Observed	$(R_2 - R_1)$ Eq. (7)	$(R_2 - R_1)$ Fig. 25
2.6	27, 26	Fence	3,540	...	3,600	4,200,000	4,300,000
3.7	20, 19	Fence	3,310	...	3,460	4,650,000	5,050,000
4.5	23, 22	Fence	2,960	...	3,120	4,600,000	5,150,000
4.5	76, 62	Air jet	...	2,440	2,340	3,400,000	3,850,000

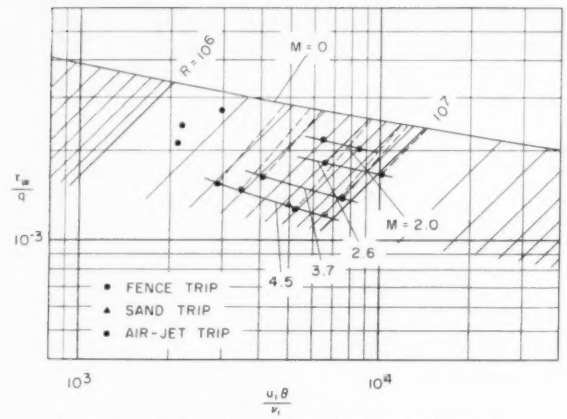

FIG. 25. Determination of ideal Reynolds Number.

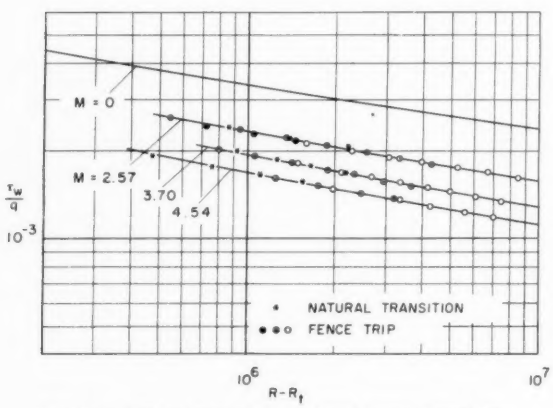

FIG. 26. Equivalence of natural and forced transition.

(6) allows the data of Fig. 26 to be transferred to the coordinate system of Fig. 25, with the result shown in Fig. 27.

Finally, a joint test of the hypotheses of uniqueness and momentum balance can be carried out by direct calculation from Eq. (5). Choosing a value for R' of 290,000 per in., local friction distributions can be estimated as shown by the dashed lines in Figs. 7–12. The relationship between R_θ and τ_w/q obtained by integration of Eq. (5) is found in each case to j oin smoothly onto the appropriate experimental curve, as shown in Fig. 27.

For the fence trip, the computed values of R_θ at the most downstream station are found to be a few per cent smaller than values obtained by experimental continuation—i.e., than values measured directly. This discrepancy, while not important in Fig. 27, should be compared to the result of a less equivocal investigation of momentum balance at a Mach Number of 4.5 with the airjet trip. The relevant profile data at two stations at the same tunnel pressure have already been presented in Fig. 15. Table 1 lists the experimentally observed increment $(R_{\theta_2} - R_{\theta_1})$, together with the increment calculated from Eq. (5) with $\theta_0 = 0$; the observed increase in R_θ between the two probe stations is perhaps 4 per cent smaller than the integral of $\tau_w/2q$ over the same interval. The discrepancy of 4 per cent, by coincidence or otherwise, agrees with an estimate[13] of the probable effect of the clearance gaps around the floating surface element.

An inspection of the velocity profile data tabulated in reference 14 indicates that the profiles with the airjet trip are probably free of residual effects from the tripping device and may in fact be taken as typical of the supersonic turbulent boundary layer. Returning to Fig. 27, it follows that the fence data probably do not deviate from the fully developed condition by more than the observed discrepancy between the fence and airjet data at $M = 4.5$. The collected points in Fig. 27 are therefore certified as representing the fully developed turbulent boundary layer, within the degree of accuracy implied both by the comparison just given and by the estimate already made of possible systematic error in measurement of shearing stress.

(4) Reynolds Number

One method of obtaining Reynolds Numbers for the present data requires the supersonic measurements to be compatible with measurements at zero Mach Number and to be internally consistent in terms of the momentum-integral equation, Eq. (3). Given a pair of boundary-layer profiles at the same Mach Number but different Reynolds Numbers, an average local friction coefficient can be defined by

$$C_{f_{\text{avg.}}} = \frac{1}{R_2 - R_1}\int_{R_1}^{R_2} C_f\, dR = 2\,\frac{R_{\theta_2} - R_{\theta_1}}{R_2 - R_1} \qquad (7)$$

It is easily shown that the average coefficient expressed by Eq. (7) is, for practical purposes, identical with that given by

$$C_{f_{\text{avg.}}} = \frac{1}{R_{\theta_2} - R_{\theta_1}}\int_{R_{\theta_1}}^{R_{\theta_2}} C_f\, dR_\theta \qquad (8)$$

when a power law is assumed for the variation of C_f with R_θ within the interval in question—i.e., a straight line in

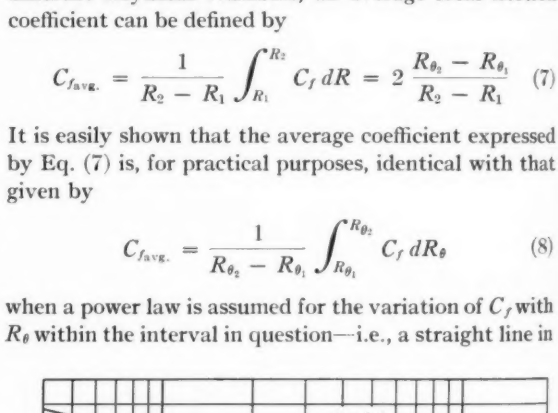

FIG. 27. The ideal boundary layer.

TABLE 2
Tentative Reduction to Ideal Conditions

M	Test	Trip	u_1x/ν_1	R	R_θ	C_f	C_F	C_f/C_{f_i}	C_F/C_{F_i}
2.3	27	Fence	4,840,000	6,080,000	6,600	0.00181	0.00217	0.795	0.715
2.3	26	Fence	8,320,000	10,260,000	10,200	0.00165	0.00193	0.700	0.710
3.7	20	Fence	3,540,000	3,980,000	4,100	0.00162	0.00236	0.595	0.635
3.7	19	Fence	7,250,000	8,630,000	7,550	0.00138	0.00175	0.570	0.610
4.5	76	Air jet	3,370,000	2,810,000	2,900	0.00155	0.00206	0.535	0.600
4.5	24	Fence	3,520,000	3,570,000	3,470	0.00148	0.00194	0.530	0.590
4.5	62	Air jet	6,910,000	6,200,000	5,240	0.00125	0.00169	0.495	0.560
4.5	22	Fence	6,830,000	8,170,000	6,590	0.00122	0.00161	0.500	0.560

Fig. 25. Taking $C_f = AR_\theta^{-1/n}$ in Eq. (8), then

$$C_{f_{avg.}} = \frac{(R_{\theta_2}C_{f_2} - R_{\theta_1}C_{f_1})/(R_{\theta_2} - R_{\theta_1})}{1 - \ln(C_{f_1}/C_{f_2})/\ln(R_{\theta_2}/R_{\theta_1})} \tag{9}$$

Values of $(R_2 - R_1)$ calculated from Eq. (7), using the average coefficient from Eq. (9), are listed in Table 1. As has been pointed out, the second entry for $M = 4.5$ involves two profiles at different plate stations at the same tunnel pressure, with the airjet trip, and the remaining data involve two profiles at different pressures at the same station, with the fence trip.

Consulting Fig. 25, a straight line that slopes up and to the right at 45° is a line on which $C_f(M)/C_f(0)$ and $R_\theta(M)/R_\theta(0)$ are equal; it may be assumed initially to be also a line of constant Reynolds Number. Absolute values of R follow on integrating Eq. (2) in an asymptotic sense already defined; the result[15] for $M = 0$ is shown in Fig. 25. Values of R for the ideal supersonic boundary layer are conveniently determined by interpolation, and the increment $(R_2 - R_1)$ thus derived for the various paired profiles is given in Table 1.

The second method for calculating $(R_2 - R_1)$ may be reconciled with the first by assuming that lines of constant R in Fig. 25 have a slope which is not 45° but is at least independent of Reynolds Number in the range being considered. The problem is then reduced to one of determining the proper slope so that the intercepts on the curve $M = 0$ are separated by the desired increment in R. Such lines are shown in the figure; they correspond to the values of R, and of $C_f/C_{f_i} = C_f(M)/C_f(0)$ and $C_F/C_{F_i} = R_\theta(M)/R_\theta(0)$ at constant R, which are listed in Table 2. The result of the calculation is relatively insensitive to errors in measurement of either shearing stress or momentum thickness. In particular, it is easily shown that the value of $(C_f/C_{f_i})/(C_F/C_{F_i})$ for a given pair of profiles would be unaffected if the measured values of τ_w/q or R_θ were corrected by a small fixed percentage to account for a suspected experimental error. It follows that the development leading to Table 2 does not depend significantly on the question of uniqueness raised in the preceding sections.

It should be pointed out that difficulty in defining an ideal Reynolds Number is not necessarily material in practical calculations of flat-plate drag. For example, the original values of u_1x/ν_1 for a typical curve in Fig. 27 can obviously be recovered by integrating Eq. (2),

$$\frac{u_1x}{\nu_1} = 2\int_{R'_{\theta_0}}^{R_\theta} \frac{dR_\theta}{g(R_\theta)} \tag{10}$$

with $g(R_\theta) = C_f(R_\theta)$ defined experimentally. A corresponding calculation can be carried out for any plate flow for which the transition curve in Fig. 27 is known or can be estimated. In practice, it may be convenient to begin with the coordinate system $C_f(R)$ of Figs. 5–14, taking the laminar flow as an initial state and assuming a distribution of local friction for the first half of the transition region. The function $R_\theta(R)$ then follows on integrating the conventional expression for momentum balance, Eq. (5). The result of the integration can be transferred to the coordinate system $C_f(R_\theta)$ of Fig. 27 and can be suitably connected to the curve describing the known final state of the boundary layer. Eq. (10) may then be used to continue the calculation indefinitely.

(5) *The Ideal Boundary Layer*

The uniqueness criterion expressed by Eq. (2) is clearly a vital concept in any evaluation of experimental data obtained in turbulent boundary layers. For low-speed flow, this concept leads immediately to an intuitive definition of ideal Reynolds Number and eventually to a quantitative definition based on certain characteristic properties of the mean-velocity profile. According to the evidence considered in reference 15, the development of a turbulent boundary layer with constant density may be divided roughly into four regions:

(1) For momentum-thickness Reynolds Numbers R_θ greater than about 5,000, the turbulent mean-velocity profile follows certain well-defined laws of similarity. The contribution of the sublayer to the streamwise flow of mass or momentum is negligible.

(2) For R_θ between 2,000 and 5,000, the similarity laws apply, but the sublayer flow should be taken into account.

(3) For R_θ between 500 and 2,000, the mean-velocity profile is probably unique, but the similarity laws are not strictly valid.

(4) For R_θ less than about 500, fully turbulent flow is rarely observed.

In the region (1), the relationship between τ_w/q and R_θ has a simple analytic form involving four dimensionless parameters. If this expression is arbitrarily adopted

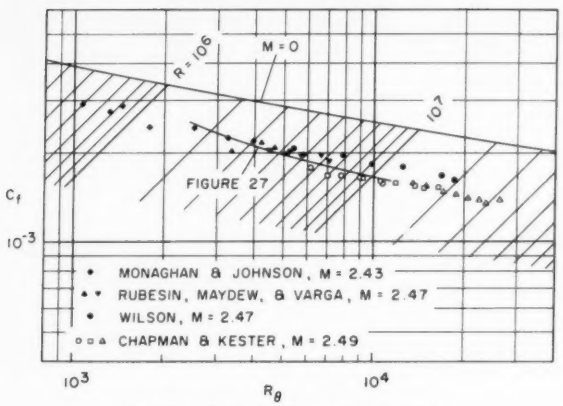

FIG. 28. Collected data at $M = 2.5$.

as the uniqueness relationship of Eq. (2), then the Reynolds Number defined by integration[15] will be valid in an asymptotic sense for large values of R_θ.

As the generalized similarity laws for the compressible mean-velocity profile are unknown, the corresponding definition of Reynolds Number in terms of an asymptotic state is not yet possible. It is therefore necessary to classify as tentative any quantitative results of the present report which are not independent of, or at least insensitive to, the definition of an ideal Reynolds Number. In particular, emphasis should be placed on Fig. 27 rather than on Fig. 26, and more importance should be attached to the values of C_f/C_{f_i} in Table 2 than to the values of C_F/C_{F_i}.

One of the original objectives of the research reported here was to discriminate among several theoretical analyses of the compressible turbulent boundary layer. However, during study of the experimental data it became obvious that the most conspicuous effect of compressibility is to move the various stages of boundary-layer development toward larger values of R_θ. For example, the effect of surface heating at large Mach Numbers is known to be manifested in thickening of the sublayer,[12, 14] so that the final stage of turbulent boundary-layer flow must be reached at progressively larger values of R_θ as M increases. This effect is overlooked in the theoretical literature with one exception.[18]

Finally, it is important to note in Fig. 27 that fully developed turbulent flow was apparently not observed in the JPL experiments for R_θ smaller than about 2,000. In the absence of other evidence, therefore, it is recommended that values of R_θ substantially larger than 2,000 be stipulated for any fundamental future study of friction, heat transfer, or other phenomena in supersonic turbulent boundary layers.

APPENDIX.—COMPARISON WITH OTHER DATA AT $M = 2.5$

For two-dimensional flow over a flat plate, it is readily shown that the complete form of the momentum-integral equation (3) is†

$$\frac{\tau_w}{q} = 2\frac{d\theta}{dx} - (2 - M^2 + \delta^*/\theta)\frac{\theta}{q}\frac{dp}{dx} \qquad (11)$$

It has been found experimentally[14, 19–21] that the value of the profile parameter δ^*/θ is very nearly 4.2 for turbulent flow at Mach Numbers near 2.5, and it follows that the combination $(2 - M^2 + \delta^*/\theta)$ in Eq. (11) is negligibly small. This property of the momentum-integral equation is an important reason for studying experimental data at $M = 2.5$, since the boundary layer should be insensitive to local variations in static pressure.

Profile measurements in turbulent boundary layers at Mach Numbers between 2.4 and 2.5 have been reported by Wilson,[19] by Monaghan and Johnson,[20] and by Rubesin, Maydew, and Varga.[21] In each of these investigations the momentum-thickness distribution $\theta(x)$ on a flat plate was observed for a fixed tunnel condition, and $2d\theta/dx$ can be computed immediately as a function of R_θ. Values calculated by the writer are represented by solid symbols in Fig. 28, and the corresponding curve for $M = 0$ from reference 15 is also shown.

The data derived from profile surveys appear at first glance to define a unique boundary layer. Moreover, the fact that the experimental curves for $M = 0$ and $M = 2.5$ are parallel suggests that $C_f(M)/C_f(0)$ is, in fact, independent of Reynolds Number. The slope and ordinate of the function $R_\theta(R)$ are therefore affected equally and uniformly by compressibility, and a line of constant R has a slope of 45° in Fig. 28.

Values of R obtained by interpolation in Fig. 28 are plotted against u_1x/ν_1, the Reynolds Number measured from the leading edge, in Fig. 29. In each case the ordinate and abscissa differ by a constant that agrees closely with the value chosen in the original paper. This result is not surprising, since each of the original analyses determined an apparent origin by referring the supersonic measurements to flow at $M = 0$ and by assuming the effect of compressibility to be nearly or exactly independent of Reynolds Number.

Chapman and Kester[9] have recently measured directly the friction drag on the cylindrical afterbody of a cone-cylinder model at a Mach Number of 2.5. Small corrections were introduced to compensate for a starting length upstream of the region of measurement, using the fact that $C_F(M)/C_F(0)$ was found experimentally to be independent of Reynolds Number at constant Mach Number. Since the mean and local friction coefficients satisfy a relationship $C_f = d(C_FR)/dR$, where by definition $C_f = \tau_w/q$ and $C_F = D/2\pi rqx$, it is convenient to represent C_F in a limited region by the power law $C_F = AR^{-1/n}$; then $C_f = C_F[1 - (1/n)]$. Assuming that a value of $1/n = 0.17$ is appropriate to the data for $M = 2.5$ in Fig. 8 of reference 9, the meas-

† $\delta^* = \int_0^\delta \left(1 - \frac{\rho}{\rho_1}\frac{u}{u}\right) dy.$

urements in question lie as shown by the open points in Fig. 28. Because R_θ was not measured in these experiments, the data have been plotted against $C_F R/2$, which is supposedly equivalent to R_θ when the latter is suitably defined in cylindrical coordinates. No attempt has been made to correct the original values of C_F for the influence of curvature, although it is clear that any such correction should affect ordinate and abscissa equally in Fig. 28. Values of R obtained by interpolation are found to agree with values given in reference 9 for a length/diameter ratio of 8 and are found to be a few per cent smaller for length/diameter ratios of 13 and 23.

If any conclusion can be drawn from the experience of the several investigators who have measured turbulent friction in supersonic flow, it is that more study of experimental techniques is needed. Fig. 28 in some cases exhibits a serious disagreement between measurements of drag and of momentum loss at a Mach Number of 2.5. The only direct verification of momentum balance known to the writer is the one reported here, which was obtained on a smooth but unpolished surface at $M = 4.5$ with an airjet trip. It is entirely possible that surface roughness may be a factor in causing the disagreement noted in Fig. 28. However, the writer's personal conviction is that too much attention, rather than too little, is probably paid to surface finish in investigations concerned primarily with flow downstream of transition.

Experience at JPL does not suggest an explanation for the discrepancies in Fig. 28. The effects of pressure gradient have already been discounted, and any systematic error in momentum-thickness measurements should be common to all the experiments considered here.

It should be noted in connection with profile surveys that the momentum thickness at large Mach Numbers is highly sensitive to the shape of the velocity profile at the outer edge of the boundary layer. On assuming constant stagnation temperature and static pressure, so that a relationship between ρ and u is known, the maximum value of the integrand in Eq. (1) can be computed as a function of Mach Number. The value in question is 0.250 at $M = 0$, 0.131 at $M = 2.55$, and 0.067 at $M = 4.55$. However, the integrand in Eq. (1) behaves like $[1 - (u/u_1)]$ near the outer edge of the boundary layer. On referring to Fig. 15 for a typical profile, it is clear that a given error in velocity must lead to relatively larger errors in the ordinate, and therefore in θ, as the Mach Number increases. Moreover, if the phenomenon of intermittence observed in low-speed flow persists at supersonic speeds, the velocity deduced from impact by pressure measurements may depend on the nature of the intermittence and on the probe response to a fluctuating signal.

It is also possible that the ambient flow in a typical supersonic wind tunnel deviates sufficiently far from the two-dimensional condition to account for all or part of the inconsistency observed in Fig. 28. The practice

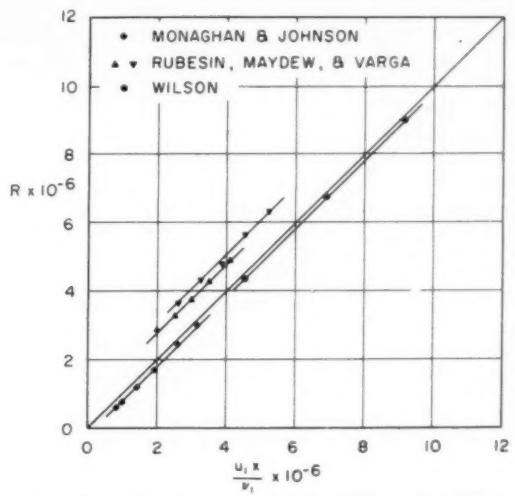

FIG. 29. Comparison of real and ideal Reynolds Numbers.

of making an adjustment in the top and bottom nozzle contours, to account for the presence of a boundary layer on all four tunnel walls, leads inevitably to three-dimensional flow in the test section. The flow is slightly converging in the plan view and slightly diverging in the elevation. The two effects cancel as far as the pressure distribution on the tunnel axis is concerned, yielding there a uniform value of static pressure. In the 20-in. tunnel at JPL, pressure and flow inclination surveys off the nozzle centerline at a Mach Number of 2.6 have definitely established the presence of this peculiarity in the supposedly uniform flow.

REFERENCES

[1] Kempf, G., *Neue Ergebnisse der Widerstandsforschung*, Werft-Reederei-Hafen, Vol. 10, No. 11, pp. 234–239; No. 12, pp. 247–253, 1929.

[2] Schultz-Grunow, F., *Neues Reibungswiderstandsgesetz für glatte Platten*, Luftfahrtforschung, Vol. 17, No. 8, pp. 239–246, August, 1940; translated as *New Frictional Resistance Law for Smooth Plates*, NACA TM No. 986, September, 1941.

[3] Ginsburgh, A. S., *Supersonic Skin Friction Drag Measurements at a Mach Number of 1.72*, United Aircraft Corporation, Project Meteor, Rep. No. UAC-17, February, 1948.

[4] Liepmann, H. W., and Dhawan, S., *Direct Measurements of Local Skin Friction in Low-speed and High-speed Flow*, Proc. First U.S. National Congress of Applied Mechanics, pp. 869–874, Chicago, 1951; see also Dhawan, S., *Direct Measurements of Skin Friction*, Guggenheim Aeronautical Laboratory, California Institute of Technology, Pasadena, Calif., Thesis, 1951, or NACA TN No. 2567, January, 1952.

[5] Hakkinen, R. J., *Measurements of Skin Friction in Turbulent Boundary Layers at Transonic Speeds*, Guggenheim Aeronautical Laboratory, California Institute of Technology, Pasadena, Calif., Thesis, 1953.

[6] Weiler, J. E., and Hartwig, W. H., *The Direct Determination of Local Skin Friction Coefficient*, Defense Research Laboratory, University of Texas, Austin, Tex., Rep. No. DRL-295 (CF-1747), January, 1952.

[7] Eimer, M., *Experimental Skin Friction at Hypersonic Mach Numbers*, Guggenheim Aeronautical Laboratory, California Institute of Technology, Pasadena, Calif., Thesis, 1953.

[8] Bradfield, W. S., DeCoursin, D. G., and Blumer, C. B., *Characteristics of Laminar and Turbulent Boundary Layer at Supersonic Velocity*, Institute of Technology, University of Minnesota, Minneapolis, Research Rep. No. 83, July, 1952.

[9] Chapman, D. R., and Kester, R. H., *Measurements of Turbulent Skin Friction on Cylinders in Axial Flow at Subsonic and Supersonic Velocities*, Journal of the Aeronautical Sciences, Vol. 20, No. 7, pp. 441–448, July, 1953.

[10] Coles, D., *Direct Measurement of Supersonic Skin Friction*, Readers' Forum, Journal of the Aeronautical Sciences, Vol. 19, No. 10, p. 717, October, 1952.

[11] Coles, D., *Measurements in the Boundary Layer on a Smooth Flat Plate in Supersonic Flow*, Guggenheim Aeronautical Laboratory, California Institute of Technology, Pasadena, Calif., Thesis, 1953.

[12] Coles, D., *Measurements in the Boundary Layer on a Smooth Flat Plate in Supersonic Flow. I. The Problem of the Turbulent Boundary Layer*, Jet Propulsion Laboratory, California Institute of Technology, Pasadena, Calif., Rep. No. 20-69, June, 1953.

[13] Coles, D., *Measurements in the Boundary Layer on a Smooth Flat Plate in Supersonic Flow. II. Instrumentation and Experimental Techniques at the Jet Propulsion Laboratory*, Jet Propulsion Laboratory, California Institute of Technology, Pasadena, Calif., Rep. No. 20–70, June, 1953.

[14] Coles, D., *Measurements in the Boundary Layer on a Smooth Flat Plate in Supersonic Flow. III. Measurements in a Flat Plate Boundary Layer at the Jet Propulsion Laboratory*, Jet Propulsion Laboratory, California Institute of Technology, Pasadena, Calif., Rep. No. 20–71, June, 1953.

[15] Coles, D., *The Problem of the Turbulent Boundary Layer*, submitted to the editor, Zeitschrift für angewandte Mathematik und Physik, July, 1953; to be published in 1954.

[16] Schaevitz, H., *The Linear Variable Differential Transformer*, Proc. Society for Experimental Stress Analysis, Vol. 4, No. 2, pp. 79–88, 1947.

[17] Fage, A., and Sargent, R. F., *An Air-injection Method of Fixing Transition from Laminar to Turbulent Flow in a Boundary Layer*, British ARC, R. & M. No. 2106, June, 1944.

[18] Donaldson, C. du P., *Skin Friction and Heat Transfer through Turbulent Boundary Layers for Incompressible and Compressible Flows*, 1952 Heat Transfer and Fluid Mechanics Institute, Los Angeles, pp. 19–35, June, 1952; see also *On the Form of the Turbulent Skin Friction Law and its Extension to Compressible Flows*, NACA TN No. 2692, May, 1952.

[19] Wilson, R. E., *Turbulent Boundary Layer Flow on a Smooth Flat Plate at Supersonic Speeds*, unclassified paper in NavOrd Rep. No. 1651 (*Confidential*), pp. 245–278, November, 1951.

[20] Monaghan, R. J., and Johnson, J. E., *The Measurement of Heat Transfer and Skin Friction at Supersonic Speeds. Part II. Boundary Layer Measurements on a Flat Plate at M = 2.5 and Zero Heat Transfer*, British ARC, CP No. 64, December, 1949.

[21] Rubesin, M. W., Maydew, R. C., and Varga, S. A., *An Analytical and Experimental Investigation of the Skin Friction of the Turbulent Boundary Layer on a Flat Plate at Supersonic Speeds*, NACA TN No. 2305, February, 1951.

IAS Twenty-Third Annual Meeting

Hotel Astor, New York City, January 24–28, 1955

The Meetings Committee is planning sessions on Aerodynamics, Aeroelasticity, Structures, Rotating Wing Aircraft, Aircraft Design, Meteorology, etc.

Authors wishing to have papers considered for presentation at this meeting should submit outlines or short abstracts to the Meetings Committee, 2 East 64th St., New York 21, N.Y., no later than September 15, 1954.

Strength Under Combined Tension and Bending in the Plastic Range

J. M. FRANKLAND* AND R. E. ROACH†

Chance Vought Aircraft, Inc.

ABSTRACT

A rational method is presented for the strength of rectangular sections under combined tension and bending in the plastic range. The analysis is based on the accepted theory of plastic bending as presented by Osgood[2] and others. Nondimensional interaction curves between axial load and bending are presented for three types of stress-strain characteristics representative of artificially aged aluminum alloys. Strength is presented in terms of allowable plastic strain at the extreme fiber. Some comparisons are made with tests on 75ST-6bars in pure bending. It is also shown how the change in curvature under load may be obtained, and suggestions are given for the use of this to calculate strength under statically indeterminate conditions.

INTRODUCTION

RATIONAL METHODS OF ANALYSIS for bending in the plastic range have been available for some time. Cozzone[1] has published a practical method that has found wide acceptance among aeronautical engineers, and Osgood[2] has written a review of the theoretical approach to the problem. The theory is based on the assumption of a linear distribution of strain over the depth of the section, the stresses being derived from the strains by use of the uniaxial stress-strain curve of the material. Tests, such as those by Rappleyea and Eastman,[3] have confirmed the theory satisfactorily.

Several criteria for ultimate strength in bending have been proposed. Cozzone[1] recommends that the conventional tensile strength of the material be used for the maximum bending stress, although it is possible to use his charts for any assumed value of extreme fiber stress. Brush, Sidebottom, and Smith[4] take the ultimate bending moment to be that at which plastic yielding has penetrated halfway to the centroidal axis. Barrett[5] uses the 0.5 per cent offset yield strength for the maximum bending stress, justifying this choice on the basis of British proof-load requirements.

It should be observed that the tensile strength is not, in principle, a limiting stress for bending, since for ductile materials the tensile strength is merely the conventional stress at which a tensile specimen begins to neck, and necking does not occur in bending failures of compact specimens.

The point of view expressed in this paper derives mainly from experience with aluminum-alloy forged fittings, which in heavier sections sometimes show low ductility and thus have only a limited capacity for plastic redistribution. It has consequently seemed desirable to present the strength data in terms of extreme fiber strain rather than in terms of stress and to use various values of limiting strain ranging from low to high ductility. Data are presented here only for the rectangular cross section in order to direct attention to the effects of ductility and the interaction of axial load and bending moment.

METHOD OF ANALYSIS

The Ramberg-Osgood[6] expression for the stress-strain curve will be used. This can be written in the form

$$e = s + (3/7)s^n \qquad (1)$$

where

e = ϵ/ϵ_Y
s = σ/σ_Y
σ_Y = secant yield strength in tension, the secant having a slope of $0.7E$
ϵ_Y = σ_Y/E
n = a constant characteristic of the material
σ = true stress
ϵ = natural strain‡

The first term on the right-hand side of Eq. (1) represents the elastic component of the strain, and the second term represents the plastic component.

The exponent n will be taken as an odd integer, since this appears sufficiently accurate in view of material variation and it permits Eq. (1) to apply in both tension and compression. The assumption is made that the compressive stress-strain curve is symmetrical to the tensile branch. This is an adequate representation of the facts for the artificially aged alloys 14ST-6 and 75ST-6 but is somewhat in error for work-hardened materials and 24ST-3. It should be noted that Eq. (1) ceases to apply when unloading occurs, as unloading changes only the elastic component of strain. It is

Presented at the Structures Session, Twenty-Second Annual Meeting, IAS, New York, January 25–29, 1954.

* Technical Assistant to Chief of Structures.

† Lead Structural Development Engineer.

‡ In the strain range of interest, the difference between conventional strain, $\Delta l/l$, and natural strain, $\log_e [1 + (\Delta l/l)]$, is not large. The reader can interpret ϵ as conventional strain without appreciable error if he so prefers.

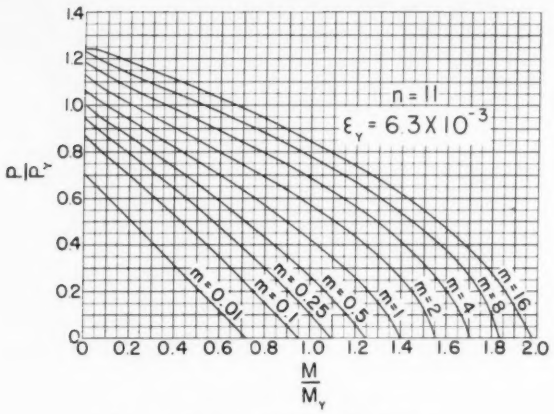

FIG. 1. Interaction curves for $n = 11$.

further assumed that the material is free of appreciable internal stresses.

The undeformed cross section is a rectangle of depth $2h$ and breadth $2b$. Rectangular coordinates x and y are chosen with the origin at the center, so the section is bounded by

$$x = \pm b, \qquad y = \pm h$$

The section is loaded in tension by an axial force P applied at the centroid and in bending by a moment M about the x-axis. The sense of the bending moment is such that the tensile stresses due to bending appear in the upper half of the section ($y > 0$).

The basic assumption of the theory is that the distribution of strain is linear over the section, and hence

$$e = c_0 + c_1\eta \tag{2}$$

where $\eta = y/h$.

Under load, the section deforms from its original rectangular shape. There is a change in area and depth, and the centroid is no longer at mid-height. An approximate treatment is adequate for the range of conditions considered in this paper.

It will be assumed that the transverse contraction is half of the longitudinal extension and that the distorted section is a trapezoid. Anticlastic curvature and anisotropy of plastic flow are thus neglected. The components of displacement in the cross section are, in the x-direction,

$$u = -(1/2)xe\ \epsilon_Y \tag{3}$$

and, in the y-direction,

$$v = -\frac{1}{2}\epsilon_Y \int_0^y e\, dy$$
$$= -(1/2)h\ \epsilon_Y[c_0\eta + (1/2)c_1\eta^2] \tag{4}$$

by virtue of Eq. (2).

Let η_1 be the value of η at the top of the deformed section and η_2 be the value at the bottom. The same subscripts will be used to denote extreme fiber values of e and s. Terms containing higher powers of ϵ_Y than the first will be dropped in the following calculations:

From Eq. (4) one finds

$$\left.\begin{aligned}\eta_1 &= 1 - (1/2)\ \epsilon_Y[c_0 + (1/2)c_1]\\ \eta_2 &= -1 + (1/2)\epsilon_Y[c_0 - (1/2)c_1]\end{aligned}\right\} \tag{5}$$

The strains in the extreme fibers are

$$e_1 = c_0 + c_1\eta_1$$
$$e_2 = c_0 + c_1\eta_2$$

Solving the last pair of equations for c_0 and c_1 and using Eqs. (5), the following values are obtained:

$$c_0 = \frac{1}{2}(e_1 + e_2) + \frac{1}{16}\epsilon_Y(e_1 - e_2)^2 \tag{6}$$

$$c_1 = \frac{1}{2}(e_1 - e_2) + \frac{1}{8}\epsilon_Y(e_1^2 - e_2^2) \tag{7}$$

The centroid of the deformed section drops to η^*, where

$$\eta^* = -(5/12)c_1\ \epsilon_Y \tag{8}$$

It is convenient to characterize the strain distribution in terms of the plastic components of the strains e_1 and e_2 at the extreme fibers. Let m be the maximum plastic strain, occurring at η_1, and let αm be the plastic strain at η_2.

Then

$$\left.\begin{aligned}m &= (3/7)s_1^n\\ \alpha m &= (3/7)s_2^n\end{aligned}\right\} \tag{9}$$

For pure bending α is approximately minus one, and, in the presence of axial load, it increases to the upper limit of plus one for pure axial load with no bending. Thus m is a measure of the severity of straining, and α gives an indication of the relative amounts of bending and tension.

Now the axial load is

$$P = \sigma_Y \int s\, dA \tag{10}$$

and the bending moment is

$$M = h\sigma_Y \int s(\eta - \eta^*)\, dA \tag{11}$$

the integration extending over the deformed section.

The axial load and the bending moment will be measured in terms of the load P_Y and the moment M_Y, which acting separately would produce a maximum stress of the secant yield strength—viz.,

$$P_Y = 4bh\sigma_Y$$
$$M_Y = (4/3)bh^2\sigma_Y$$

Using Eq. (3),

$$dA = bh(2 - e\ \epsilon_Y)\, d\eta \tag{12}$$

Whenever there is bending in addition to pure axial load, Eq. (2) can be solved for η to give

$$\eta = (1/c_1)(e - c_0), \quad d\eta = (1/c_1)\, de$$

By means of the last two equations, the integrals of Eqs. (10) and (11) can be written in terms of

$$B = \int s\, de, \quad C = \int se\, de, \quad D = \int se^2\, de$$

These integrals can be evaluated by use of Eq. (1) with the following results:

$$B = \frac{1}{2}(s_1^2 - s_2^2) + \frac{mn}{n+1}(s_1 - \alpha s_2) \tag{13}$$

$$C = \frac{1}{3}(s_1^3 - s_2^3) + m\frac{n+1}{n+2}(s_1^2 - \alpha s_2^2) + \frac{m^2 n}{2n+1}(s_1 - \alpha^2 s_2) \tag{14}$$

$$D = \frac{1}{4}(s_1^4 - s_2^4) + m\frac{n+2}{n+3}(s_1^3 - \alpha s_2^3) + m^2\frac{2n+1}{2n+2}(s_1^2 - \alpha^2 s_2^2) + \frac{m^3 n}{3n+1}(s_1 - \alpha^3 s_2) \tag{15}$$

One obtains

$$P/P_Y = (1/2c_1)[B - (1/2)\,\epsilon_Y C] \tag{16}$$

$$\frac{M}{M_Y} = \frac{3}{2c_1^2}\left(C - \frac{1}{2}\epsilon_Y D\right) - 3\left(\frac{c_0}{c_1} + \eta^*\right)\frac{P}{P_Y} \tag{17}$$

Eqs. (16) and (17) now express the axial loading and the bending moment in terms of quantities that are determined by the stress-strain curve of the material, which is defined by ϵ_Y and n, and the extreme fiber stresses and strains. The parameters c_0 and c_1 can be calculated from Eqs. (6) and (7), α and m are defined by Eqs. (9), and η^* can be found from Eq. (8).

Interaction Curves for Bending and Tension

Nondimensional interaction charts plotting P/P_Y against M/M_Y are presented in Figs. 1, 2, and 3. Each chart gives curves showing the combinations of axial load and bending moment for which the maximum plastic tensile strain is constant—that is, for constant values of m. These curves of constant strain are also curves of constant maximum stress. The actual plastic deformation is, of course, obtained from the normalized strain m as the product $m\,\epsilon_Y$.

Each chart presents the conditions for a single material characterized by the strain-hardening exponent n. Values for n of 11, 15, and 21 have been chosen as representative of artificially aged aluminum alloys. For 75ST-6, n can be taken as 15, while $n = 21$ is suitable for the 24ST-80 series and 14ST-6. For calculation of the correction terms due to deformation of the cross section, ϵ_Y has been taken as 6.3×10^{-3} throughout.

It will be apparent that the strength is greatly affected by small changes in ductility if the ductility is low, say for $m = 4$ or less. On the other hand, the strength becomes substantially independent of ductility at larger values of extreme fiber strain, say for $m > 10$. In prac-

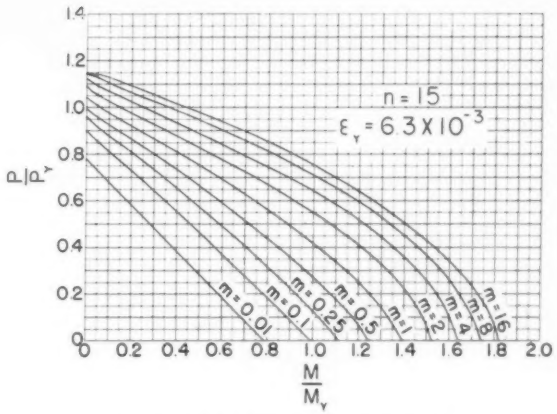

Fig. 2. Interaction curves for $n = 15$.

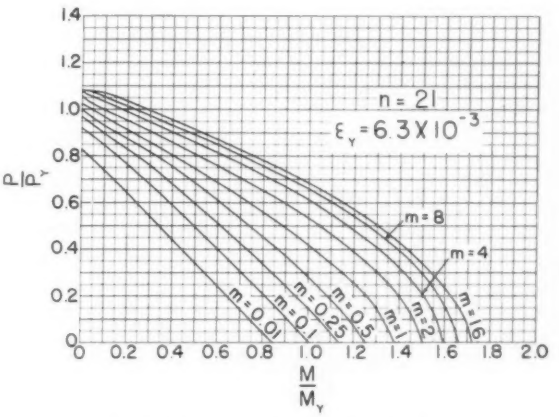

Fig. 3. Interaction curves for $n = 21$.

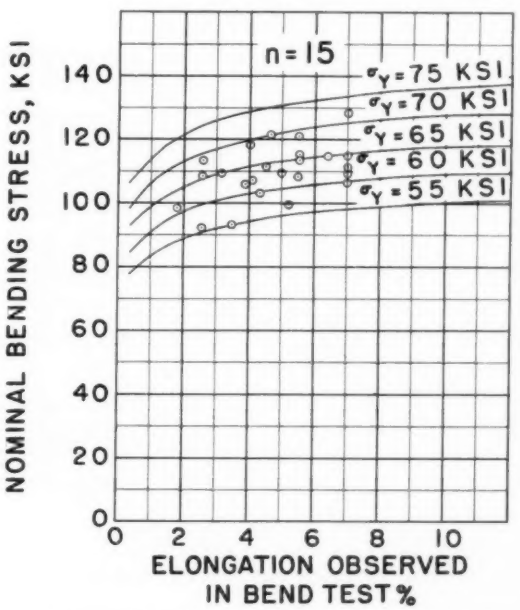

Fig. 4. Nominal bending stress versus maximum permanent strain for $n = 15$.

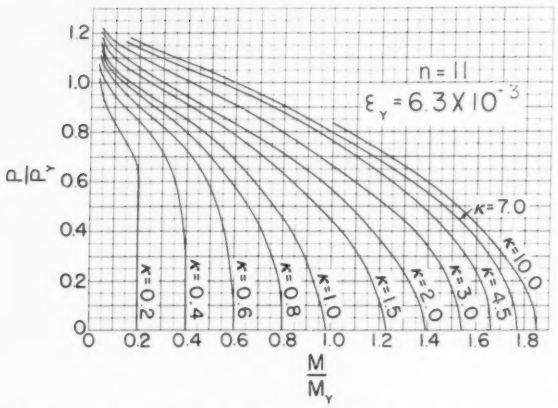

FIG. 5. Curvature as a function of loading for $n = 11$.

tice, these larger values of m are not often usable because of excessive deflection. For instance, for $m = 10$ under pure bending, the radius of curvature of a 75ST-6 bar would be about eight times the depth.

PURE BENDING

The relation between nominal bending stress and extreme fiber strain can be obtained for a given material by the methods of the previous section. Nominal bending stress is defined here as the quotient of bending moment by section modulus. The nominal bending stress at failure is the modulus of rupture.

Curves of nominal bending stress versus the permanent strain in the extreme fiber are shown in Fig. 4, which is drawn for a material characterized by $n = 15$ and having yield strengths from 55 to 75 kips per sq.in. This is representative of 75ST-6. Also shown are experimental data obtained from square bars of 75ST-6 loaded by uniform bending moment. Because of limitations of the loading jig, strains greater than 7 per cent could not be obtained, so that the experimental points at this strain were obtained on unbroken specimens. Points at lower strains represent fracture and are moduli of rupture.

CURVATURE DUE TO BENDING MOMENT AND AXIAL LOAD

From the analysis given earlier, the deformations accompanying various combinations of loading can be obtained. Of greatest interest is the curvature.

If R_0 is the radius of curvature of the centroidal axis in the unloaded state, and R is the radius under load, the difference of the extreme fiber strains is given by

$$\epsilon_Y(e_1 - e_2) = 2h[(1/R_0) - (1/R)] \qquad (18)$$

It is convenient to use a nondimensional curvature, κ, which is defined as

$$\kappa = (h/\epsilon_Y)[(1/R_0) - (1/R)] \qquad (19)$$

From Eq. (18),

$$\kappa = (1/2)(e_1 - e_2) \qquad (20)$$

It should be noted that κ is always positive.

To any pair of load values, M/M_Y and P/P_Y, there will correspond a definite value of κ. Curves of constant κ are given in these coordinates for $n = 11$, 15, and 21 in Figs. 5, 6, and 7. The curves illustrate the increase in bending flexibility at constant bending moment when the axial load is increased in the plastic range.

When the relation of bending moment to axial load is not statically determinate, it is necessary to know the significant deformations in order to follow the loading history in bending moment and axial load coordinates. The most important case is primary axial load accompanied by secondary bending.

To illustrate the use of the κ-curves, the case of axial loading of a member that is initially curved will be considered. A rectangular bar of uniform section and length l is loaded by a tensile force P applied at the centroids of the end sections. Let x be the longitudinal coordinate with origin at the center of the bar, the ends of the bar being at $\pm(1/2)l$. The centroidal axis under no load is assumed to be the sinusoid given by

$$y = a_0 \cos \pi x/l$$

The maximum value of y is found at mid-length and is equal to a_0. Under load, it is assumed that the centroidal axis takes the shape

$$y = a \cos \pi x/l$$

An assumption of this character has been found suitable by Westergaard and Osgood[7] for the analysis of columns with initial curvature. It should be an even better approximation under axial tension, at least for values of a_0/h which are not large.

The critical section is at mid-length, and

$$R_0 = l^2/(\pi^2 a_0)$$
$$R = l^2/(\pi^2 a)$$

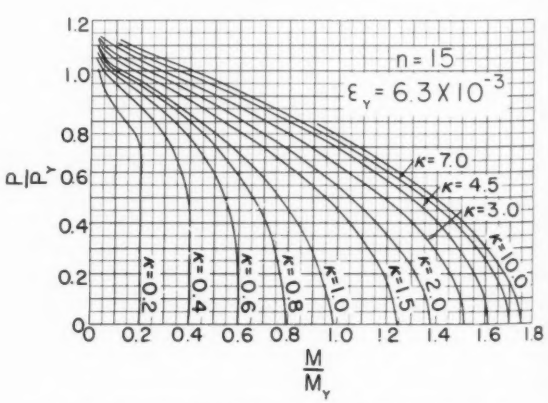

FIG. 6. Curvature as a function of loading for $n = 15$.

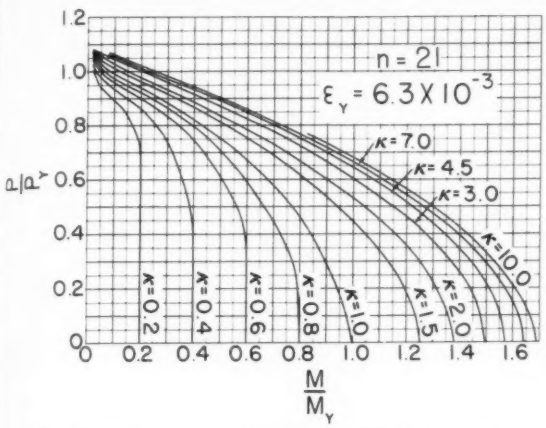

FIG. 7. Curvature as a function of loading for $n = 21$.

and thus

$$\kappa = (\pi^2 h/\epsilon_Y l^2)(a_0 - a) \tag{21}$$

Also $M = Pa$, or

$$M/M_Y = (3a/h)(P/P_Y) \tag{22}$$

Eliminating a between Eqs. (21) and (22), one obtains

$$\frac{M}{M_Y} = \left(\frac{3a_0}{h} - \frac{3\,\epsilon_Y \kappa l^2}{\pi^2 h^2}\right)\frac{P}{P_Y} \tag{23}$$

This is the equation of a straight line through the origin of graphs such as Figs. 5, 6, and 7. Assuming a value of κ, one may therefore find the associated values of M/M_Y and P/P_Y for a particular problem from the intersection of that straight line with the appropriate κ curve.

For a specific example, take

$$l = 16.2h, \quad a_0 = (1/3)h, \quad \epsilon_Y = 6.3 \times 10^{-3}$$

A material for which $n = 21$ is assumed, so Fig. 7 applies.

Eq. (23) reduces to

$$M/M_Y = (1 - 0.5\kappa)P/P_Y$$

When κ is equal to 2, the parenthesis on the right-hand side vanishes. This is the limiting value of κ at which the bar becomes straight and no higher values of κ can be obtained.

At $\kappa = 0.2$,

$$M/M_Y = 0.9P/P_Y$$

The intersection of this line with the curve for $\kappa = 0.2$ in Fig. 7 gives

$$M/M_Y = 0.20, \qquad P/P_Y = 0.22$$

At $\kappa = 0.4$,

$$M/M_Y = 0.8P/P_Y$$

and the intersection of this with the κ curve yields another point

$$M/M_Y = 0.38, \qquad P/P_Y = 0.47$$

Repetition of this for other κ values yields further points through which a curve can be drawn. This curve, Fig. 8, shows the values of bending moment as a function of axial load while the load is increasing.

A maximum value of $M/M_Y = 0.46$ is reached at $P/P_Y = 0.70$, after which the bending moment decreases with axial load. Curves of constant m taken from Fig. 3 are also shown as the dashed lines in Fig. 8. These give the maximum plastic strain in the section at each stage of the loading. It will be seen that a normalized plastic strain of $m = 4$ is needed for elimination of secondary bending by plastic readjustment. For the material properties assumed, this corresponds to a necessary ductility of (4)(0.63) = 2.5 per cent.

Application of this method to curved members under compressive axial load is possible. However, such use is limited by the requirement that no significant unloading should occur in the member, and this restriction may rule out most of the cases of interest.

Of course some problems will not yield to such a simple approach. The deflection shapes represented above by a single parameter family of curves might have to be replaced by families of two or more parameters in order to obtain a satisfactory relation between deflection and curvature. A method of successive approximations by trial and liquidation of error could be used to satisfy the conditions at two or more stations along the length of the member. But no matter what elaborations might be found necessary in a particular case, the information provided by the κ curves is fundamental.

(*Continued on page 474*)

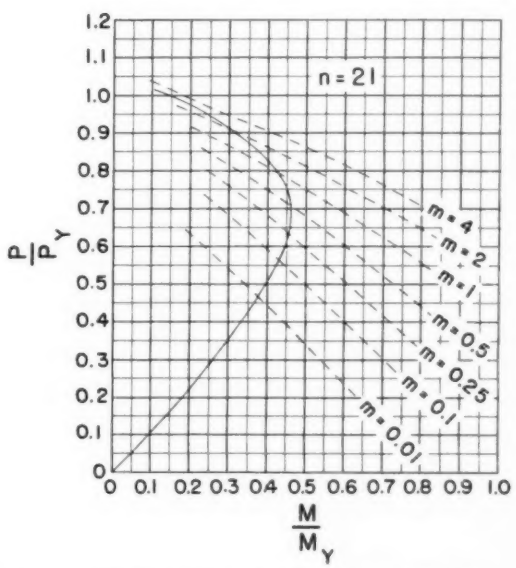

FIG. 8. Loading history of a curved bar under tension.

The Transfer Function of a Rocket-Type Guided Missile with Consideration of Its Structural Elasticity

JACK L. BEHARRELL* AND HANS R. FRIEDRICH†

Convair-San Diego Division of General Dynamics Corporation

ABSTRACT

Assuming that the pitching or yawing motion of a rockes type guided missile under the influence of thrust and air forces normal to its longitudinal axis can be described by the motion of an elastic free-free beam with given mass distribution and given stiffness distribution, the transfer function of the missile is deduced. It relates the deflection angle δ of the control agent to the angle θ_0 measured by a displacement gyro at any point x_θ on the longitudinal axis of the missile. This transfer function is to be used in future investigations to replace the simple transfer function of a rigid body in the block diagram of the overall missile control loop.

INTRODUCTION

IN MOST THEORETICAL investigations regarding guided missile control problems, it is customary to formulate the transfer function of the missile itself under the assumption of a rigid body. A selection of the fundamental frequency of the closed control loop by a considerable factor smaller than the lowest natural frequency of the bending modes is considered sufficient for introducing this simplification.

However, the present trend to increase the overall performance of guided missiles by reducing the fabricated weight per pound propellant for a given payload and range, makes it doubtful whether the simplification, mentioned above, is still accurate enough. It is thought vitally important to consider more rigorously in closed loop control investigations the elasticity of the missile.

It is the object of this paper, as a basic step in this direction, to formulate the transfer function of an elastic missile. This transfer function is to relate the deflection angle of the control agent to the angle measured by an angular displacement gyro at any point on the longitudinal axis of the missile.

THEORY

The pitching and yawing motion of the missile in space under the influence of thrust and air forces normal to its longitudinal axis can be described with good approximation by the motion of an elastic free-free beam with given mass distribution and given stiffness distribution. The following partial differential equation is the mathematical expression for this rotary motion.

$$\frac{\partial^2}{\partial x^2}\left[EI(x)\frac{\partial^2 y(x,t)}{\partial x^2}\right] + g(x)\left|\frac{y(x,t)}{[\partial y(x,t)]/\partial t}\right|\frac{\partial y(x,t)}{\partial t} + m(x)\frac{\partial^2 y(x,t)}{\partial t^2} + F(x)\frac{\partial y(x,t)}{\partial x} + D(x)\frac{\partial}{\partial t}\left[\frac{\partial y(x,t)}{\partial x}\right] = T\delta(t)\Delta(x - x_l) \quad (1)$$

The boundary conditions to be fulfilled for a free-free beam are

$$\frac{\partial^2 y(0,t)}{\partial x^2} = \frac{\partial^3 y(0,t)}{\partial x^3} = 0; \qquad \frac{\partial^2 y(x_l,t)}{\partial x^2} = \frac{\partial^3 y(x_l,t)}{\partial x^3} = 0 \quad (2)$$

In Eqs. (1) and (2) the following nomenclature applies:

- x = distance of any arbitrary point on the longitudinal axis of the missile measured from the tip of the nose
- x_l = length of the missile
- t = instantaneous time
- y = deflection of any point x normal to the desired position of the longitudinal axis of the missile
- EI = local stiffness distribution along the longitudinal axis of the missile
- g = local distribution of the structural damping coefficient along the longitudinal axis of the missile
- m = local mass distribution along the longitudinal axis of the missile

Received June 23, 1953. Revised and received February 19, 1954.

* Dynamics Engineer.

† Design Specialist—Dynamics Group.

F = local coefficient of the restoring air forces normal to the longitudinal axis of the missile

D = local coefficient of the damping air forces normal to longitudinal axis of the missile

$T\delta$ = control force normal to longitudinal axis of missile

δ = deflection of the control agent

$\Delta(x - x_l)$ = dirac Δ function such that for

$$x \neq x_l;\ \Delta(x - x_l) = 0$$

$$x = x_l;\ \int_0^{x_l} \Delta(x - x_l)dx = 1$$

For the sake of simplification, the following permissible assumptions will be introduced:

(1) The structural damping is small enough to be neglected:

$$g(x) = 0 \tag{3}$$

(2) The restoring air forces and damping air forces normal to the longitudinal axis of the missile are dependent only on the rotary motion of an equivalent rigid missile having the same aerodynamic shape and the same mass distribution

$$F(x)\frac{\partial y(x,t)}{\partial x} \approx F(x)\frac{\partial y_R(x,t)}{\partial x} \tag{4}$$

$$D(x)\frac{\partial}{\partial t}\left[\frac{\partial y(x,t)}{\partial x}\right] \approx D(x)\frac{\partial}{\partial t}\left[\frac{\partial y_R(x,t)}{\partial x}\right] \tag{5}$$

For the rotary motion of the equivalent rigid body, the following equation holds:

$$y_R(x,t) = (x - x_{cg})\theta(t) \tag{6}$$

where

x_{cg} = location of the center of gravity

θ = rigid body rotation about cg

From Eqs. (4) through (6) follows:

$$F(x)\frac{\partial y(x,t)}{\partial x} \approx F(x)\theta(t) \tag{7}$$

$$D(x)\frac{\partial}{\partial t}\left[\frac{\partial y(x,t)}{\partial x}\right] \approx D(x)\frac{d\theta(t)}{dt} \tag{8}$$

With the first assumption mentioned above and utilizing Eqs. (1) and (6) the rotary rigid body motion is described by the following differential equation:

$$m(x)(x - x_{cg})\frac{d^2\theta(t)}{dt^2} + D(x)\frac{d\theta(t)}{dt} + F(x)\theta(t) = T\delta(t)\Delta(x - x_l) \tag{9}$$

Multiplication of Eq. (9) with $(x - x_{cg})$, application of the Laplace transformation with regard to time t, and integration over the length of the missile results in the following equation:

$$s^2\theta(s)\int_0^{x_l} m(x)(x - x_{cg})^2dx + s\theta(s)\int_0^{x_l} D(x)(x - x_{cg})dx + \theta(s)\int_0^{x_l} F(x)(x - x_{cg})dx = T(x_l - x_{cg})\delta(s) \tag{10}$$

where

$$I = \int_0^{x_l} m(x)(x - x_{cg})^2\,dx \tag{11}$$

represents the moment of inertia about an axis through the cg normal to the longitudinal axis of the missile.

Introducing for the sake of abbreviation

$$d_0 = \frac{1}{I}\int_0^{x_l} D(x)(x - x_{cg})dx \tag{12}$$

$$\mu_{r0} = \frac{1}{I}\int_0^{x_l} F(x)(x - x_{cg})dx \tag{13}$$

$$\mu_{c0} = \frac{1}{I}\,T(x_l - x_{cg}) \tag{14}$$

the following equation is obtained from Eq. (10):

$$\theta(s) = \{[\mu_{c0}/(s^2 + d_0s + \mu_{r0})]\,\delta(s)\} \tag{15}$$

and from Eqs. (6) and (15) follows

$$y_R(x,s) = \{[\mu_{c0}/(s^2 + d_0s + \mu_{r0})]\,(x - x_{cg})\delta(s)\} \tag{16}$$

From Eqs. (1), (2), (3), (7), and (8) follows for the rotary motion of the elastic missile

$$\frac{\partial^2}{\partial x^2}\left[EI(x)\frac{\partial^2 y(x,t)}{\partial x^2}\right] + m(x)\frac{\partial^2 y(x,t)}{\partial t^2} = T\delta(t)\Delta(x - x_l) - F(x)\theta(t) - D(x)\frac{d\theta(t)}{dt} \tag{17}$$

with the boundary conditions

$$\frac{\partial^2 y(0,t)}{\partial x^2} = \frac{\partial^3 y(0,t)}{\partial x^3} = 0; \qquad \frac{\partial^2 y(x_l,t)}{\partial x^2} = \frac{\partial^3 y(x_l,t)}{\partial x^3} = 0 \tag{18}$$

Application of the Laplace transformation with respect to time transforms the partial differential Eqs. (17) and (18) into the following set of ordinary differential equations:

$$\frac{d^2}{dx^2}\left[EI(x)\frac{d^2 y(x,s)}{dx^2}\right] + s^2 m(x)y(x,s) = T\delta(s)\Delta(x - x_l) - [sD(x) + F(x)]\theta(s) \tag{19}$$

with the boundary conditions

$$\frac{d^2 y(0,s)}{dx^2} = \frac{d^3 y(0,s)}{dx^3} = 0; \qquad \frac{d^2 y(x_l,s)}{dx^2} = \frac{d^3 y(x_l,s)}{dx^3} = 0 \tag{20}$$

Inserting Eq. (15) into Eq. (19) gives

$$\frac{d^2}{dx^2}\left(EI\frac{d^2 y}{dx^2}\right) + s^2 m(x)y = \left\{T\Delta(x - x_l) - \frac{\mu_{c0}}{s^2 + d_0 s + \mu_{r0}}[sD(x) + F(x)]\right\}\delta(s) \tag{21}$$

As a first step in the direction to find the general solution of this inhomogeneous differential equation, solutions of the following homogeneous differential equation will be obtained.

$$\frac{d^2}{dx^2}\left(EI\frac{d^2 y_H}{dx^2}\right) + s^2 m(x)y_H = 0 \tag{22}$$

with the boundary conditions

$$\frac{d^2 y_H(0,s)}{dx^2} = \frac{d^3 y_H(0,s)}{dx^3} = 0; \qquad \frac{d^2 y_H(x_l,s)}{dx^2} = \frac{d^3 y_H(x_l,s)}{dx^3} = 0 \tag{23}$$

Since $EI(x)$ and $m(x)$ are positive functions, and since Eq. (22) is self-adjoint, the system, on setting $s^2 = -\lambda$ has a complete set of real eigenvalues λ_K and corresponding orthogonal eigenfunctions $\phi_K(x,\lambda_K)$ reference 1, pages 62, 65.

These eigenvalues are related to the natural frequencies through

$$s_K = \sqrt{-\lambda_K} = \pm i\omega_K \tag{24}$$

The eigenfunctions $\phi_K(x, \pm i\omega_K)$ may then be identified with the bending mode shapes.

The general solution of the inhomogeneous differential equation Eq. (21) may be written

$$y(x,s) = A(s) + A_0(s)(x - x_{cg}) + \sum_{K=1}^{\infty} A_K(s)\phi_K(x, \pm i\omega_K) \tag{25}$$

Combining Eqs. (21), (22), (24), and (25) results in the following three equations:

$$s^2 m(x)A(s) = \left\{T\Delta(x - x_l) - \frac{\mu_{c0}}{s^2 + d_0 s + \mu_{r0}}[sD(x) + F(x)]\right\}\delta(s) \tag{26}$$

$$s^2 m(x)(x - x_{cg})A_0(s) = \left\{T\Delta(x - x_l) - \frac{\mu_{c0}}{s^2 + d_0 s + \mu_{r0}}[sD(x) + F(x)]\right\}\delta(s) \tag{27}$$

$$\sum_{K=1}^{\infty} A_K(s)(s^2 + \omega_K{}^2)m(x)\phi_K(x, \pm i\omega_K) = \left\{T\Delta(x - x_l) - \frac{\mu_{c0}}{s^2 + d_0 s + \mu_{r0}}[sD(x) + F(x)]\right\}\delta(s) \tag{28}$$

Integrating Eq. (26) over the length of the missile results in

$$A(s) = \frac{1}{s^2}\frac{1}{M}\left[T - \frac{\mu_{c0}}{s^2 + d_0 s + \mu_{0r}}(sD + F)\right]\delta(s) \tag{29}$$

where

$$M = \int_0^{x_l} m(x)dx = \text{total mass of missile} \tag{17}$$

$$D = \int_0^{x_l} D(x)dx = \text{resultant damping air force normal to longitudinal axis of missile}$$

$$F = \int_0^{x_l} F(x)dx = \text{resultant restoring air force normal to longitudinal axis of missile} \tag{18}$$

Eq. (29) characterizes the rigid body translatory motion of the missile.

Multiplying Eq. (27) by $(x - x_{cg})$ and integrating over the length of the missile results in

$$A_0(s)s^2 \int_0^{x_l} m(x)\ (x - x_{cg})^2 dx = \left\{ T(x_l - x_{cg}) - \frac{\mu_{c0}}{s^2 + d_0 s + \mu_{r0}} \left[s \int_0^{x_l} D(x)\ (x - x_{cg})dx + \int_0^{x_l} F(x)(x - x_{cg})dx \right] \right\} \delta(s) \tag{19, 30}$$

Utilizing Eqs. (11), (12), (13), and (14) from Eq. (30), there follows

$$A_0(s) = \{ [\mu_{c0}/(s^2 + d_0 s + \mu_{r0})]\delta(s) \} \tag{20, 31}$$

Comparing Eq. (31) with Eq. (15) reveals that $A_0(s) = \theta(s)$ describes the rotary rigid body motion of the missile.

Multiplying Eq. (28) by $\phi_j(x, \pm i\omega_j)$ and integrating over the length of the missile results in

$$\sum_{K=1}^{\infty} A_K(s)(s^2 + \omega_K{}^2) \int_0^{x_l} m(x)\phi_j\ (x, \pm i\omega_j)\phi_K(x, \pm i\omega_K)dx = \left\{ T\phi_j(x_l, \pm i\omega_j) - \frac{\mu_{c0}}{s^2 + d_0 s + \mu_{r0}} \left[s \int_0^{x_l} D(x)\phi_j(x, \pm i\omega_j)\ dx + \int_0^{x_l} F(x)\phi_j(x, \pm i\omega_j)dx \right] \right\} \delta(s) \tag{21, 22, 32}$$

Since the eigenfunctions $\phi_K(x, \pm i\omega_K)$ are orthogonal

$$A_K(s) = \frac{T\phi_K(x_l) - \frac{\mu_{c0}}{s^2 + d_0 s + \mu_{r0}} \left[s \int_0^{x_l} D(x)\phi_K\, dx + \int_0^{x_l} F(x)\phi_K\, dx \right]}{(s^2 + \omega_K{}^2) \int_0^{x_l} m(x)\phi_K{}^2 dx} \delta(s) \tag{23, 33}$$

From Eqs. (25), (29), (31), and (33), then follows

$$y(x,s) = \left\{ \frac{1}{s^2} \frac{1}{M} \left[T - \frac{\mu_{c0}}{s^2 + d_0 s + \mu_{r0}} (sD + F) \right] + \frac{\mu_{c0}}{s^2 + d_0 s + \mu_{r0}} (x - x_{cg}) + \sum_{K=1}^{\infty} \frac{T\phi_K(x_l, \pm i\omega_K) - \frac{\mu_{c0}}{s^2 + d_0 s + \mu_{r0}} \left[s \int_0^{x_l} D(x)\phi_K dx + \int_0^{x_l} F(x)\phi_K dx \right]}{(s^2 + \omega_K{}^2) \int_0^{x_l} m(x)\phi_K{}^2 dx} \phi_K \right\} \delta(s) \tag{24, 25, 34}$$

With the help of Eq. (34) the desired transfer function, relating the control agent deflection angle δ to the angle θ_g measured by any position gyro, can be found.

Assuming that the gyro is located at $x = x_g$ on the longitudinal axis of the missile, the gyro measures the local slope of the function $y(x,t)$. Thus

$$\theta_g(t) = \frac{\partial}{\partial x} y(x,t)\Big|_{x = x_g} \tag{26, 35}$$

or after application of the Laplace transformation

$$\theta_g(s) = \frac{d}{dx} y(x,s)\Big|_{x = x} \tag{27, 36}$$

From Eqs. (34) and (36) finally follows

$$\frac{\theta_g}{\delta}(s) = \left\{ \frac{\mu_{c0}}{s^2 + d_0 s + \mu_{r0}} \left[1 - \sum_{K=1}^{\infty} \frac{\int_0^{x_l} [sD(x) + F(x)]\phi_K dx \dfrac{d\phi_K}{dx}}{(s^2 + \omega_K{}^2) \int_0^{x_l} m(x)\phi_K{}^2 dx} \right] + \sum_{K=1}^{\infty} \frac{T\phi_K(x_l, \pm i\omega_K) \dfrac{d\phi_K}{dx}}{(s^2 + \omega_K{}^2) \displaystyle\int_0^{x_l} m(x)\phi_K{}^2 dx} \right\}_{x = x_g} \tag{37}$$

Recognizing in

$$M_{GK} = \int_0^{x_l} m(x)\phi_K{}^2 dx \tag{38}$$

the generalized mass for the kth mode and in

$$D_{GK} = \int_0^{x_l} D(x)\phi_K dx \tag{39}$$

the generalized air damping for the kth mode and in

$$F_{GK} = \int_0^{x_l} F(x)\phi_K dx \tag{40}$$

the generalized restoring air force for the kth mode and in

$$T_{GK} = T\phi_K(x_l, \pm i\omega_K) \tag{41}$$

the generalized control force for the kth mode, then Eq. (37) can be rewritten as

$$\frac{\theta_g}{\delta}(s) = \left\{ \frac{\mu_{c0}}{s^2 + d_0 s + \mu_{r0}} \left[1 - \sum_{K=1}^{\infty} \frac{sD_{GK} + F_{GK}}{(s^2 + \omega_K{}^2) M_{GK}} \frac{d\phi_K}{dx} \right] + \sum_{K=1}^{\infty} \frac{T_{GK}}{(s^2 + \omega_K{}^2) M_{GK}} \frac{d\phi_K}{dx} \right\}_{x = x_g} \tag{42}$$

For technical applications, it will be sufficient in general to consider only the first or the first and second mode.

Conclusions

From Eq. (37) it can be seen that the representation of the transfer function of an elastic rocket type guided missile in a general control block diagram consists of a basic block representing the rigid body motion of the missile and parallel to it one additional block for each vibration mode considered.

With such a block diagram describing the pitching or yawing motion of the missile, it is now possible to investigate the influence of the location of the angular displacement gyro and/or rate gyro on the longitudinal stability quality of the closed control loop in order to find such a location that the influence is minimized.

References

[1] Collatz, L., *Eigenwert Probleme Und Ihre Numerische Behandlung*, Akademische Verlagsgesellschaft, Leipzig, pp. 59–65, 1945.

[2] Kamke, E., *Differentialgleichungen: Loesungsmethoden Und Loesungen. I.* Akademische Verlagsgesellschaft, Leipzig, p. 537, 1944.

Changes of Address

Since the Post Office Department does not as a rule forward magazines to forwarding addresses, it is important that the Institute be notified of changes in address 30 days in advance of publishing date to ensure receipt of every issue of the JOURNAL and REVIEW.

Notices should be printed legibly and sent directly to:

Institute of the Aeronautical Sciences, Inc.
2 East 64th Street, New York 21, New York

Effect of Large Temperature Changes (Including Viscous Heating) upon Laminar Boundary Layers with Variable Free-Stream Velocity*

SOLOMON LEVY†

University of California at Berkeley

SUMMARY

This is a theoretical investigation concerned with the determination of skin friction and heat transfer for a laminar boundary-layer flow with variable free-stream velocity. The effects of frictional heating and the variation of properties are considered for a constant wall temperature and a constant product of viscosity and density.

Characteristics of the flow are computed from the laminar boundary-layer partial differential equations, which are first transformed into ordinary differential equations. Numerical solutions to these equations were calculated on the differential analyzer for low Mach Number flows (Mach Number approaching 0) with a Prandtl Number of 0.7 and 1.0 and for the entire Mach Number range with a Prandtl Number of 1. Approximate solutions are presented for high Mach Number flows (Mach Number larger than 5) with a Prandtl Number of 0.7. All the computations deal with a power variation of the free-stream Mach Number, $M_1 = P(2s)^{\beta/2}$, and with a permeable and an impermeable surface either insulated or maintained at constant temperature. A calculation method is presented for the determination of heat transfer and skin friction for an isothermal surface and an arbitrary free-stream velocity variation, utilizing the results derived from the numerical analysis of the differential equations.

Comparison of the various solutions, as well as their application to a specific flow example, leads to the following conclusions:

(1) The temperature difference between the wall and the free stream exerts a substantial effect on the skin-friction coefficient. The heat-transfer coefficient is not affected radically. The separation point moves to regions of greater deceleration as the body surface is cooled.

(2) For a constant product of viscosity and density the skin friction increases in an accelerating flow and decreases in a decelerating flow when the dissipation term is included in the energy equation. The same trend prevails for the heat-transfer coefficient but on a smaller scale.

(3) For accelerating flows the skin friction increases as the Prandtl Number is reduced from 1 to 0.7. With extremely small or large Mach Number values the increase in the skin friction is of the order of 1 or 10 per cent, respectively, and the solutions for a Prandtl Number of 1 may be utilized to yield an approximate answer if the Prandtl Number is not too different from 0.7. On the other hand, the changes in the heat-transfer coefficient are excessive for the case of dissipative flow, and multiplication of the results for a Prandtl Number of 1 by the factor (Prandtl Number)$^{1/3}$ does not lead to the correct answer with the exception of low Mach Number flows (nondissipative flows).

Received July 21, 1953. Revised and received February 19, 1954.

* The author wishes to acknowledge his indebtedness to Dr. R. A. Seban for his guidance throughout the conduct of the investigation. The author is indebted especially to J. Killeen for performing all the calculations on the differential analyzer.

† Presently, Engineer at Knolls Atomic Power Laboratory, General Electric Company, Schenectady, N.Y.

NOMENCLATURE

c_p	=	specific heat at constant pressure, B.t.u./lb. °F.
D	=	significant dimension of the body, ft.
F	=	function appearing in Eq. (42)
f	=	function of the independent variable η
g	=	temperature ratio, T_s/T_{s_1} as
h	=	heat-transfer coefficient, B.t.u./hr. ft.^{2}/°F.
K	=	constant equivalent to $1 - T_w/T_{s_1}$
k	=	thermal conductivity, B.t.u./hr. ft.^{2} °F./ft.
M_1	=	free-stream Mach Number
m	=	exponent appearing in Eq. (50)
n	=	constant appearing in Eq. (50)
p	=	pressure in the boundary-layer, lbs. per sq.ft.
q	=	local heat rate, B.t.u./hr. ft.^{2}
R	=	constant appearing in perfect gas relation
r	=	recovery factor
s	=	function of x defined by $ds = \mu_1 \rho_1 u_1 dx$
T	=	temperature in the boundary-layer, °F.
T_{aw}	=	temperature of insulated surface, °F.
T_s	=	stagnation temperature, °F.
u	=	velocity component in the x direction, ft. per sec.
$\tilde{u}_1$	=	nondimensional velocity, u_1/u_a
v	=	velocity perpendicular to body surface, ft. per sec.
v_0	=	suction velocity, ft. per sec.
x	=	distance along the body surface, ft.
$\tilde{x}$	=	nondimensional distance, x/D
y	=	distance normal to the body surface, ft.
z^*	=	nondimensional displacement thickness
z_i	=	nondimensional momentum thickness
β	=	velocity distribution parameter
δ^*	=	displacement thickness, ft.
η	=	independent variable defined by Eq. (5)
θ	=	momentum thickness, ft.
$\tilde{\theta}$	=	nondimensional momentum thickness, $(\theta/D)\sqrt{u_a D/\nu_a}$
μ	=	absolute viscosity, lb. sec./ft.^{2}
ν	=	kinematic viscosity, ft.^{2}/sec.
$\tilde{\nu}_1$	=	nondimensional viscosity, ν_1/ν_a
ρ	=	density of the flowing fluid, slugs per cu.ft.
σ	=	Prandtl Number, nondimensional
τ	=	shear stress, lbs. per sq.ft.
χ	=	nondimensional ratio, $\mu\rho/\mu_1\rho_1$
ψ	=	stream function

Subscripts

1	=	condition at the edge of the boundary layer
w	=	condition at the surface of the body
a	=	condition at arbitrarily selected point

Introduction

Specifying the skin friction and heat transfer in a laminar boundary-layer flow is important in designing high-speed aircraft. Since Prandtl first derived the boundary-layer equations in 1904, many investigators have tried to derive new solutions to these equations. Their aim was to obtain the boundary-layer characteristics for an arbitrary body in high-speed flight. A complete analysis of the problem, including dissipation, variation of properties, free-stream velocity, and wall temperature, is difficult. For a constant free-stream velocity, complete solutions have been presented by Chapman and Rubesin[1] and by Crocco.[2] Complexity of the boundary-layer equations is substantially increased with variable free-stream velocity, and the problem must be attacked under additional simplifying assumptions.

In this investigation solutions are presented for a nonuniform free-stream velocity, assuming a constant wall temperature and a constant product of density and viscosity. The solutions are computed from the partial differential equations, which are first transformed into ordinary differential equations, and these results are utilized in the integral methods to supply a calculation method for cases in which the boundary conditions are more general. Ordinary differential equations are obtained for the following conditions:

(1) Nondissipative flows ($M_1 \to 0$) for any constant value of the Prandtl Number. The free-stream velocity is a power function of the distance measured along the body, and the equations specify the effects of the variation of the properties.

(2) Dissipative flows over the entire Mach Number range for a Prandtl Number of unity and for a power function of the free-stream Mach Number, $M_1 = P(2s)^{\beta/2}$.

(3) Dissipative flows at high Mach Numbers ($M_1 > 5$) for any constant value of the Prandtl Number and for $M_1 = P(2s)^{\beta/2}$. Even though solutions over this Mach Number range have little practical value because of shock-wave interaction and large pressure gradient across the boundary layer the obtained results help to specify the changes in the dissipation flow characteristics as the Prandtl Number is reduced from 1 to 0.7, typical of air.

Previously, exact numerical solutions were obtained by Brown and Donoughe[3] only for the nondissipative flows of item (1). The other two types of flow have not been investigated. The purpose of this work is to recompute the nondissipative solutions of Brown and Donoughe on a differential analyzer for the simplified case of $\rho\mu$ = constant; to obtain numerical solutions for the flows of items (2) and (3); to extend the results for all three types of flow to the more general case of flow about an arbitrary body; and to determine the effects of dissipation and variation of properties through a specific numerical example.

Part I—Solutions of the Differential Equations

Basic Equations

The boundary-layer forms of the continuity, momentum, and energy equations for two-dimensional steady flow of a gas with constant Prandtl Number and specific heat are

$$\frac{\partial}{\partial x}(\rho u) + \frac{\partial}{\partial y}(\rho v) = 0 \tag{1}$$

$$\rho\left(u\frac{\partial u}{\partial x} + v\frac{\partial u}{\partial y}\right) = -\frac{\partial p}{\partial x} + \frac{\partial}{\partial y}\left(\mu\frac{\partial u}{\partial y}\right) \tag{2}$$

$$\rho\left(u\frac{\partial T_s}{\partial x} + v\frac{\partial T_s}{\partial y}\right) = \frac{\partial}{\partial y}\left(\mu\frac{\partial T_s}{\partial y}\right) + \left(\frac{1}{\sigma} - 1\right)\frac{\partial}{\partial y}\left(\mu\frac{\partial T}{\partial y}\right) \tag{3}$$

where T_s is the local stagnation temperature defined as

$$T_s = T + (u^2/2c_p)$$

For $\partial p/\partial y = 0$, the equation of state, $p = R\rho T$, specifies that the density ρ at any x position is inversely proportional to the temperature T.

The variation of the free-stream pressure p and free-stream stagnation temperature T_{s_1} is obtained from Eqs. (2) and (3) for large values of y,

$$-\partial p/\partial x = \rho_1 u_1 (du_1/dx)$$

with

$$\rho_1 u_1 (dT_{s_1}/dx) = 0$$

$$(\partial u/\partial y)_{y\to\infty} = (\partial^2 u/\partial y^2)_{y\to\infty} = 0$$

The continuity equation is satisfied if the stream function ψ is defined so that

$$\rho u = \partial\psi/\partial y, \qquad \rho v = -\partial\psi/\partial x \tag{4}$$

In reference 5 Illingworth transformed the momentum and energy equations without the dissipation term into ordinary differential equations. The same transformation is applied here to Eqs. (2) and (3), including the dissipation term.

The variables x and y are replaced by the variables s and η,

$$s = \int_0^x \mu_1\rho_1 u_1\, dx, \quad \eta = \frac{u_1\rho_1}{(2s)^{1/2}}\int_0^y \frac{T_1}{T}\, dy \tag{5}$$

and the change of variables is governed by the relations

$$\frac{\partial}{\partial y} = \frac{\rho u_1}{(2s)^{1/2}}\frac{\partial}{\partial \eta} + \frac{\partial s}{\partial y}\frac{\partial}{\partial s}$$

$$\frac{\partial}{\partial x} = \mu_1\rho_1 u_1\left(\frac{\partial}{\partial \eta}\frac{\partial \eta}{\partial s} + \frac{\partial}{\partial s}\right)$$

The velocity and the stagnation temperature are assumed to be defined by

$$u = u_1 f'(\eta) \tag{6}$$

$$T_s = T_{s_1}\, g(\eta) \tag{7}$$

where primes indicate derivatives with respect to the independent variable η. The form of Eqs. (6) and (7) presumes that Eqs. (2) and (3) can be transformed into ordinary differential equations. The end results of the transformation validate this assumption, but they do not show by any means that the obtained equations are unique.†

For $\eta = 0$, Eq. (7) specifies that the wall temperature T_w is equal to $T_{s_1}g(0)$, and the solutions are restricted to a constant wall temperature, since the free-stream stagnation temperature previously was found to be invariant with x.

Integration of Eq. (6) with respect to η gives

$$\psi = (2s)^{1/2} f(\eta) \tag{8}$$

The terms of Eqs. (2) and (3) can now be evaluated in terms of s and η from Eqs. (5), (6), (7), and (8), and the momentum and energy equations become

$$\frac{\partial}{\partial \eta}(\chi f'') + f f'' - \frac{2s}{u_1}\frac{du_1}{ds}\left(f'^2 - \frac{T}{T_1}\right) = 0 \tag{9}$$

$$\frac{\partial}{\partial \eta}(\chi g') + f g' + \left(\frac{1}{\sigma} - 1\right)\frac{T_1}{T_{s_1}}\frac{\partial}{\partial \eta}\left(\chi \frac{\partial}{\partial \eta}\frac{T}{T_1}\right) = 0 \tag{10}$$

with $\chi = \mu\rho/\mu_1\rho_1$.

For the purpose of simplification χ is assumed equal to 1. Chapman and Rubesin[1] have shown that solutions of the boundary-layer equations for flat-plate flow with $\chi = 1$ agree well with the more exact solutions if an appropriate constant is used in the skin-friction and heat-transfer relations. They took $\mu\rho = C$ with the constant C being evaluated from the wall temperature condition and being incorporated in the skin-friction and heat-transfer expressions.

The ratio T/T_1 is computed from Eq. (7),

$$\frac{T}{T_1} = g(\eta) + \frac{\gamma - 1}{2} M_1^2 [g - f'^2] \tag{11}$$

where

$$[(\gamma - 1)/2]\, M_1^2 = u_1^2/2c_pT_1$$

Substituting for T/T_1, the momentum and energy equations become

† Krzywoblocki[6] recently investigated the general problem of uniqueness of the boundary-layer solutions and showed that the Jacobian of the transformation

$$J\left[\frac{x(s),\ y(s,\eta)}{s,\ \eta}\right]$$

vanishes identically and that the transformation is not one-to-one, indicating the corresponding solutions may not be unique.

TABLE 1 - SOLUTIONS OF THE DIFFERENTIAL EQUATIONS

Investigator	Equation Solved	Velocity & Mach Number	Property Variation	Prandtl Number	Thermal Condition at Wall	Type of Solution	Transformation
Hartree[7]	Momentum	$u_1 = Px^{\beta/2-\beta}$, $M_1 = 0$	Constant	Any constant	Variable	Exact	$\eta = \frac{y}{x^{1/2-\beta}}\sqrt{\frac{u_1}{\nu x}}$
Eckert[8]	Energy				Constant Temperature		
Schuh[9] Levy[10] Tifford-Chu[11]	Energy				Variation of Power Type		
Eckert-Drewitz[12]	Energy				Insulated		
Brown-Donoughe[3]	Momentum Energy		Variable	0.7	Constant Temperature		$\eta = y\sqrt{\frac{\rho u_1}{\mu_w x}}$
Present Solutions	Momentum Energy		$\mu\rho$=constant	0.7, 1.0			$\eta = \frac{u_1\rho_1}{(2s)^{1/2}}\int_0^y \frac{T_1}{T}dy$, $s = \int_0^x \mu_1\rho_1 u_1 dx$
Crocco[2]		u_1=constant, M_1=constant	Variable	0.725, 1.0			
Chapman-Rubesin[1]			$\mu\rho$=constant	Any constant	Variation of Power Type		
Stewartson[13]	Momentum	$M_1 = P(2s)^{\beta/2}$	$\mu\rho$=constant	1.0	Insulated		$y = \left(\frac{T}{T_{s_1}}\right)^{\frac{\omega+1}{2(\omega-1)}}\int_0^\eta \frac{T_1}{T}d\eta$, $x = \int_0^s \left(\frac{T_1}{T_{s_1}}\right)^{\frac{3\omega+1}{2(\omega-1)}} ds$
Present Solutions	Momentum Energy		$\mu\rho$=constant	1.0	Constant Temperature		
Levy-Seban[14]		$u_1 = Px^{\beta/2-\beta}$, $M_1 = 0$	$\mu\rho$=constant	0.7, 1.0		Approximate	$\eta = \frac{u_1\rho_1}{(2s)^{1/2}}\int_0^y \frac{T_1}{T}dy$, $s = \int_0^x \mu_1\rho_1 u_1 dx$
Present Solutions	Momentum Energy	$M_1 = P(2s)^{\beta/2}$, $M_1 > 5$	$\mu\rho$=constant	Any constant	Constant Temperature & Insulated		

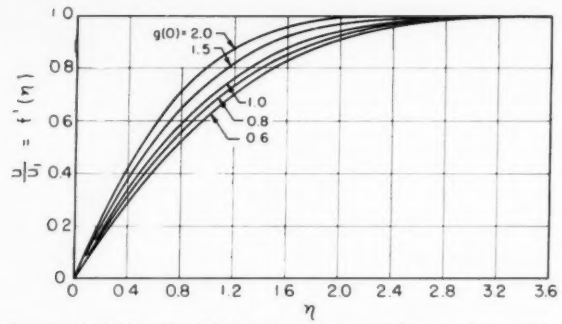

FIG. 1. Velocity distributions for constant β flows with $\sigma = 0.7$, $f(0) = 0$, and $\beta = 0.5$.

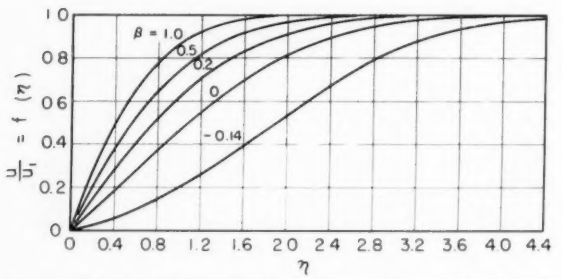

FIG. 2. Velocity distributions for constant β flows with $\sigma = 0.7$, $g(0) = 1.5$, and $f(0) = 0$.

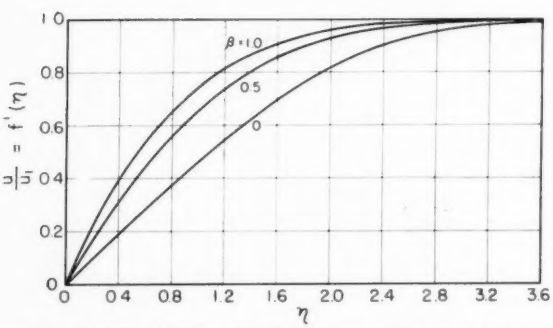

FIG. 3. Velocity distributions for constant β flows with $\sigma = 1.0$, $g(0) = 0.8$, and $f(0) = 0$.

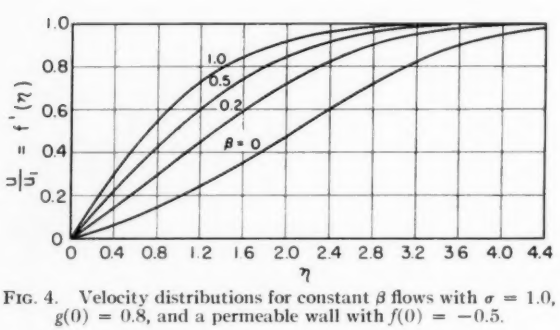

FIG. 4. Velocity distributions for constant β flows with $\sigma = 1.0$, $g(0) = 0.8$, and a permeable wall with $f(0) = -0.5$.

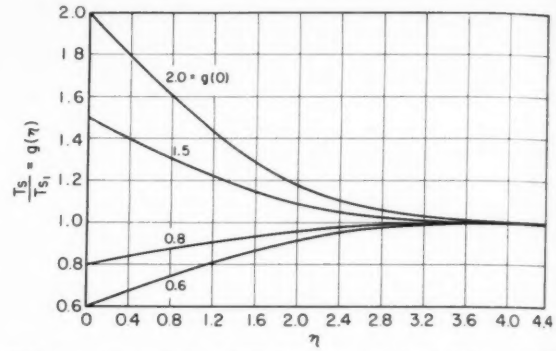

FIG. 5. Temperature distributions for constant β flows with $\sigma = 0.7$, $\beta = 0.5$, and $f(0) = 0$.

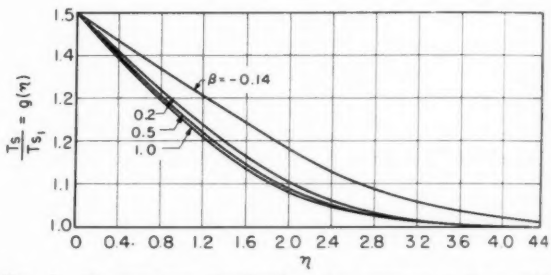

FIG. 6. Temperature distributions for constant β flows with $\sigma = 0.7$, $f(0) = 0$, and $g(0) = 1.5$.

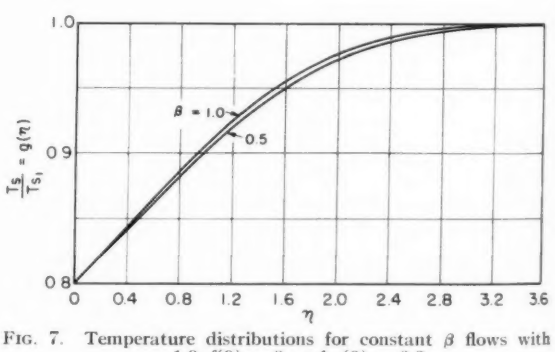

FIG. 7. Temperature distributions for constant β flows with $\sigma = 1.0$, $f(0) = 0$, and $g(0) = 0.8$.

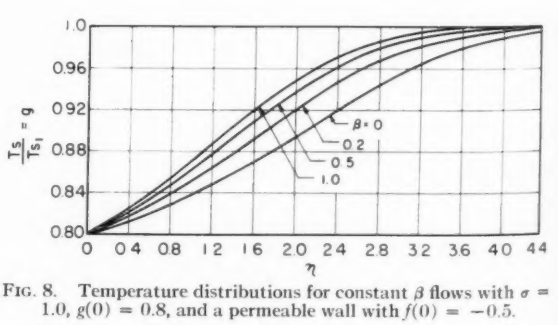

FIG. 8. Temperature distributions for constant β flows with $\sigma = 1.0$, $g(0) = 0.8$, and a permeable wall with $f(0) = -0.5$.

$$f''' + ff'' - \frac{2s}{u_1}\frac{du_1}{ds}\left(1 + \frac{\gamma - 1}{2}M_1^2\right) \times (f'^2 - g) = 0 \quad (12)$$

$$g'' + fg' + \left(\frac{1}{\sigma} - 1\right)\frac{T_1}{T_{s_1}}\left(1 + \frac{\gamma - 1}{2}M_1^2\right)g'' - \frac{T_1}{T_{s_1}}\left(\frac{1}{\sigma} - 1\right)\left(\frac{\gamma - 1}{2}M_1^2\right)\frac{d^2}{d\eta^2}f'^2 = 0 \quad (13)$$

The terms T_1/T_{s_1} and

$$\frac{2s}{u_1}\frac{du_1}{ds}\left(1 + \frac{\gamma - 1}{2}M_1^2\right)$$

appearing in Eqs. (12) and (13) are written

$$\frac{T_1}{T_{s_1}} = 1\Big/\left(1 + \frac{\gamma - 1}{2}M_1^2\right)$$

$$\left(1 + \frac{\gamma - 1}{2}M_1^2\right)\frac{2s}{u_1}\frac{du_1}{ds} = \frac{2s}{M_1}\frac{dM_1}{ds} \equiv \beta$$

with the latter expression obtained from the differentiation of $[(\gamma - 1)/2]M_1^2 = u_1^2/2c_pT_1$ and from the evaluation of dT_1/ds from the statement that the free-stream stagnation temperature is invariant with x.

The final forms of the momentum and energy equations are

$$f''' + ff'' + \beta(g - f'^2) = 0 \quad (14)$$

$$g'' + \sigma fg' - (1 - \sigma)\frac{[(\gamma - 1)/2]M_1^2}{1 + [(\gamma - 1)/2]M_1^2} \times \frac{d^2}{d\eta^2}f'^2 = 0 \quad (15)$$

Eqs. (14) and (15) must be ordinary differential equations if the definitions of u and T_s in terms of a single variable η are to be valid. This occurs for β = constant and for any of the following conditions:

(1) $M_1 \to 0$ or nondissipative flow. The Prandtl Number can assume any constant value, and the free-stream velocity satisfies the relation

$$u_1 = P(2s)^{\beta/2}$$

(2) The Prandtl Number is equal to 1 and $M_1 = P(2s)^{\beta/2}$. No restriction is imposed upon the magnitude of the Mach Number, and the dissipation term is included.

(3) $M_1 \to \infty$ and $M_1 = P(2s)^{\beta/2}$. The effects of dissipation are again included, but the flow is limited to high Mach Numbers. Any value of Prandtl Number can be used. The boundary-layer equations are no longer valid at high Mach Numbers, and the usefulness of the results as $M_1 \to \infty$ is limited. The equations presented here can be utilized, however, to specify the characteristics of a dissipative boundary layer with a Prandtl Number different from 1 and will be used primarily for comparison purposes.

For all three cases the momentum equation is Eq. (14). The corresponding energy equations are, respectively,

$$g'' + \sigma fg' = 0 \quad (16)$$

$$g'' + fg' = 0 \quad (17)$$

$$g'' + \sigma fg' - (1 - \sigma)(d^2/d\eta^2)f'^2 = 0 \quad (18)$$

The associated boundary conditions are, for all three cases,

$$\eta = 0, \quad f = 0 \text{ or } f = \text{const.}, \quad f' = 0 \quad g = 1 - K$$
$$\eta \to \infty, \quad f' = 1, \quad g = 1$$

which correspond to

$$y = 0, \ v = 0 \text{ or } v = v_0(x), \ u = 0, \quad T_w = (1 - K)T_{s_1}$$
$$y \to \infty, \quad u = u_1, \quad T_s = T_{s_1}$$

Exact solutions of Eqs. (14), (16), and (17) have been computed on the differential analyzer for various values of β and a large range of K values. On the other hand, the system of Eqs. (14) and (18) was solved by an approximate method. Before proceeding to discussion of the numerical results, a review of available solutions is shown in Table 1. The present types of solutions are included for comparison purposes. Examination of Table 1 reveals that the case of $M_1 \to 0$ and $\sigma = 0.7$ has been investigated previously. The other two types of numerical solutions presented here have not been considered by other investigators.

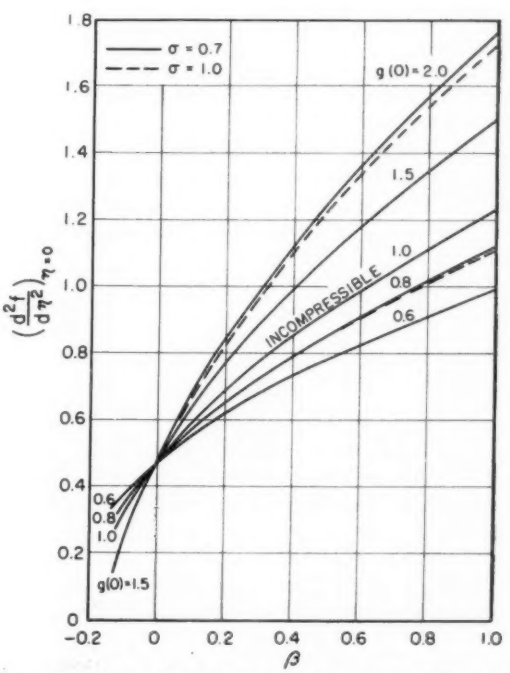

FIG. 9. Velocity gradients at the wall for constant β flows with $f(0) = 0$.

Exact Solutions—Nondissipative Flows

In the absence of frictional heating the free-stream Mach Number is 0 and $T/T_1 = g(\eta)$. The free-stream variation is determined from the relations $ds = \mu_1\rho_1 u_1\, dx$ and $\beta = (2s/u_1)\,(du_1/ds)$. There results

$$u_1 = P(2s)^{\beta/2} = Px^{(\beta/2-\beta)}$$

This corresponds to the wedge flows considered by Hartree,[7] the parameter β being identical in the present equation and in Hartree's solutions.

The momentum equation and energy equation are Eqs. (14) and (16), respectively, which were derived previously. They are identical to the equations obtained by Illingworth.[5] Exact solutions to the system of Eqs. (14) and (16) were computed on the differential analyzer. Calculations were carried out for a sufficient number of values of β and $g(0)$ to describe the combined effect of free-stream velocity and properties variation. These cases are indicated in the following tabulation:

$$\begin{cases} \beta &= 1.0, 0.5, 0.2, 0, -0.14 \\ g(0) &= 0.6, 0.8, 1.0, 1.5, 2.0 \\ \sigma &= 0.7 \\ f(0) &= 0 \end{cases}$$

$$\begin{cases} \beta &= 1.0, 0.5, 0.2, 0 \\ g(0) &= 0.8, 1.0, 2.0 \\ \sigma &= 1.0 \\ f(0) &= 0 \end{cases}$$

$$\begin{cases} \beta &= 1.0, 0.5, 0.2, 0 \\ g(0) &= 0.8 \\ \sigma &= 1.0 \\ f(0) &= -0.5 \end{cases}$$

The large number of cases considered prohibits presentation of all the results. Typical velocity profiles are shown in Figs. 1, 2, 3, 5, 6, and 7, and these demonstrate the effects of changing β or T_w/T_1. The changes in these profiles with respect to β are illustrated in Figs. 4 and 8 for the case of $f(0) = -0.5$, which corresponds to a permeable wall with a suction velocity of the form

$$v_0 = \frac{\mu_w u_1 f(0)}{(2s)^{1/2}} = u_1 f(0)\sqrt{\frac{\mu_w}{u_1\rho_w x}} = -\frac{1}{2}\,u_1\sqrt{\frac{\mu_w}{u_1\rho_w x}} \qquad (19)$$

The gradients of the velocity and temperature functions at the wall are shown for all cases in Figs. 9, 10, 11, and 12. The knowledge of these gradients enables the calculation of the skin friction and heat rate at the wall,

$$\frac{\tau_w}{\rho_w u_1^2} = \frac{\mu_w}{\rho_w u_1^2}\left(\frac{\partial u}{\partial y}\right)_{y=0} = \frac{f''(0)}{\sqrt{2-\beta}}\sqrt{\frac{\mu_w}{u_1\rho_w x}} \qquad (20)$$

$$\frac{q_w}{T_w - T_1}\frac{x}{k_w} = \frac{hx}{k_w} = \frac{g'(0)}{K\sqrt{2-\beta}}\sqrt{\frac{u_1 x\rho_w}{\mu_w}} \qquad (21)$$

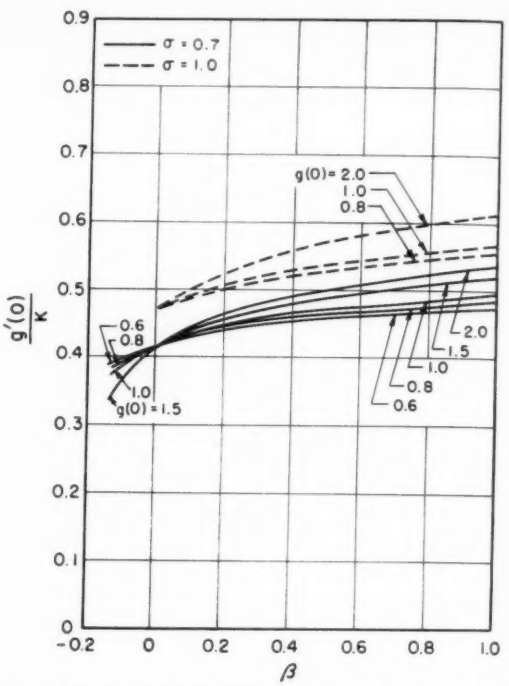

FIG. 10. Temperature gradients at the wall for constant β flows with $\sigma = 0.7$, $\sigma = 1.0$, and $f(0) = 0$.

The displacement thickness δ^* and the momentum thickness θ can be computed if they are expressed in their nondimensional form. Introduction of η into the definitions

$$\delta^* = \int_0^\infty \left(1 - \frac{\rho}{\rho_1}\frac{u}{u_1}\right) dy$$

$$\theta = \int_0^\infty \frac{\rho}{\rho_1}\frac{u}{u_1}\left(1 - \frac{u}{u_1}\right) dy$$

yields

$$z_i = \frac{\theta}{(2s)^{1/2}}\,u_1\rho_1 = \int_0^\infty f'(1-f')\,d\eta$$

$$z^* = \frac{\delta^*}{(2s)^{1/2}}\,u_1\rho_1 = \int_0^\infty (1-f')\,d\eta - \int_0^\infty \left(1 - \frac{T}{T_1}\right) d\eta$$

Values of z_i and z^* were calculated from the known velocity and temperature profiles and are presented in the second part of the paper, where they are utilized to solve the momentum integral equation. Figs. 14 and 15 show these results.

All the solutions presented here show the effects of the variation of properties. Examination of Figs. 9 to 12 reveals that the skin friction increases considerably from the incompressible value when the surface of the body is heated or cooled. Conversely, the heat-transfer coefficient is only slightly affected. The effects of the variation of properties decreases until no effect is ob-

served for flat-plate flow ($\beta = 0$), which verifies the classical result for this flow for $\mu\rho$ a constant. Even though the calculations were not carried out for separation flow, $f''(0) = 0$, the results for $\beta = -0.14$ show that separation occurs for larger unfavorable pressure gradients when the body is cooled.

The solutions for a Prandtl Number of 0.7 for the simplified case of $\rho\mu$ = constant are a repetition of the calculations of Brown and Donoughe.[3] However, the solutions are obtained here by a different numerical technique and might help to clarify some of the difficulties of solution reported by Brown and Livingood,[4] who noticed that f'' and f''' did not approach zero as η became large for the large values of T_w/T_1 considered in reference 3. Comparison of the present results with those of Brown and Donoughe shows agreement within 5 per cent for the skin friction and heat transfer. Correspondence in the values of the nondimensional displacement and momentum thickness is not too satisfactory as the ratio T_w/T_1 becomes large, with a maximum deviation of 20 per cent noted for $T_w/T_1 = 2.0$. As T_w/T_1 increases, the velocity profiles obtained here and in reference 3 tend to approach 1 from above as $\eta \to \infty$. The corresponding values of $f''(0)$ and $g'(0)$ are defined well, but a small change in the fourth significant figure of these gradients leads to a 5 per cent change in the velocity profiles for $\eta > 2.0$. The functions f'' and f''' will approach zero at large values of η only if the gradients at the wall can be specified within five to six significant figures, and these exceed the accuracy of the differential analyzer. Asymptotic solutions were substituted instead to determine the velocity profiles at large values of η.

Levy and Seban[14] have obtained an approximate solution of Eqs. (14) and (16) with a considerable reduction in the amount of calculations. The degree of accuracy of these approximate results can be determined by comparing them with the present exact solutions. Agreement within at least 5 per cent exists between the approximate and the exact solutions for skin friction and heat transfer, the discrepancy becoming larger as T_w/T_1 increases; the same trend is noticed for the values of the displacement and momentum thicknesses, the maximum deviation being approximately 10 per cent.

The results presented here are exact for $M_1 = 0$. Their application to $M_1 > 0$ is possible if the term

$$(1 - \sigma)\frac{[(\gamma - 1)/2]M_1^2}{1 + [(\gamma - 1)/2]M_1^2}\frac{d^2}{d\eta^2}f'^2 \qquad (22)$$

is small as compared to the other terms of Eq. (15). For a Mach Number of 1, Eq. (22) has a maximum value $0.4\,(1 - \sigma)f''^2(0)$ at $\eta = 0$. This term becomes larger as T_w/T_1 or β increases. For stagnation flow with $\sigma = 0.7$, it is equal to 0.27 and 0.37 for $T_w/T_1 = 1.5$ and 2.0, respectively. Since the other terms of the energy equation are equal to zero at $\eta = 0$, the neglect of the term of Eq. (22) is open to question unless the Prandtl Number is much closer to 1 or the Mach Number not too large ($M_1 < 0.7$).

Exact Solutions—Dissipative Flow with a Prandtl Number of 1

For a Prandtl Number of 1 the solutions to the boundary-layer equations become much simpler. For flat-plate flow, the Crocco-Stoddola relation specifies that the stagnation temperature is proportional to the velocity. For the case of variable free-stream velocity, Stewartson[13] has shown that the dissipative flow system can be reduced to the incompressible wedge flows if the surface is insulated. For no heat transfer at the wall, a particular solution of Eq. (17), which satisfies all the boundary conditions, is $g(\eta) = 1$, and the momentum equation becomes

$$f''' + ff'' + \beta(1 - f'^2) = 0 \qquad (23)$$

Solutions to Eq. (23) have already been obtained by Hartree[7] and can be used to compute the skin friction for dissipative flow over an insulated surface.

The correspondence noted between the dissipative and nondissipative solutions for an insulated surface also exists for a surface maintained at constant temperature. When the wall temperature is constant, Eqs. (14) and (17) must be solved simultaneously to obtain the temperature and velocity profiles. These equations are identical to the low Mach Number Eqs. (14) and (16) if the Prandtl Number is replaced by 1 in Eq. (16). The solutions of the previous section for nondissipative flow with a Prandtl Number of 1 are applicable therefore to the dissipative flow considered here if the ratio T_s/T_{s_1} is substituted for T/T_1 and the velocity u_1 is replaced by M_1 in the expression $u_1 = P(2s)^{\beta/2}$. Therefore, Figs. 3 and 6 represent typical velocity and stagnation temperature profiles for various

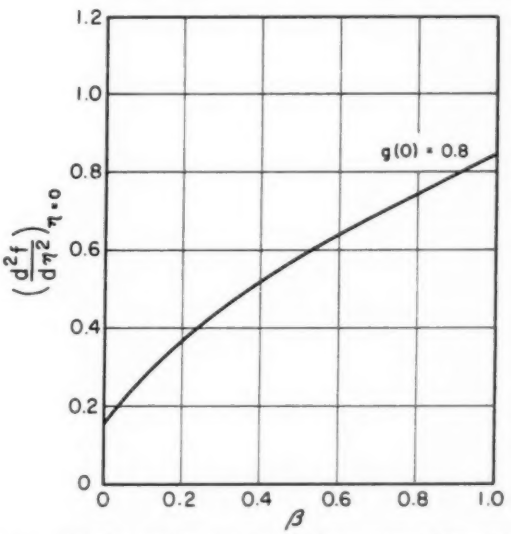

FIG. 11. Velocity gradients at the wall for constant β flows with $\sigma = 1.0$ and a permeable wall with $f(0) = -0.5$.

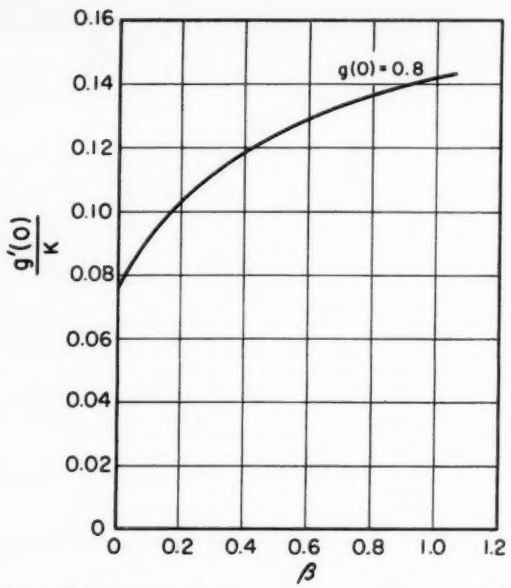

FIG. 12. Temperature gradients at the wall for constant β flows with $\sigma = 1$ and a permeable wall with $f(0) = -0.5$.

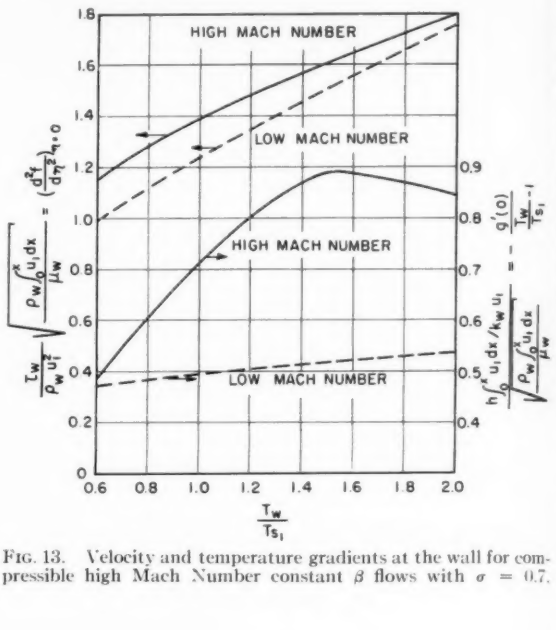

FIG. 13. Velocity and temperature gradients at the wall for compressible high Mach Number constant β flows with $\sigma = 0.7$.

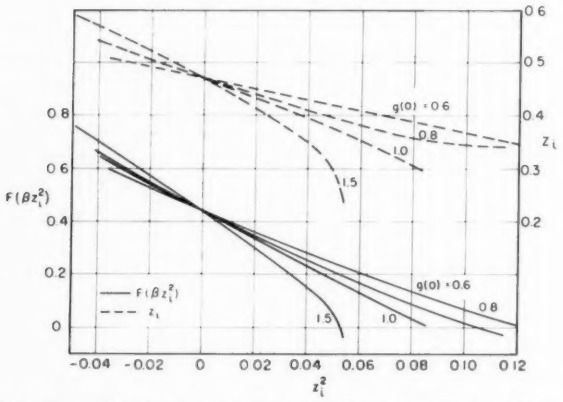

FIG. 14. $F(\beta z_i^2)$ and z_i vs. form parameter βz_i^2 for low Mach Number flow.

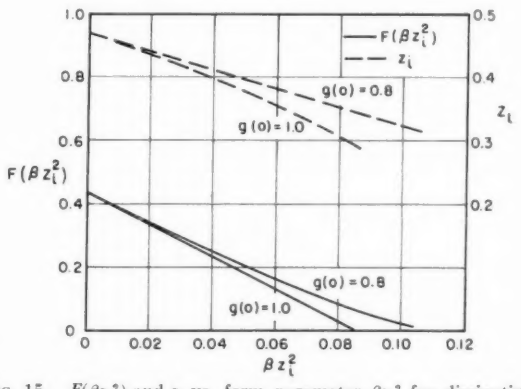

FIG. 15. $F(\beta z_i^2)$ and z_i vs. form parameter βz_i^2 for dissipative flow with $\sigma = 1.0$.

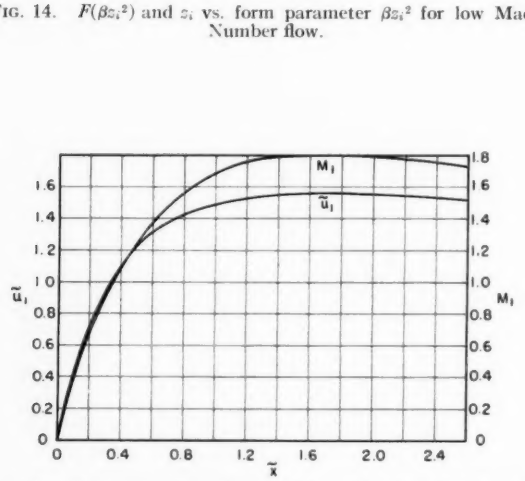

FIG. 16. Free-stream velocity and Mach Number distribution.

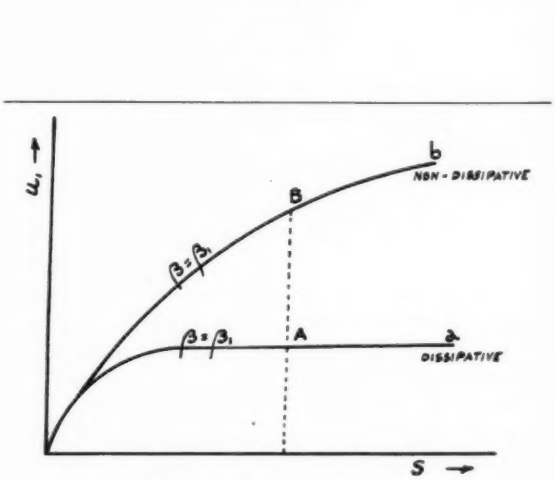

SKETCH 1. Free-stream velocity.

values of β and T_w/T_{s_1}, and Figs. 4 and 8 show the changes in these profiles with respect to β when the wall becomes permeable and has a suction velocity defined by $f(0) = -(1/2)$. The suction velocity is obtained now from

$$v_0 = \frac{\mu_w u_1 f(0)}{(2s)^{1/2}} = -\frac{1}{2}\frac{u_1}{\sqrt{2}}\sqrt{\frac{\mu_w}{\rho_w \int_0^x u_1\,dx}} \tag{24}$$

The velocity and temperature gradients at the wall are identical to those presented for a Prandtl Number of 1 in the previous section. The skin friction and heat-transfer coefficient are obtained from these gradients by the expressions

$$\frac{\tau_w}{\rho_w u_1^2} = \frac{\mu_w}{\rho_w u_1^2}\frac{T_1}{T_w}\frac{u_1^2\rho_1}{(2s)^{1/2}} f''(0) = \frac{f''(0)}{\sqrt{2}}\sqrt{\frac{\mu_w}{\rho_w \int_0^x u_1\,dx}} \tag{25}$$

$$\frac{q_w}{T_w - T_{s_1}}\frac{\int_0^x u_1\,dx}{u_1 k_w} = \frac{h\int_0^x u_1\,dx}{k_w u_1} = \frac{g'(0)}{\sqrt{2}\,K}\sqrt{\frac{\rho_w \int_0^x u_1\,dx}{\mu_w}} \tag{26}$$

The local heat-transfer coefficient is defined as

$$h = \frac{q_w}{T_w - T_{s_1}} = \frac{q_w}{T_w - T_{aw}}$$

since, for an insulated surface with a Prandtl Number of 1, $T_{s_1} = T_{aw}$, the adiabatic wall temperature.

For $M_1 \to 0$, Eqs. (24), (25), and (26) reduce to the corresponding nondissipative equations. However, this correspondence between the dissipative and nondissipative flows does not help to specify the effects of dissipation, since the free-stream velocity distributions are different for the two flows. In the case of dissipative flow, the free-stream velocity u_1 is

$$u_1 = \left(2c_p T_{s_1}\frac{[(\gamma-1)/2]M_1^2}{1 + [(\gamma-1)/2]M_1^2}\right)^{1/2} \tag{27}$$

Substitution of Eq. (27) into the definition $dx = ds/\mu_1\rho_1 u_1$ determines x in terms of s

$$dx = \frac{ds}{\mu_1\rho_1\sqrt{2c_p T_{s_1}}}\sqrt{\frac{1 + [(\gamma-1)/2]M_1^2}{[(\gamma-1)/2]M_1^2}} \tag{28}$$

for

$$M_1 = P(2s)^{\beta/2} \tag{29}$$

Once x is known as a function of s, the variation of the free-stream velocity u_1 with x is obtained from Eq. (27). The resulting expression is entirely different from the simple relation $u_1 = Px^{(\beta/2-\beta)}$ obtained for the nondissipative flows. In spite of this difference in the free-stream velocity variation from one set of solutions to the other, a qualitative description of the dissipation effects is possible by referring to the variable s. The dissipative flow free-stream velocity approaches a constant as s goes to infinity, while for the nondissipative flow it continually increases with s. At s equal to zero, $(2s/u_1)\,(du_1/ds) = \beta$ for the two flows, and at the origin the two curves for the free-stream velocity are tangent to each other, as shown in Sketch 1 for $\beta = \beta_1 > 0$. Curve Aa corresponds to the dissipative flow and curve Bb to the nondissipative one.

For the same value of s, the skin friction is identical for the nondissipative flow and the dissipative flow shown in Sketch 1. On the other hand, there also exists a nondissipative flow with β not constant which has a free-stream velocity distribution of the type Aa. At the point A such a flow has a β value smaller than β_1 because du_1/ds there is less than at the point B, and the skin friction for this variable nondissipative flow is lower than the value corresponding to the point B—i.e., less than the dissipative value. For accelerating flows, addition of the dissipation term to the energy equation corresponds to an increase in the skin friction. The reverse is true for decelerating flows, since the positions of the curves Aa and Bb are interchanged.

The number of numerical solutions obtained on the differential analyzer for dissipative flow with a Prandtl Number of 1 is relatively small. Most flows involve a wider variation of wall temperatures and of suction and blowing conditions. Approximate values can be obtained for all these conditions by using the method of reference 14. Examination of Figs. 9 and 10 reveals another alternative, since the skin friction is not affected by the Prandtl Number, while the heat-transfer coefficient for the two Prandtl Numbers considered can be deduced from one another by the use of the factor $\sigma^{1/3}$. Utilization of the results for a Prandtl Number of 0.7 becomes possible if proper care is taken in their conversion to a Prandtl Number of unity.

Approximate Solutions—High-Speed Dissipative Flow

The energy equation, Eq. (15), can be written

$$g'' + \sigma f g' - (1-\sigma)\frac{d^2}{d\eta^2}f'^2 + (1-\sigma)\frac{1}{1 + [(\gamma-1)/2]\,M_1^2} \times \frac{d^2}{d\eta^2}f'^2 = 0 \tag{30}$$

As the free-stream Mach Number becomes larger and approaches infinity, the last term of Eq. (30) vanishes and the energy equation becomes

$$g'' + \sigma f g' - (1 - \sigma)\,(d^2/d\eta^2)\,f'^2 = 0 \tag{18}$$

For a Mach Number of 5 or 10, the neglected factor amounts to $^1/_6$ or $^1/_{21}$ of the term $(1 - \sigma)\,(d^2/d\eta^2)f'^2$ retained in Eq. (18). Then, the solutions of Eq. (18) are expected to be valid for $M_1 > 5$ and can be computed for an insulated wall or a constant wall temperature.

For no heat transfer at the wall Eq. (18) can be integrated to yield the temperature distribution in terms of the velocity function

$$g = \frac{T_s}{T_{s_1}} = 1 - (1 - \sigma) \int_\eta^\infty e^{-\sigma \int_0^\eta f\,d\eta} \left(\int_0^\eta e^{\sigma \int_0^\eta f\,d\eta} \frac{d^2}{d\eta^2} f'^2\,d\eta \right) d\eta \tag{31}$$

Let $\eta = 0$, and the adiabatic wall temperature is

$$\frac{T_{aw}}{T_{s_1}} = 1 - (1 - \sigma) \int_0^\infty e^{-\sigma \int_0^\eta f\,d\eta} \left(\int_0^\eta e^{\sigma \int_0^\eta f\,d\eta} \frac{d^2}{d\eta^2} f'^2\,d\eta \right) d\eta$$

The recovery factor $r = (T_{aw} - T_1)/(u_1^2/2c_p)$ becomes

$$r = 1 - (1 - \sigma) \left\{ 1 + \frac{1}{[(\gamma - 1)/2]M_1^2} \right\} \int_0^\infty e^{-\sigma \int_0^\eta f\,d\eta} \left(\int_0^\eta e^{\sigma \int_0^\eta f\,d\eta} \frac{d^2}{d\eta^2} f'^2\,d\eta \right) d\eta \tag{32}$$

and it increases as the Mach Number increases. As the free-stream Mach Number approaches infinity, the recovery factor reaches the maximum value

$$r = 1 - (1 - \sigma) \int_0^\infty e^{-\sigma \int_0^\eta f\,d\eta} \left\{ \int_0^\eta e^{\sigma \int_0^\eta f\,d\eta} \frac{d^2}{d\eta^2} f'^2\,d\eta \right\} d\eta \tag{33}$$

For flat-plate flow, $\beta = 0$, Eq. (33) leads to the same solution as the complete energy equation, Eq. (15) or (30), and the recovery factor is equal to the square root of the Prandtl Number. For β different from zero, the evaluation of the recovery factor requires successive approximations. The first approximation is obtained by substituting the incompressible value of the function f in Eq. (33) and gives $r = 0.798$ for $\sigma = 0.7$ and $\beta = 1.0$. This value may vary as more approximations are carried out, but it is close enough to the incompressible values[15] to indicate that the effect of the Mach Number upon the recovery factor is relatively small.

When the wall is not insulated, Eqs. (14) and (18) may be solved simultaneously according to the methods of Ringleb[16] and of reference 14. Exponential functions are assumed for both the velocity and temperature profiles. These in turn are determined by satisfying Eqs. (14) and (18) along $\eta = 0$ as far as possible. The details of the method are given in reference 14. The gradients at the wall $f''(0) = -a$ and $g'(0) = -KA$ are specified from the following two equations:

$$10\beta KA(2a^2 - \beta) = 24a^5 - 5a^3[12\beta(1 - K) - 2\beta\sigma + 1] + 2\beta a[15\beta(1 - K)^2 - 2(1 - K) - 3\beta\sigma(1 - K)] \tag{34}$$

$$24A^5 + \frac{120}{K}(1 - \sigma)A^3a^2 - 5\left[\sigma - 7\beta(1 - \sigma) + \frac{24}{K}(1 - \sigma)\,(1 - K)\beta\right]A^2a + A\left[\frac{30}{K}(1 - \sigma)\,(1 - K)^2\beta^2 + \frac{120}{K^2}(1 - \sigma)^2a^4 + \sigma(1 - K)\beta + 19(1 - \sigma)\,(1 - K)\beta^2\right] = \frac{8a^3}{K}(1 - \sigma)\left[\frac{15}{K}(1 - \sigma)\,(1 - K)\beta - 2\beta\sigma + 1\right] \tag{35}$$

Examination of Eq. (34) reveals that it reduces to the low Mach Number equation as presented in reference 14 when the Prandtl Number is reduced to 1. The similarity between the low and high Mach Number equations for the term a indicates that the skin friction for the same constant β flow is not affected relatively as the Mach Number becomes large. However, the form of Eq. (35) is different entirely from the corresponding low Mach Number flow equation, and large changes in the heat-transfer coefficient may be expected. These effects are demonstrated in Fig. 13 where the skin friction and heat transfer are shown for $\beta = 1$ and various values of K. The heat-transfer coefficient is now defined as $h = q_w/T_w - T_{s_1}$. This change permits the use of Eq. (26). The skin friction is still defined by Eq. (25).

The curves for dissipative flow with a Prandtl Number of 1 are not included in Fig. 13. Comparison of

Figs. 9 and 13 reveals that for $\beta = 1$ the skin friction of a dissipative flow increases at most by 10 per cent as the Prandtl Number is reduced from 1 to 0.7. This result, coupled with the practical independence of the skin friction upon the Prandtl Number for the non-dissipative case, shows that the results for a Prandtl Number of 1 can be utilized to predict the skin friction over a body maintained at constant temperature. The resulting error will not exceed 10 per cent for Mach Number values between 0 and 5 or larger. The same argument is not valid for the heat-transfer coefficient because the curves of Figs. 10 and 13 are too different.

The results presented in this section have led to some interesting conclusions, but they should be used with extreme caution. The approximate method utilized to solve the system of Eqs. (14) and (18) is subject to error. This error cannot be estimated, since no exact solutions to the same problem have been obtained. Further, the pressure gradient in the direction normal to the body cannot be neglected, and the derived solutions are not correct. They serve to demonstrate, however, that, as the Prandtl Number is reduced from 1.0 to 0.7, the skin friction does not change at large Mach Numbers if the pressure is taken constant across the boundary layer.

Part II—Solutions of the Integral Equations

The exact solutions presented in the previous section show that a considerable amount of mathematical and numerical work is necessary to solve the laminar boundary-layer equations. Yet the flows dealt with a special type of free-stream velocity variation. Particularly, the problem of flow about an arbitrary body cannot be solved exactly. When the free-stream velocity varies arbitrarily, the von Kármán-Pohlhausen integral equations are used generally to yield an approximate answer to the problem. Several solutions based upon the integral methods have been proposed in the past and are briefly reviewed in Table 2. The solutions to be obtained in this section are listed for comparison purposes. While two of the flows considered have been analyzed already,[24, 26] the present methods will yield different answers from those proposed by the other authors for all cases specified in Table 2.

Basic Equations

The method of solution starts from the integral momentum equation

$$2u_1\rho_1\theta\frac{du_1}{dx} + u_1^2\frac{d}{dx}(\rho_1\theta) + \rho_1 u_1\,\delta^*\frac{du_1}{dx} = \left(\mu\frac{\partial u}{\partial y}\right)_{y=0} \tag{36}$$

together with the boundary condition at the wall

$$\left[\frac{\partial}{\partial y}\left(\mu\frac{\partial u}{\partial y}\right)\right]_{y=0} = -\rho_1 u_1\frac{du_1}{dx} \tag{37}$$

and with the definitions

TABLE 2 - SOLUTIONS OF THE INTEGRAL EQUATIONS

Investigator	Equation Solved	Mach Number	Property Variation	Prandtl Number	Thermal Condition at Wall	Additional Assumptions
Pohlhausen[17]	Momentum	$M_1 = 0$	Constant	Any constant	Variable	Polynomial Profiles
Kroujiline[18]	Energy	↓	↓	↓	Constant	↓
Gruschwitz[19] Low[21] Weil[20]	Momentum	Variable	$\mu\rho$=constant	1.0	Insulated	
Morduchow[22]	Momentum Energy	↓	↓	↓	Constant Temperature	Ratio of hydrodynamical to thermal boundary layer is constant
Eckert[8]	↓	$M_1 = 0$	↓	↓	↓	One-Parameter Profiles
Seban[23]	↓	↓	↓	↓	Variable	↓
Levy-Seban[14]	↓	↓	$\mu\rho$=constant	0.7, 1.0	Constant Temperature	↓
Eckert-Livingood[24]	↓	↓	Variable	0.7	↓	↓
Present Solutions	↓	↓	$\mu\rho$=constant	0.7, 1.0	↓	↓
Rott[25] Rott-Crabtree[26]	Momentum	Variable	↓	0.7 1.0	Insulated	↓
Present Solutions	Momentum	↓	↓	1.0	Insulated	↓
Present Solutions	Momentum Energy	↓	↓	↓	Constant Temperature	↓
Present Solutions	↓	$M_1 > 5$	↓	Any constant	Constant Temperature & Insulated	↓

$$\delta^* = \int_0^\infty \left(1 - \frac{\rho}{\rho_1}\frac{u}{u_1}\right) dy \tag{38}$$

$$\theta = \int_0^\infty \frac{\rho}{\rho_1}\frac{u}{u_1}\left(1 - \frac{u}{u_1}\right) dy \tag{39}$$

If one chooses to determine the momentum thickness θ in terms of x, Eq. (36) becomes a first-order differential equation for the unknown variable θ. Solutions to this differential equation are based upon the simplifying assumption that the velocity and temperature profiles about an arbitrary body belong to a one-parameter family of profiles

$$T_s/T_{s_1} = g(\eta, \beta), \quad u/u_1 = f'(\eta, \beta) \tag{40}$$

where the proper free-stream velocity u_1 and the proper equivalent value of s have been substituted in the definition of η. The functions f' and g are also dependent upon the specified thermal condition at the wall.

Introduction of Eq. (40) into Eqs. (36) to (39) yields

$$\beta z_i^2 = \frac{\theta^2\rho_1}{\mu_1}\left(1 + \frac{\gamma - 1}{2} M_1^2\right)\frac{du_1}{dx} \tag{41}$$

$$u_1 \frac{d}{dx}\left(\frac{\theta^2\rho_1}{\mu_1}\right) = F(\beta z_i^2) + 2\beta z_i^2 \frac{[(\gamma - 1)/2]M_1^2}{1 + [(\gamma - 1)/2]M_1^2} \tag{42}$$

where for

$$\xi = \int_0^\infty (1 - f')d\eta \text{ and } \zeta = \int_0^\infty (1 - g)d\eta$$

$$F(\beta z_i^2) = 2\left[f''(0)z_i - \beta z_i^2\left(2 + \frac{\xi - \zeta}{z_i}\right)\right]$$

Equations (41) and (42), together with the known distribution of M_1 and the prescribed thermal condition at the wall, determine the development of θ in terms of x. Estimates of $\theta^2\rho_1/\mu_1$ yield of βz_i^2 from Eq. (41) and thus determine $(d/dx)\ (\theta^2\rho_1/\mu_1)$ from Eq. (42).

The local values of the skin friction and heat-transfer coefficient are obtained from the computed values of the momentum thickness θ. From Eqs. (25) and (26) there results, for $2s = \theta^2\rho_1{}^2u_1{}^2/z_i^2$,

$$\tau_w/(1/2)\rho_w u_1{}^2 = 2f''(0)z_i/(u_1\theta\rho_1/\mu_1) \tag{43}$$

$$h = k_1\,[g'(0)z_i/\theta K] \tag{44}$$

where $h = q_w/(T_w - T_{s_1})$.

The numerical solutions are considerably simplified when Eqs. (41), (42), (43), and (44) are written in nondimensional form. These are

$$\beta z_i^2 = \frac{\tilde\theta^2}{\tilde\nu_1}\left(1 + \frac{\gamma - 1}{2} M_1^2\right)\frac{d}{d\tilde x}{}_1 \tag{45}$$

$$\tilde u_1 \frac{d}{d\tilde x}\left(\frac{\tilde\theta^2}{\tilde\nu_1}\right) = F(\beta z_i^2) + 2\beta z_i^2 \frac{[(\gamma - 1)/2]M_1^2}{1 + [(\gamma - 1)/2]M_1^2} \tag{46}$$

$$\frac{\tau_w}{(1/2)\rho_1 u_1{}^2}\sqrt{\frac{u_a D}{\nu_a}} = \frac{2f''(0)z_i}{\tilde u_1\tilde\theta/\tilde\nu_1} \tag{47}$$

$$\frac{hD}{k_1}\sqrt{\frac{\nu_a}{u_a D}} = \frac{g'(0)z_i}{\tilde\theta K} \tag{48}$$

where the nondimensional quantities are defined as follows:

$$u_1 = u_1/u_a, \qquad \tilde\nu_1 = \nu_1/\nu_a$$

$$\tilde\theta = \frac{\theta}{D}\sqrt{\frac{u_a D}{\nu_a}}, \qquad \tilde x = x/D$$

Here D is some significant dimension of the body and the subscript a refers to conditions at an arbitrarily selected point.

The system of Eqs. (45) to (48) determines all the important characteristics of the flow about an arbitrary body for a specified initial condition of $\tilde\theta$. The initial value of $\tilde\theta$ is obtained from a limiting process at the stagnation point for $\tilde x \to 0$. For a small region near the stagnation point, the free-stream velocity is proportional to the distance $\tilde x$ and the momentum thickness $\tilde\theta$ is obtained for $\tilde x$ approaching zero from the expression $2s = \theta^2\rho_1{}^2u_1{}^2/z_i^2$

$$\tilde\theta = z_i/\sqrt{(du_1/d\tilde x)_{\tilde x = 0}} \tag{49}$$

The system of Eqs. (45) to (48) is reduced further if $F(\beta z_i^2)$ is a linear function of βz_i^2

$$F(\beta z_i^2) = -m\beta z_i^2 - n$$

and there results

$$\frac{\tilde\theta^2}{\tilde\nu_1} = n\,\frac{\{1 + [(\gamma - 1)/2]M_1^2\}^{(2-m)/2}}{\tilde u_1{}^m} \times \int_0^{\tilde x} \tilde u_1{}^{m-1}\left(1 + \frac{\gamma - 1}{2}M_1^2\right)^{(m-2)/2} d\tilde x \tag{50}$$

where the constants vary with the particular type of flow considered and with the prescribed thermal condition at the wall.

The functions $f''(0)$, $g'(0)$, and $F(\beta z_i^2)$, which are essential to the solution of the problem, vary with the specific type of flow considered. On the other hand, Eq. (45) shows that the form parameter βz_i^2 is defined from the same equation for all the flows. Specific flow cases will be considered now.

Incompressible Flow

For this particular case the free-stream Mach Number M_1 is equal to 0, $z^* = \xi$, and $\tilde\nu_1 = 1$. The solution has been indicated by Seban[23] and can be written

$$\tilde\theta^2 = n\ {}_1{}^{-m}\int_0^{\tilde x} \tilde u_1{}^{m-1}\,d\tilde x$$

where

$n = 0.45$,	$m = 5.12$,	$0 < \beta z_i^2 < 0.09$
$n = 0.45$,	$m = 5.32$,	$-0.06 < \beta z_i^2 < 0$

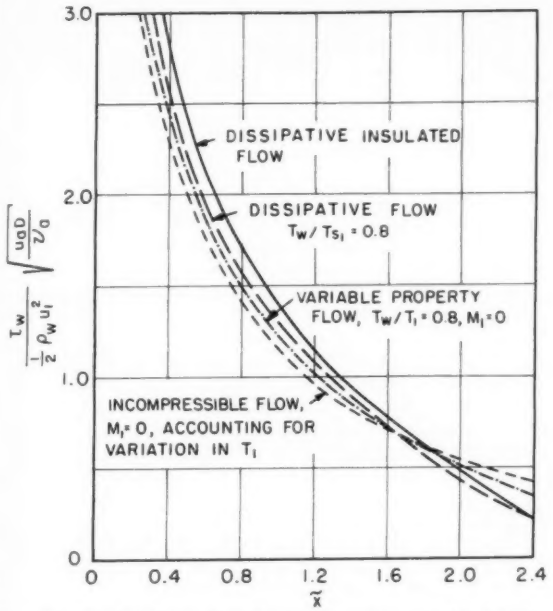
DISSIPATIVE INSULATED FLOW
DISSIPATIVE FLOW
$T_w/T_{s_1} = 0.8$
VARIABLE PROPERTY FLOW, $T_w/T_1 = 0.8$, $M_1 = 0$
INCOMPRESSIBLE FLOW, $M_1 = 0$, ACCOUNTING FOR VARIATION IN T_1
$\sqrt{\frac{u_0 D}{2\nu_0}} \frac{\tau_w}{\frac{1}{2}\rho_w u_1^2}$
$\tilde{x}$

FIG. 17. Dissipation and cooling effects upon the skin friction for flow over an arbitrary body with $\sigma = 1.0$.

The function $f''(0)$, $g'(0)$, and Z_i, which are necessary for the computation of the skin friction and heat transfer, are given in reference 23 for a Prandtl Number of 0.7, typical of air.

Nondissipative Flow with Variable Properties

Here again, $M_1 = 0$ and $z^* = \xi$. The momentum thickness $\tilde{\theta}$ is obtained from the simultaneous solution of the equations

$$\beta z_i^2 = (\tilde{\theta}^2/\tilde{\nu}_1)\,(d\tilde{u}_1/d\tilde{x})$$

$$\tilde{u}_1 \frac{d}{d\tilde{x}}\left(\frac{\tilde{\theta}^2}{\tilde{\nu}_1}\right) = F(\beta z_i^2)$$

The functions $F(\beta z_i^2)$ and z_i are plotted versus the form parameter βz_i^2 in Fig. 14 for various values of the ratio T_w/T_1 and for a Prandtl Number of 0.7. The gradients at the wall which determine the skin friction and heat transfer are given in Figs. 9 and 10. The linearity of the function $F(\beta z_i^2)$ is noted for specific cases only. These are:

	T_w/T_1	0.6	0.8	1.0
$0 < \beta z_i^2 < 0.011$		$m = 3.79$	$m = 4.28$	$m = 5.12$
$-0.04 < \beta z_i^2 < 0$		$m = 4.45$	$m = 5.10$	$m = 5.32$

with $n = 0.45$. The momentum thickness $\tilde{\theta}$ is

$$\frac{\tilde{\theta}^2}{\tilde{\nu}_1} = n\tilde{u}_1^{-m} \int_0^{\tilde{x}} \tilde{u}_1^{m-1}\, d\tilde{x}$$

Dissipative Flow with a Prandtl Number of 1

When the wall is insulated $g = 1$ and

$$z^* = \frac{\gamma - 1}{2} M_1^2 + \left(1 + \frac{\gamma - 1}{2} M_1^2\right) \xi$$

and the problem reduces to the corresponding incompressible one. The functions $f''(0)$ and z_i are given in reference 23. The momentum thickness is obtained from

$$\frac{\tilde{\theta}^2}{\tilde{\nu}_1} = n \frac{\{1 + [(\gamma - 1)/2] M_1^2\}^{(2-m)/2}}{\tilde{u}_1^m} \times \int_0^{\tilde{x}} \tilde{u}_1^{m-1} \left(1 + \frac{\gamma - 1}{2} M_1^2\right)^{(m-2)/2} d\tilde{x}$$

where m and n are the constants specified in the section for incompressible flow. The form parameter is

$$\beta z_i^2 = \frac{\tilde{\theta}^2}{\tilde{\nu}_1}\left(1 + \frac{\gamma - 1}{2} M_1^2\right) \frac{d\tilde{u}_1}{d\tilde{x}}$$

The derived equations are different from the solutions proposed by Rott and Crabtree[26] for the same type of flow—namely,

$$\tilde{\theta}^2 = 0.45\, \tilde{\nu}_{s_1} \left(1 + \frac{\gamma - 1}{2} M_1^2\right)^3 \tilde{u}_1^{-6} \times \int_0^{\tilde{x}} \tilde{u}_1^5 \left(1 + \frac{\gamma - 1}{2} M_1^2\right)^{-1.5} d\tilde{x}$$

When the wall is not insulated, the characteristics of the flow are determined by Eqs. (45) to (48). The functions $F(\beta z_i^2)$ and z_i are shown in Fig. 15. The gradients at the wall are obtained from Figs. 9 and 10. As evaluated from Fig. 15, the constants m and n appearing in Eq. (50) are, for $\beta z_i^2 > 0$:

T_w/T_{s_1}	0.8	1.0
m	4.20	5.12
n	0.45	0.45

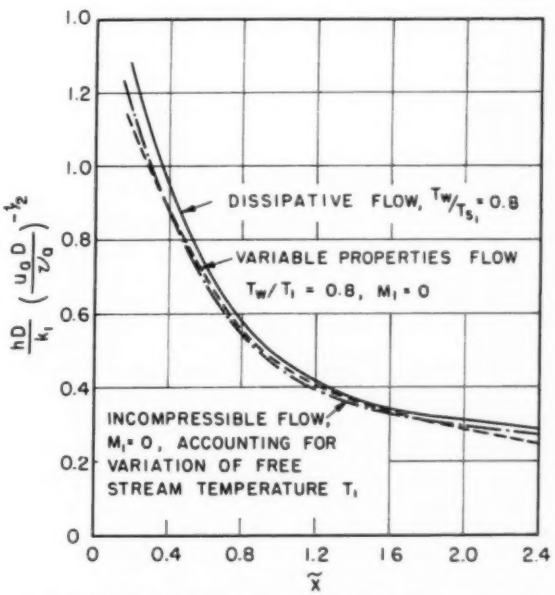
DISSIPATIVE FLOW, $T_w/T_{s_1} = 0.8$
VARIABLE PROPERTIES FLOW
$T_w/T_1 = 0.8$, $M_1 = 0$
INCOMPRESSIBLE FLOW, $M_1 = 0$, ACCOUNTING FOR VARIATION OF FREE STREAM TEMPERATURE T_1
$\frac{hD}{k_1}\left(\frac{u_0 D}{2\nu_0}\right)^{-\frac{1}{2}}$
$\tilde{x}$

FIG. 18. Dissipation and cooling effects upon the heat transfer for flow over an arbitrary body with $\sigma = 1.0$.

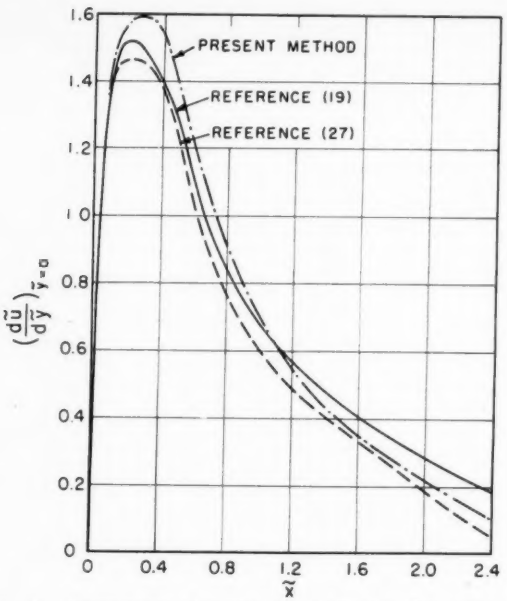

FIG. 19. Comparison of results for dissipative flow over an insulated arbitrary body with $\sigma = 1.0$.

High Mach Number Flow with a Prandtl Number of 0.7

In the first part of this work, a limited number of results were presented for the case of dissipative flow with free-stream Mach Number values greater than 5. The gradients at the wall can be evaluated for any specific condition from Eqs. (34) and (35), and, in turn, these specify the velocity and temperature profiles.[14] The functions $F(\beta z_i^2)$ and z_i can be computed then according to the method of reference 14. The solutions are defined here by the equations

$$\beta z_i^2 = \frac{\tilde{\theta}^2}{\tilde{\nu}_1}\left(1 + \frac{\gamma - 1}{2} M_1^2\right)\frac{d\tilde{u}_1}{d\tilde{x}}$$

$$\tilde{u}_1 \frac{d}{d\tilde{x}}\left(\frac{\tilde{\theta}^2}{\tilde{\nu}_1}\right) = F(\beta z_i^2) + 2\beta z_i^2$$

since for large Mach Number

$$\frac{\gamma - 1}{2} M_1^2 \Big/ \left(1 + \frac{\gamma - 1}{2} M_1^2\right)$$

is equal to 1.

Applications of the Method of Solution

The effects of dissipation and variation of properties upon the skin friction and heat-transfer coefficient can be demonstrated best by a numerical example. All the calculations presented here were carried out for the body specified in reference 19. The free-stream velocity and the conditions at the point a are taken as follows:

$$\tilde{u}_1 = \tilde{x}(\tilde{x} + 5)/(\tilde{x} + 1)^2$$
$$u_a = 304 \text{ m. per sec.} = 997.4 \text{ ft. per sec.}$$
$$T_a = 241.5°\text{K.} = 460°\text{R.}$$

The point a is chosen in the undisturbed flow upstream of the body, and isentropic flow may be assumed to exist between the reference point a and the free stream. Thus

$$\rho_a/\rho_1 = (T_1/T_a)^{2.5}$$

The velocity and Mach Number distribution in the free stream are shown in Fig. 16. Calculations were carried out for the following cases:

Incompressible flow, constant wall temperature, $\sigma = 1$
Nondissipative flow, $T_w/T_1 = 0.8$, $\sigma = 1$
Dissipative flow, $T_w/T_{s_1} = 0.8$, $\sigma = 1$
Dissipative flow, insulated surface, $\sigma = 1$

The results of the computation are shown in Figs. 17, 18, and 19. Figs. 17 and 18 show the effects of dissipation and variation of properties.

Fig. 19 is a comparison of the present results with those of references 19 and 27. Examination of Figs. 17, 18, and 19 reveals the following facts:

Addition of the dissipation term to the energy equation decreases the value of the momentum thickness $\tilde{\theta}$. It increases the form parameter βz_i^2 for an accelerating flow and decreases βz_i^2 for a decelerating flow. These two effects combine to increase the skin friction for a positive gradient of the free-stream velocity and compensate for each other for a negative gradient of the free-stream velocity. The calculations show that the separation point moves closer to the forward stagnation point.

Cooling reduces the skin friction and delays separation. The heat transfer is not affected. For an insulated surface, agreement within 10 per cent of the present method with those of references 19 and 27 is observed.

The incompressible solutions obtained for a value of $\tilde{\nu}_1$ equal to 1 do not agree with the other results. Good agreement is obtained if one uses the relation

$$\frac{\tilde{\theta}^2}{\tilde{\nu}_1} = n\tilde{u}_1{}^{-m}\int_0^{\tilde{x}} \tilde{u}_1{}^{m-1}\, d\tilde{x}$$

with $\tilde{\nu}_1$ evaluated from the local free-stream conditions. This agreement may be fortuitous because of the flatness of the velocity curve and also because the amount of cooling considered in the numerical example was small.

REFERENCES

[1] Chapman, D. R., and Rubesin, M. W., *Temperature and Velocity Profiles in the Compressible Laminar Boundary Layer with Arbitrary Distribution of Surface Temperature*, Journal of the Aeronautical Sciences, Vol. 16, No. 9, p. 547, September, 1949.

[2] Crocco, L., *The Laminar Boundary-Layer in Gases* (Translation), APL/NAA/CF-1038, 1948.

[3] Brown, W. B., and Donoughe, P. L., *Tables of Exact Laminar Boundary-Layer Solutions When the Wall is Porous and Fluid Properties are Variable*, NACA TN No. 2479, 1951.

[4] Brown, W. B., and Livingood, J. N. B., *Solutions of Laminar Boundary-Layer Equations which result in Specific-Weight-Flow Profiles Locally Exceeding Free Stream Values*, NACA TN No. 2800, 1952.

[5] Illingworth, C. R., *Steady Flow in the Laminar Boundary-Layer of a Gas*, Proc. Royal Society of London, Vol. 199, 1949.

[6] Krzywoblocki, M. Z., *On the Fundamentals of the Boundary-Layer Theory*, Journal of the Franklin Institute, April, 1953.

[7] Hartree, D. R., *On an Equation Occurring in Falkner and Skan's Approximate Treatment of the Equations of the Boundary-Layer*, Proc. Cambridge Philosophical Society, Vol. 33, 1937.

[8] Eckert, E., *The Computation of the Heat Transfer in the Laminar Boundary-Layer of Bodies in Flow*, V.D.I. Forschungsheft No. 416, Berlin, 1942.

[9] Schuh, H., *Laminar Heat Transfer in Boundary-Layers at High Velocities*, R. & T. 810, British M.A.P., April, 1947.

[10] Levy, S., *Heat Transfer to Constant-Property Laminar Boundary-Layer Flows with Power-Function Free Stream Velocity and Wall-Temperature Variation*, Journal of the Aeronautical Sciences, Vol. 19, No. 5, p. 341, May, 1952.

[11] Tifford, A. N., and Chu, S. T., *Heat Transfer in Laminar Boundary-Layer Subject to Surface Pressure and Temperature Distribution*, Proc. of the Second Midwestern Conference on Fluid Mechanics, 1952.

[12] Eckert, E., and Drewitz, O., *Calculation of the Temperature Field in the Laminar Boundary-Layer of an Unheated Body in a High Speed Flow*, R.T.P. Trans. No. 1594, M.A.P.

[13] Stewartson, K., *Correlated Incompressible and Compressible Boundary-Layers*, Proc. Royal Society of London, Vol. 200, 1949.

[14] Levy, S., and Seban, R. A., *Skin Friction and Heat Transfer for Laminar Boundary-Layer Flow with Variable Properties and Variable Free Stream Velocity*, Paper 53-SA-3, ASME, 1953.

[15] Levy, S., and Seban, R. A., *Recovery Factors for the Laminar Boundary-Layer Separation and Stagnation Flows*, Readers' Forum, Journal of the Aeronautical Sciences, Vol. 19, No. 5, p. 355, May 1952.

[16] Ringleb, F. O., *Computation of the Laminar Boundary-Layer with Suction*, Journal of the Aeronautical Sciences, Vol. 19, No. 1, p. 48, January, 1952.

[17] Pohlhausen, K., Z. angew Math. Mech., Vol. 1, 1921.

[18] Kroujiline, G., *Transmission of Heat Past a Circular Cylinder in a Transverse Current of Fluid*, Sci. Abstract, Sec. A—Physics, Vol. 34, No. 4267, 1936.

[19] Gruschwitz, E., *Calcul Approche de la Couche Limite Laminaire en Ecoulement Compressible sur une Paroi Non Conductrice de la Chaleur*, Office National d'Etudes et de Recherches Aeronautiques, Publication No. 47, 1950.

[20] Weil, H., *Effects of Pressure Gradient on Stability and Skin Friction in Laminar Boundary-Layers in Compressible Fluids*, Journal of the Aeronautical Sciences, Vol. 18, No. 5, p. 311, May, 1951.

[21] Low, G. M., *Simplified Method for Calculation of Compressible Laminar Boundary-Layer with Arbitrary Free Stream Pressure Gradient*, NACA TN 2351, 1951.

[22] Morduchow, M., *On Heat Transfer over a Sweat-Cooled Surface in Laminar Compressible Flow with a Pressure Gradient*, Journal of the Aeronautical Sciences, Vol. 19, No. 10, p. 705, October, 1952.

[23] Seban, R. A., *Calculation Method for Two-Dimensional Laminar Boundary-Layers with Arbitrary Free Stream Velocity Variation and Arbitrary Wall Temperature Variation*, Report "2-12, University of California, 1950.

[24] Eckert, E. R. G., and Livingood, J. N. B., *Method for Calculation of Heat Transfer in Laminar Region of Air Flow Around Cylinders of Arbitrary Cross Section (Including Large Temperature Differences and Transpiration Cooling)*, NACA TN No. 2733, 1952.

[25] Rott, N., *Compressible Boundary-Layer on a Heat-Insulated Body*, Readers' Forum, Journal of the Aeronautical Sciences, Vol. 20, No. 1, p. 67, January, 1953.

[26] Rott, N., and Crabtree, L. F., *Simplified Laminar Boundary-Layer Calculations for Bodies of Revolution and for Yawed Wings*, Journal of the Aeronautical Sciences, Vol. 19, No. 8, p. 533, August, 1952.

[27] Flugge-Lotz, I., and Eichelbrenner, E. A., *La Couche Limite Laminaire dans l'Ecoulement Compressible le long d'une Surface Courbe*, Office National d'Etudes et de Recherches Aeronautiques, Rapport 1/694, 1948.

Appendix (A)—Differential Analyzer Solutions

Eq. (14) is a third-order differential equation, and Eq. (16) is of the second order. The simultaneous solution to these equations involves a total of five integrations on the differential analyzer. The method of solution consists of assuming the values $f''(0)$ and $g'(0)$ and proceeding to generate the functions f and g. The values of $f''(0)$ and $g'(0)$ are found by trial and error. Different sets of values are assumed until one is found for which the boundary conditions at infinity are satisfied—namely, $f' \to 1$ and $g \to 1$.

For each set of starting values, the functions f', f, and g were recorded graphically, and inspection of these figures enabled the operator to decide whether or not the assumed values of $f''(0)$ and $g'(0)$ were satisfactory.

The differential analyzer used was of the mechanical type with an estimated accuracy of 1 per cent per integration. The error of the solutions presented here is not expected to exceed 5 per cent for the five integrations leading to the results. In all cases the values of $f''(0)$ and $g'(0)$ were determined within three significant figures, and the error in these two quantities is not expected to exceed a fraction of 1 per cent. For incompressible flow the present values of $f''(0)$ and $g'(0)$ were within 0.5 per cent of the exact solutions.[7, 8] Even though the gradients at the wall are defined accurately, the uncertainty in the velocity profile remains large as $\eta \to \infty$ if the ratio T_w/T_{e_1} exceeds 1.5. For large values of T_w/T_{e_1}, the velocity profile is sensitive to the initial assumptions of $f''(0)$ and $g'(0)$, which makes the determination of the solution more difficult. Fig. 20 presents a typical case. A minor change in the value of $g'(0)$ changes the velocity profile, and calcu-

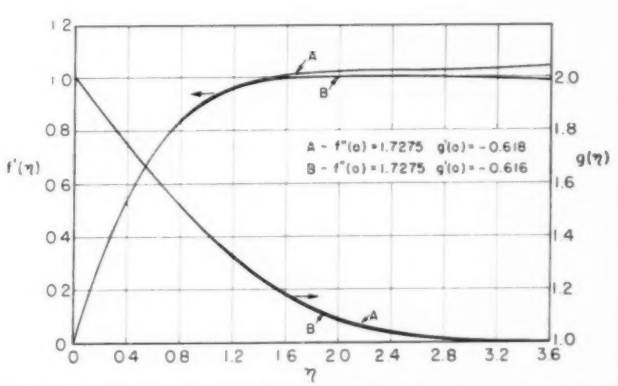

Fig. 20. Velocity and temperature profile for $\beta = 1.0$, $\sigma = 1.0$, and $g(0) = 2.0$.

lations beyond the cases A and B shown in the figure were not carried out because they would exceed the accuracy of the differential analyzer. Instead, asymptotic solutions were used to compute the velocity and temperature profile at large values of η. The solutions A and B coincide from $\eta = 0$ to $\eta = 0.8$, and the rest of the solutions can be determined from the asymptotic equations for $\eta > 0.8$.

Asymptotic solutions were utilized for T_w/T_{s_1} equal to 2. For these cases, the function f' approaches 1 from above, which means that a reversal occurs in the normal gradient of the velocity within the boundary layer. Such a solution was obtained by Hartree[7] for the incompressible case with $\beta < 0$, but it was abandoned in favor of another possible solution for which the velocity gradient does not become negative. It is possible that there exists another solution of the system of Eqs. (14) and (16) for which the velocity gradient does not become negative for large values of $g(0)$. No attempt was made to find whether this solution exists because it would mean that a discontinuity occurs in the values of $f''(0)$ in terms of $g(0)$ for a constant β value.

Strength Under Combined Tension and Bending in the Plastic Range

(*Continued from page 453*)

It is of interest to record that the flexural rigidity, which reduces to EI under purely elastic coditions, is given by

$$\frac{M}{(1/R_0) - (1/R)} = \frac{1}{\kappa}\frac{M}{M_Y}EI \qquad (24)$$

Concluding Remarks

The results that have been presented have been specialized to the case of the rectangular section. Applications of the method to other compact symmetrical shapes can be made in a similar manner. For example, interaction charts have been calculated for heavy-wall round tubing. They differ little from the curves for an equivalent rectangle of the same area and section modulus. It would appear that the charts for the rectangle afford a useful approximation to the behavior of other symmetrical sections of compact type.

The problem of fitting design has become more important, as well as more difficult, with the present trend of air-frame design. Studies of the type reported here have proved useful in this field. More analytical work and experimental verification, however, are needed to amplify the somewhat specialized results presented in this paper.

References

[1] Cozzone, Frank P., *Bending Strength in the Plastic Range*, Journal of the Aeronautical Sciences, Vol. 10, No. 5, p. 137, May, 1943.

[2] Osgood, William R., *Plastic Bending*, Journal of the Aeronautical Sciences, Vol. 11, No. 3, p. 213, July, 1944.

[3] Rappleyea, F. A., and Eastman, E. J., *Flexural Strength in the Plastic Range of Rectangular Magnesium Extrusions*, Journal of the Aeronautical Sciences, Vol. 11, No. 4, p. 373, October, 1944.

[4] Brush, D. O., Sidebottom, O. M., and Smith, J. O., *Plastic Behavior of Engineering Materials, Part I, Axial Tension and Bending Interaction Curves for Members Loaded Inelastically*, Wright Air Development Center Technical Report 52-89, Part 1, August, 1952.

[5] Barrett, A. J., *The Bending of Some Common Beam Sections Into the Plastic Range*, Journal of The Royal Aeronautical Society, p. 110, February, 1953.

[6] Ramberg, Walter, and Osgood, William R., NACA TN No. 902, July, 1953.

[7] Westergaard, H. M., and Osgood, W. R., *Strength of Steel Columns*, Transactions, American Society of Mechanical Engineers, Vols. 49 and 50, APM-50-9, p. 65, 1928.

Analysis of Flutter in Compressible Flow of a Panel on Many Supports

JOHN M. HEDGEPETH,* BERNARD BUDIANSKY,† AND ROBERT W. LEONARD‡
Langley Aeronautical Laboratory, NACA

ABSTRACT

Two-dimensional linearized compressible flow theory is used, together with elementary beam theory, to analyze the dynamic stability of an infinitely long panel on equally spaced supports, having an air stream of arbitrary speed on one side and dead air on the other. It is assumed that the flutter mode has a spatial periodicity of two bays. Longitudinal stresses in the panel are taken into account.

An exact solution for the condition of neutral stability yields two independent equations in the form of rapidly converging infinite series. The results of some numerical calculations made on the basis of the first few terms of one of the series are shown, and states of stability and instability on either side of a flutter boundary are carefully distinguished. The implications of the numerical results are discussed.

INTRODUCTION

THE POSSIBILITY OF FLUTTER of thin-sheet panels on the surface of supersonic aircraft or missiles is currently of concern. The provision of adequate stiffness to prevent such flutter may indeed be a controlling design factor, particularly for lightly loaded parts of the structure where extremely thin skins satisfy static strength requirements.

Theoretical investigations, with somewhat puzzling results, have recently been performed in an attempt to provide rational criteria for the prevention of panel flutter. Miles[1] used two-dimensional, quasi-steady, linearized supersonic flow theory to analyze the dynamic stability of a two-dimensional, simply supported plate (i.e., a beam); his work, however, leads to the unhappy conclusion that all plates will flutter at supersonic Mach Numbers below $M = \sqrt{2}$. This anomaly was only partially removed by Shen,[2] who analyzed the same structure on the basis of unsteady linearized supersonic flow theory; while Shen discovered the existence of stable configurations at $M = \sqrt{2}$, his results show stability for only a finite range of plate stiffnesses, with flutter occurring for stiffnesses above, as well as below, this range.

In the present paper, the problem of panel flutter is re-examined on the same theoretical basis used by Shen, but for a different structure—namely, an infinitely long panel (beam) on equally spaced intermediate supports, having an air stream of arbitrary speed on one side and dead air on the other (Fig. 1). The motivation for the present investigation is twofold: first, the model studied bears closer geometrical similarity to an array of panels on actual aircraft surfaces than does a single isolated panel; and, second, the analysis leads to a relatively simple exact solution, the numerical predictions of which for a wide range of Mach Numbers may afford insight into the peculiarities that seem to be inherent in the problem of panel flutter.

SYMBOLS

D	= plate stiffness, $Et^3/12(1-\mu^2)$
E	= Young's modulus
F_0, F_1	= reaction forces at the supports
M	= Mach Number
M_1	= Mach Number for stationary wavy wall
P_{cr}	= buckling load per unit width, $\pi^2 D/a^2$
R	= ratio of tension load to buckling load
T	= middle plane tension per unit width
U	= velocity of airflow over the upper surface of the panel
a	= distance between adjacent supports
a_n	= complex amplitude of the nth term of the Fourier expansion for the deflection
c	= velocity of sound in air
$f(\xi, n)$	= function contained in the air force coefficients
f_0, f_1	= complex amplitudes of the reaction forces
g	= damping coefficient, ratio of viscous bending moment to elastic bending moment at ω_1
i	= $\sqrt{-1}$
k	= reduced flutter frequency, $\omega a/\pi c$
k_1	= reduced first natural frequency, $\omega_1 a/\pi c$
$l(x, \tau)$	= lift force per unit length of the panel
m, n	= integers
Δp_u, Δp_l	= pressure perturbations on upper and lower surfaces, respectively, of the panel
t	= panel thickness
w	= panel deflection
x, y	= rectangular coordinates (see Fig. 1)
x_1	= longitudinal coordinate for stationary wavy wall
z	= complex variable
β_n	= quantity defined after Eq. (10)
γ	= density of plate material
$\delta(x)$	= Dirac delta function; $\delta(x) = 0$ for $x \neq 0$, $\int_{-\infty}^{\infty} \delta(x)\,dx = 1$
ϵ	= mass ratio parameter, $\rho a/\pi\gamma t$
λ	= $\sqrt{\lvert M_1^2 - 1\rvert}$
μ	= Poisson's ratio
ρ	= air density
τ	= time
$\varphi(x_1, y)$	= perturbation velocity potential
χ_n	= air force coefficients
ω	= circular flutter frequency

Presented at the Aeroelasticity Session, Twenty-Second Annual Meeting, IAS, New York, January 25–29, 1954.

* Head, Dynamics and Aeroelasticity Section.
† Head, Structural Mechanics Branch.
‡ Aeronautical Research Scientist.

ω_1 = first natural circular frequency of the panel, $(\pi^2/a^2)\sqrt{D/\gamma t}$

Statement of the Problem

The configuration under consideration consists of an infinitely long, uniform plate, simply supported at equal intervals, with air flowing over the top and dead air below (Fig. 1). The plate is subjected to a middle-plane force in the longitudinal direction which is assumed to remain independent of the deflection. The problem is considered to be two dimensional, all quantities being constant in the direction perpendicular to the x-y plane, and the fluid is assumed to extend to infinity both above and below the plate. When the plate is stationary and undeflected, the pressure of the air below the plate is taken equal to the free-stream static pressure of the air above, so that there is no pressure differential across the plate. In the ensuing analysis, elementary beam theory is assumed to apply to the plate, and the behavior of the air both above and below the plate is described on the basis of unsteady linearized compressible flow theory.

The term "flutter," when used in a mathematical sense, generally refers to a steady, self-excited harmonic oscillation that can exist only for certain critical combinations of the pertinent physical and geometrical parameters. In the next section, an equation defining these critical combinations—the so-called "flutter equation"—is derived for the present problem. It is to be emphasized, however, that the identification of the flutter states does not settle the question of whether or not a given plate in a given air stream is unstable. First of all, the existence of a steady harmonic mode of oscillation does not by any means preclude the simultaneous existence of a different unstable mode of oscillation. Second, even if it can be shown that such an unstable mode does not coexist with a given flutter mode, it is still necessary to know whether this neutrally stable flutter mode becomes stable or unstable when the parameters of the problem are varied away from their critical values. These questions will be examined in detail after the flutter equation is derived and some of its numerical consequences are explored.

Derivation of the Flutter Equation

An oscillation of neutral stability (flutter) is specified by assuming a steady harmonic vertical motion for each point of the plate, with the various points not necessarily in phase with one another. In addition, it will be assumed that the motion has a spatial periodicity in the x-direction of two bay lengths. Then, the deflection $w(x, \tau)$ of the plate can be written with complete generality as

$$w(x, \tau) = Re\left[\left(\sum_{n=-\infty}^{\infty} a_n e^{in\pi x/a}\right) e^{i\omega\tau}\right] \qquad (1)$$

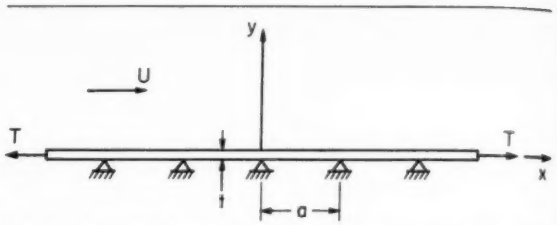

FIG. 1. Infinitely long, two-dimensional panel with flow above and dead air below.

where the Fourier coefficients a_n are complex numbers and ω is the (real) flutter frequency.

Since the individual terms of the Fourier series do not satisfy the condition of zero deflection at the supports, it is necessary that the Fourier coefficients satisfy the constraining relationships

$$\sum_{n=-\infty}^{\infty} a_n = \sum_{n=-\infty}^{\infty} (-1)^n a_n = 0 \qquad (2)$$

These relationships will be introduced in the process of satisfying the condition of equilibrium of the plate.

Derivation of Aerodynamic Forces

It is convenient at this stage to determine the magnitude of the pressure differential acting on the plate while it executes the motion expressed by Eq. (1), with a flow to the right of velocity U (Mach Number M) above the plate and dead air below. Since linearized flow theory will be used, it is possible to consider separately the pressures arising from the individual terms of Eq. (1), and then superpose them.

A general term of Eq. (1) is

$$Re[a_n e^{in\pi x/a} e^{i\omega\tau}]$$

which, for $n \neq 0$, can be written as

$$Re(a_n e^{in\pi/a[x+(\omega a/n\pi)\tau]})$$

Clearly, this term represents a traveling wave of amplitude $|a_n|$ moving in the *negative* x-direction with the velocity $\omega a/n\pi$.

If we now introduce the substitution $x_1 = x + (\omega a/n\pi)\tau$, the problem of finding the pressures acting on the traveling wave is reduced to the determination of the pressures acting on a *stationary* wavy wall of shape $Re[a_n e^{in\pi x_1/a}]$ having a flow of velocity $U + (\omega a/n\pi)$ above and a flow of velocity $\omega a/n\pi$ below (see Fig. 2).

The Ackeret solution[3] to the wavy wall problem is followed in Appendix (A) in the derivation of results for the pressure perturbation at the *upper* surface of a stationary wavy wall due to a flow of Mach Number M_1. It is found that: for subsonic flow ($M_1 < 1$) to the right *or* left,

$$\Delta p_u = -\frac{\pi\rho c^2}{a} Re\left[|n| \frac{M_1^2}{\sqrt{1 - M_1^2}} a_n e^{in\pi x_1/a}\right] \qquad (3a)$$

for supersonic flow ($M_1 > 1$) to the *right*,

$$\Delta p_u = -\frac{\pi\rho c^2}{a} Re\left[-in\frac{M_1^2}{\sqrt{M_1^2-1}} a_n e^{in\pi x_1/a}\right] \quad (3b)$$

and for supersonic flow ($M_1 > 1$) to the *left*,

$$\Delta p_u = \frac{-\pi\rho c^2}{a} Re\left[in\frac{M_1^2}{\sqrt{M_1^2-1}} a_n e^{in\pi x_1/a}\right] \quad (3c)$$

For the stationary wavy wall of Fig. 2b, the pressures on the upper surface are found from Eqs. (3a)–(3c) with $M_1 = |M + (\omega a/n\pi c)|$; the flow is to the right for $[M + (\omega a/n\pi c)] > 0$ and to the left for $[M + (\omega a/n\pi c)] < 0$.

The pressures *below* a wavy wall due to any flow are clearly the negative of those caused by the same flow *above* the wall. Hence, Δp_l, the pressure perturbation below the equivalent wavy wall of Fig. 2b, is given by Eqs. (3a)–(3c) with the signs changed and with $M_1 = |\omega a/n\pi c|$; the flow is to the right or left for $\omega a/n\pi c$ positive or negative, respectively.

The pressure differential across the wall acting in the upward direction is given by

$$l_n = \Delta p_l - \Delta p_u$$

Summarizing these facts and replacing x_1 by $x + (\omega a/n\pi)\tau$, we find that the aerodynamic lift due to the motion $w = Re[a_n e^{in\pi x/a} e^{i\omega\tau}]$ is given by

$$l_n(x, \tau) = \frac{\pi\rho c^2}{a} Re[\chi_n(M, k) a_n e^{in\pi x/a} e^{i\omega\tau}] \quad (4)$$

where, for $n \neq 0$,

$$\chi_n(M, k) = n\left[f\left(M + \frac{k}{n}, n\right) + f\left(\frac{k}{n}, n\right)\right] \quad (5)$$

with

$$k = \omega a/\pi c$$

and

$$f(\xi, n) = -i\xi^2/\sqrt{\xi^2 - 1} \qquad (\xi > 1)$$

$$= \frac{n}{|n|}\xi^2/\sqrt{1-\xi^2} \qquad (|\xi| < 1)$$

$$= i\xi^2/\sqrt{\xi^2 - 1} \qquad (\xi < -1)$$

Finally, the result for the case $n = 0$ is found by a limiting process to be given by Eq. (4) with

$$\chi_0 = -2ik$$

The total lift due to the assumed motion given by Eq. (1) then becomes, by superposition,

$$l(x, \tau) = \frac{\pi\rho c^2}{a} Re\left[\sum_{n=-\infty}^{\infty} \chi_n a_n e^{in\pi x/a} e^{i\omega\tau}\right] \quad (6)$$

Solution of the Equation of Equilibrium

By virtue of the assumed spatial periodicity of the plate deflection, it suffices to satisfy equilibrium in the interval $(-0, 2a - 0)$. In this range, the equation of equilibrium may be written

$$Dw_{zzzz} - Tw_{zz} + \gamma t w_{\tau\tau} = l(x, \tau) + F_0\delta(x) + F_1\delta(x - a) \quad (7)$$

where $\delta(x)$ is the Dirac delta function and F_0 and F_1 are the reactions at the supports at $x = 0$ and $x = a$, respectively.

Letting

$$F_0 = Re[f_0 e^{i\omega\tau}]$$
$$F_1 = Re[f_1 e^{i\omega\tau}]$$

and substituting Eqs. (1) and (6) into Eq. (7) gives

$$\sum_{n=-\infty}^{\infty}\left[D\left(\frac{n\pi}{a}\right)^4 + T\left(\frac{n\pi}{a}\right)^2 - \gamma t\omega^2 - \frac{\pi\rho c^2}{a} \times \chi_n(M, k)\right] a_n e^{in\pi x/a} = f_0\delta(x) + f_1\delta(x - a) \quad (8)$$

Multiplying Eq. (8) through by $e^{-in\pi x/a}$ and integrating from -0 to $2a - 0$ gives, for all n,

$$\left[D\left(\frac{n\pi}{a}\right)^4 + T\left(\frac{n\pi}{a}\right)^2 - \gamma t\omega^2 - \frac{\pi\rho c^2}{a}\chi_n(M,k)\right]a_n = \frac{f_0 + (-1)^n f_1}{2a} \quad (9)$$

whence

$$a_n = \frac{f_0 + (-1)^n f_1}{(2a)(\gamma t)(\pi c/a)^2\beta_n} \quad (10)$$

for $\beta_n \neq 0$, where

$$\beta_n = (n^4 + n^2 R)k_1^2 - k^2 - \epsilon\chi_n(M, k)$$

with

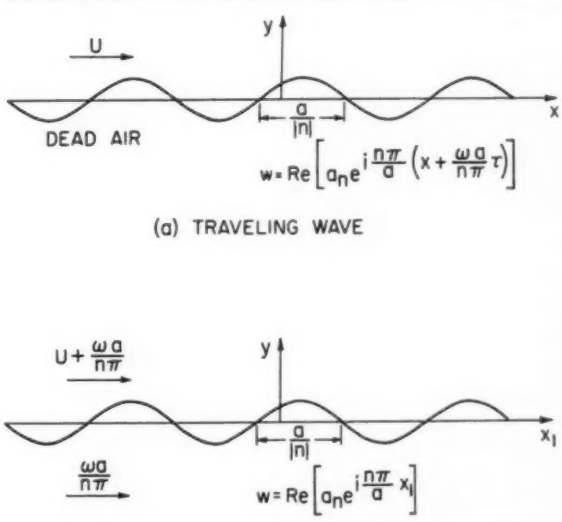

FIG. 2. A traveling wave and its equivalent stationary wavy wall.

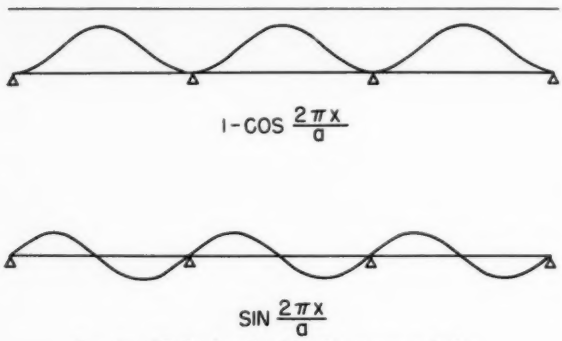

FIG. 3. Modes involved in three-term solution.

$R = T/P_{cr}$ (ratio of tension load to buckling load)
$k = \omega a/\pi c$ (reduced flutter frequency)
$k_1 = \omega_1 a/\pi c$ (reduced first natural frequency)
$\epsilon = \rho a/\pi\gamma t$ (mass ratio parameter)
$M = U/c$ (Mach Number)

Now the restraint condition on the a_n's, Eqs. (2), which may be rewritten

$$\sum_{\substack{n=-\infty \\ (n \text{ even})}}^{\infty} a_n = 0 \tag{11}$$

$$\sum_{\substack{n=-\infty \\ (n \text{ odd})}}^{\infty} a_n = 0 \tag{12}$$

must be satisfied. Substituting Eq. (10) into these conditions gives

$$(f_0 + f_1) \sum_{\substack{n=-\infty \\ (n \text{ even})}}^{\infty} (1/\beta_n) = 0$$

and

$$(f_0 - f_1) \sum_{\substack{n=-\infty \\ (n \text{ odd})}}^{\infty} (1/\beta_n) = 0$$

It can now be seen that the simultaneous satisfaction of the equilibrium equation, Eq. (8), and the constraint conditions, Eqs. (11) and (12), can be achieved in a nontrivial fashion in several independent ways. We can have either

$$\begin{cases} f_0 = f_1 \\ a_n = 0 \quad \text{for } n \text{ odd} \end{cases}$$

$$\sum_{\substack{n=-\infty \\ (n \text{ even})}}^{\infty} 1/\beta_n = 0 \tag{13}$$

or

$$\begin{cases} f_0 = f_1 \\ a_n = 0 \quad \text{for } n \text{ even} \end{cases}$$

$$\sum_{\substack{n=-\infty \\ (n \text{ odd})}}^{\infty} 1/\beta_n = 0 \tag{14}$$

or, conceivably, Eqs. (13) and (14) could hold simultaneously.

Eqs. (13) and (14) are conditions for two independent types of flutter. Examination of the nature of the terms in the Fourier expression for w reveals that Eq. (13) corresponds to a flutter mode that is identical in each bay, whereas Eq. (14) corresponds to a motion that is identical from bay to bay, but with alternating direction.

In the derivation of the above criteria it was assumed that $\beta_n \neq 0$; the implications of vanishing β_n's should be explored. It can be seen from Eq. (9) that (for n even, say) the vanishing of at least one β_n requires that $f_0 = -f_1$; then the only a_n's that can be different from zero are those for which the corresponding β_n's vanish. Consequently, the constraint relation, Eq. (11), as well as Eq. (9), can be satisfied by nonzero a_n's if *two* or more β_n's vanish simultaneously. Similar considerations apply to the satisfaction of Eqs. (9) and (12) by the vanishing of two or more β_n's for n odd.

To summarize, the criterion for flutter is Eq. (13), or Eq. (14), or the simultaneous vanishing of two or more β_n's of the same type (i.e., odd or even).

Discussion of Flutter Equations

The flutter criteria, Eqs. (13) and (14), are complex equations defining critical combinations of the five nondimensional parameters M, k, k_1, ϵ, and R. Consequently, one may expect that, when any three of these parameters are specified, the remaining two may be determined. For a given panel in a given air stream, the parameters k_1, ϵ, and R are known beforehand, and, in principle, it would therefore appear possible to solve for a flutter Mach Number M and flutter frequency k. In practice, however, it is much more convenient to assume values of M, k, and R and solve for k_1 and ϵ, since M and k are included in the equations in a complicated manner as a consequence of the way they appear in the expressions for the aerodynamic forces. Indeed, it appears desirable to survey the entire range of critical combinations of the parameters of the problem, since, as has been mentioned, the establishment of a flutter speed for a given configuration does not constitute a conclusive determination of stability or instability.

An indication of the results of such a survey is found in the next section, wherein numerical calculations are carried out for the modes of flutter corresponding to Eq. (13), with $R = 0$ and with the retention of only three terms of the infinite series.

RESULTS FOR THREE-TERM SOLUTION

If only the terms for $n = -2$, 0, and 2 are retained, Eq. (13) becomes

$$(1/\beta_0) + (1/\beta_2) + (1/\beta_{-2}) = 0 \tag{15}$$

Examination of the Fourier terms corresponding to a_0, a_2, and a_{-2} and consideration of the constraint

condition, Eq. (11), show that the three-term solution involves two degrees of freedom corresponding, effectively, to the two modes of deflection shown in Fig. 3.

Flutter Loci at Various Mach Numbers

Eq. (15) can be solved, with $R = 0$, by finding combinations of ϵ and k_1 which satisfy the equation for various combinations of M and k. At the same time, consideration should be given to the possibility of the existence of flutter modes corresponding to the simultaneous vanishing of two (or all three) of the β_n's. The solutions will be discussed separately for subsonic and supersonic Mach Numbers, since they are of different character for these two régimes.

Subsonic Speeds ($M < 1$).—It can be seen from the definition of $\chi_n(M, k)$ that for $\epsilon > 0$, $k \neq 0$, and for all $M < 1$, the imaginary part of β_0 cannot vanish and, furthermore, must have the same sign as the imaginary parts of β_2 and β_{-2}. Consequently, Eq. (15) cannot be satisfied in the subsonic régime for any $k \neq 0$; for $k = 0$, β_0 vanishes, and hence Eq. (15) is no longer applicable. For this case of $k = 0$, however, all three of the β_n's vanish simultaneously whenever

$$k_1^2 = \epsilon M^2/8\sqrt{1 - M^2} \tag{16}$$

For $k \neq 0$, it is impossible for any two β_n's to vanish simultaneously. Hence, at all subsonic speeds, flutter occurs only for those combinations of ϵ, k_1, and M which satisfy Eq. (16). Since this flutter occurs at zero frequency, it actually corresponds to a condition of neutral *static* stability. It may be noted that, since the solution of Eq. (16) is of the type that stems from the simultaneous vanishing of two or more β_n's, it remains valid even for the case where all of the terms of the original Fourier series are considered; the additional terms, however, would provide additional solutions.

Supersonic Speeds ($M > 1$).—In contrast to the situation at subsonic speeds, it can be shown that no two of the β_n's can ever vanish simultaneously at supersonic speeds, so that flutter modes can exist only by virtue of the satisfaction of Eq. (15). It turns out to be possible, for the presently considered three-term solution, to obtain from Eq. (15) explicit formulas for ϵ and k_1 in terms of M and k [see Appendix (B)]. For each supersonic Mach Number, these formulas provide a parametric relationship between ϵ and k_1 in terms of k, so that curves of ϵ versus k_1 can be constructed at each Mach Number.

The result of such a construction, for many different Mach Numbers between 1 and 2.5, is the rather complicated and bewildering array of curves in Fig. 4, some of the details of which are discussed in Appendix (B). The situation is somewhat clarified by Fig. 5, which shows schematically a pattern of flutter loci for each of several Mach Number ranges within which the pattern is typical.

In Figs. 4 and 5, the arrows on each flutter locus show the direction of increasing k values. In the subsonic range, there is, of course, only one flutter locus (Fig. 5a), given by Eq. (16), along which $k = 0$. For supersonic Mach Numbers, there may be as many as four separate curves, which have been designated as types A, B, C, and D. Each type results from a distinct range of variation of reduced frequency k, and increasing alphabetical order corresponds to increasing levels of k. (The numerals in each of the diagrams in Fig. 5 will be explained later.)

It is interesting to trace the metamorphosis of various types of flutter loci as Mach Number is increased. The type B locus, for example, starts out just above $M = 1$, as shown in Fig. 5b; pulls away from the origin at $M = \sqrt{4/3}$ (Fig. 5c); begins to form a loop at $M = 1.24493$ (Fig. 5d); "pulls through" at some (undetermined) Mach Number below $\sqrt{2}$ (Fig. 5e); starts looping again at some Mach Number slightly less than 2 (Fig. 5g); pulls through again and extends to infinity (Fig. 5h); and, finally, at $M = 2.00410$, lies down on the k_1-axis. The type A locus starts growing out from the origin gradually at $M = \sqrt{2}$ (Fig. 5f), and in the vicinity of $M = 2.05817$ it distorts radically and whips out to an infinite length (Figs. 5k, 5l). The type C curve, remarkably, appears full grown at $M = 2$ (Fig. 5i) and undergoes little change thereafter. The type D curve, on the other hand, starts to sprout at $M = 2$ and grows gradually (Figs. 5j, 5k, and 5l).

The significance of the various flutter loci must now be assessed. At any given Mach Number, every point in the k_1-ϵ plane defines a particular plate-air configuration, and we wish to know whether this configuration can have an unstable mode of oscillation. Further, it is to be realized that the configuration may possibly have *more* than *one* mode of unstable motion. We shall consider the number of such unstable modes as the *degree* of instability of the configuration. Now, certainly, a configuration corresponding to a point on one of the flutter loci possesses a *neutrally* stable mode of vibration, and it is plausible that, irrespective of the behavior of other possible modes, this mode of neutral stability becomes unstable on one side of the flutter locus and stable on the other side. Thus, at each Mach Number, *the flutter loci in the k_1-ϵ plane separate regions of various degrees of instability*. These loci might therefore be more appropriately called "stability boundaries."

It is clearly of interest to determine the degree of instability in each of the regions separated by the stability boundaries in order to discover the "safe" regions where the degree of instability is zero. This determination has been made, and the numerals in the various regions of Fig. 5 show the degree of instability; the method of calculating the degree of instability is outlined in the next section.

FIG. 4. Flutter loci for three-term solution with $R = 0$.

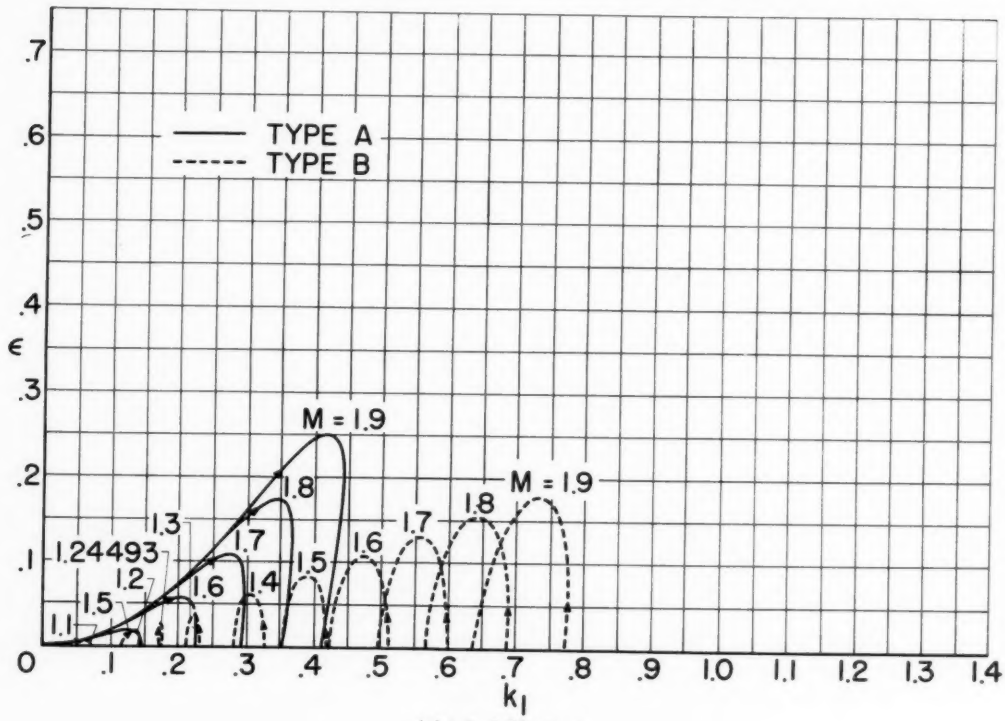

(a) $1.0 \leq M \leq 1.9$.

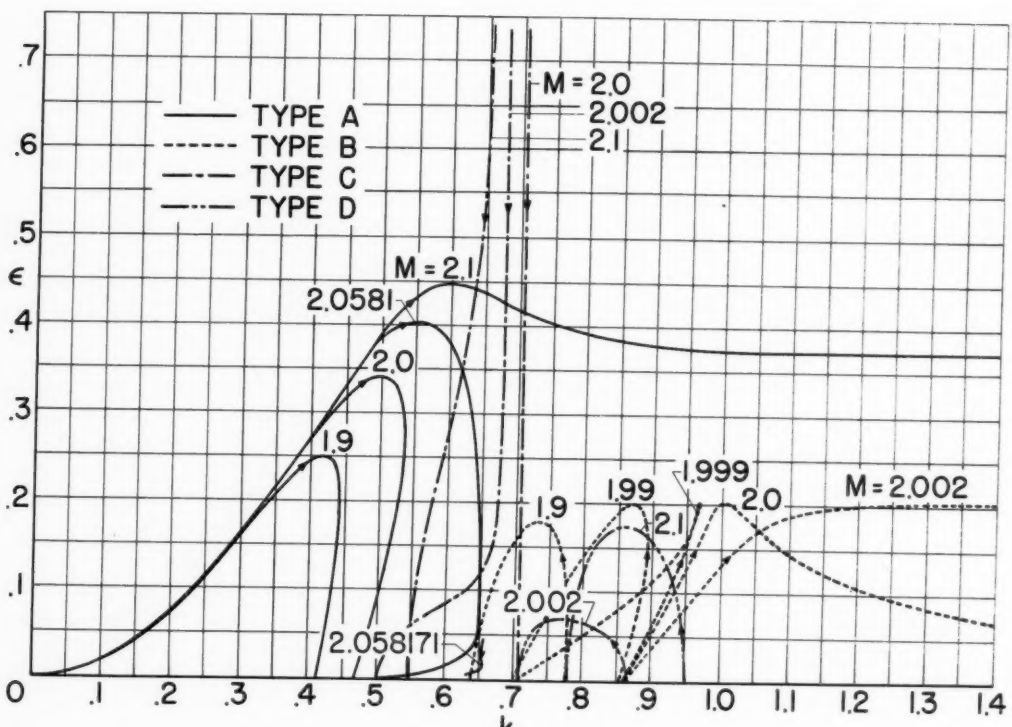

(b) $1.9 \leq M \leq 2.1$.

FIG. 4. (*continued*)

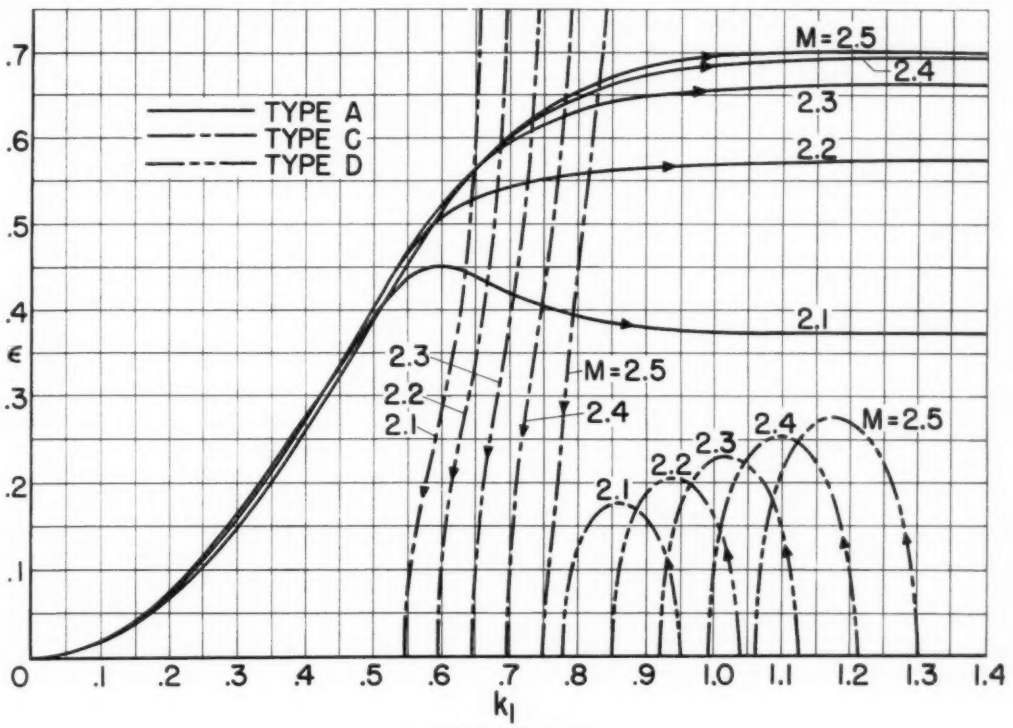

(c) $2.1 \leq M \leq 2.5$.

Identification of Regions of Instability

An unstable (divergent) mode of oscillation of the plate is represented by Eq. (1), with ω a complex number having a negative imaginary part. Consequently, if the aerodynamic loading function $\chi_n(M, k)$ could be properly defined for k in the lower half of the complex k-plane, the flutter equations, Eqs. (13) and (14), could be interpreted as frequency equations for unstable modes of oscillation, as well as for neutrally stable modes. The required extension of the domain of applicability of $\chi_n(M, k)$ is indeed possible; it can be verified that the (unique) *analytic continuation* of $\chi_n(M, k)$ into the lower half k-plane is defined as follows:

$$\chi_n(M, k) = n\left[g\left(M + \frac{k}{n}\right) + g\left(\frac{k}{n}\right)\right] \qquad (17)$$

$$[\text{for } \mathrm{Im}(k) < 0,\ n \neq 0]$$

where

$$g(z) = -iz^2/\sqrt{z^2 - 1}$$

and the single-valued branch of the multiple-valued function $g(z)$ that is chosen is the one for which the z-plane has a branch line on the real axis from -1 to 1, and $g(\sqrt{2}) = -2i$. For $\mathrm{Im}(k) \to 0$, this definition coincides with the one previously given [see Eq. (5)]. The analytic continuation of X_0 for complex k is simply $-2ik$. It can be shown, rigorously, by means of Fourier transform analysis and complex variable theory, that the formula for lift, Eq. (6), remains valid, with the use of Eq. (17) for χ_n, when ω has a negative imaginary part. [It is of interest to note that there does not exist an analytic continuation of the previously defined χ_n into the *upper* half k-plane; consequently, it appears that Eqs. (13) and (14) cannot be used to calculate complex frequencies of stable (decaying) modes of oscillation.]

With the use of the definition (17) for χ_n, a solution of the flutter equation that gives a k in the lower half plane means that the configuration represented by the selected combination of values of M, R, k_1, and ϵ is unstable. (It can be shown, incidentally, that the possibility of an unstable mode arising from the simultaneous vanishing of two β's for a complex k can be ruled out.) Thus, in the presently considered three-term solution, one could, in principle, determine the stability of a point in the k_1-ϵ plane for any Mach number by solving Eq. (15) for k and seeing whether there are any "unstable" roots (i.e., roots in lower half k-plane). Fortunately, the existence of such roots can be determined without their exhibition by use of the "Nyquist diagram" concept. This concept, which is familiar to electrical engineers and has already been used in connection with wing flutter by Dugundji,[4] is explained below.

Consider, in general, a function $F(z)$ that is analytic except for poles, for $\mathrm{Im}(z) < 0$. Let N be the number of zeros and P the number of poles of $F(z)$ having negative imaginary parts. (Each zero of order α is counted α times, and similarly for multiple poles.) Consider further the contour C shown in Fig. 6, consisting of an infinite straight line in the lower half plane, parallel to and infinitesimally close to the real axis, together with an infinite semicircle in the lower half plane. Let z traverse C once in the clockwise direction,

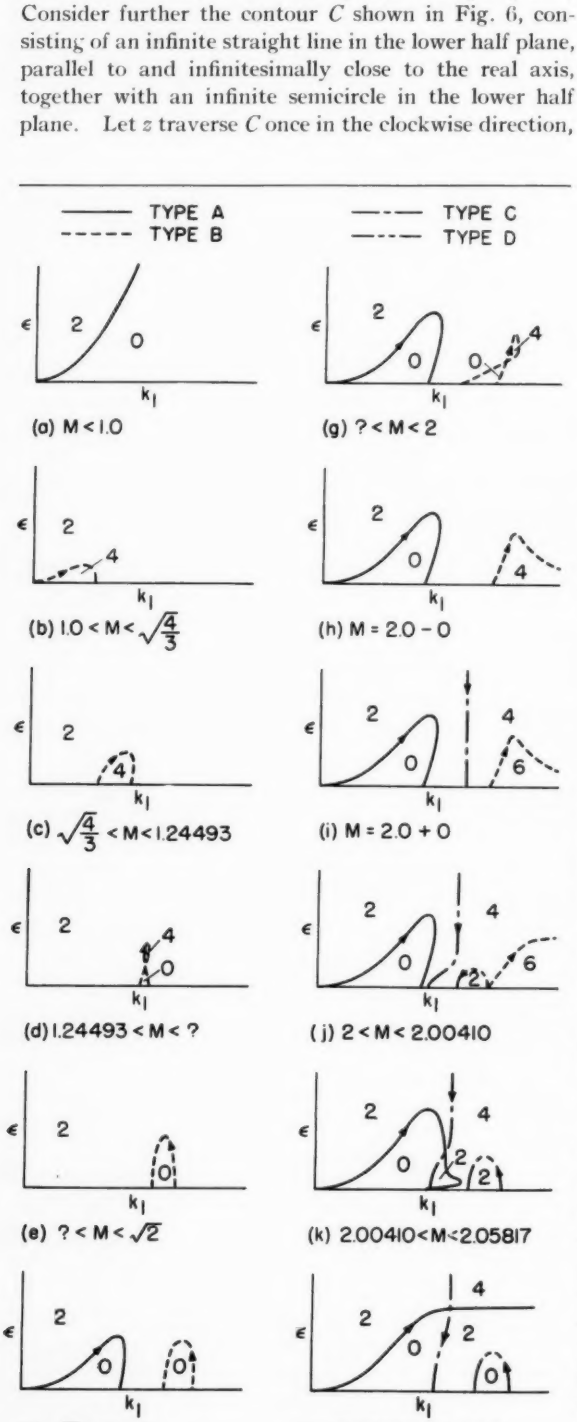

FIG. 5. Metamorphosis of flutter loci.

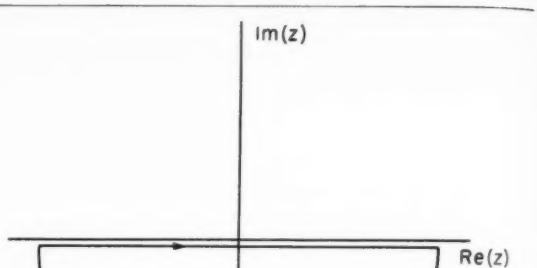

FIG. 6. Contour used in constructing the Nyquist diagram.

and trace out the corresponding path of $F(z)$—which we shall call here the "Nyquist diagram"—in the F-plane. Then, according to complex variable theory, the number of clockwise encirclements of the origin made by the Nyquist diagram is equal to $N - P$.

In the present problem, F is taken as $(1/\beta_0) + (1/\beta_2) + (1/\beta_{-2})$, and k is the independent complex variable. Clearly, for each Mach Number the number of unstable zeros of F is constant within each of the regions separated by stability boundaries in the k_1-ϵ plane (see Fig. 5). The poles of F occur only at the zeros of the β_n's; since none of the β_n's themselves have poles for $\mathrm{Im}(k) < 0$, P can readily be found by constructing an auxiliary Nyquist diagram for each of the β_n's. It is thus possible to evaluate N, and hence the degree of instability in each region of the k_1-ϵ plane, simply by the construction of Nyquist diagrams in each region. Actually, it suffices to construct a complete Nyquist diagram for F in only one of the regions and simply evaluate the change in the number of clockwise encirclements when a stability boundary is crossed. (The Nyquist diagram for each configuration represented by a point on a stability boundary must, of course, pass through the origin.)

The results of such a study by means of Nyquist diagrams are summarized in Fig. 5. The integer within each region is the degree of instability as given by the number of unstable roots of Eq. (15) determined by the Nyquist-diagram analysis. That the degree of instability in the unstable region is always even is caused by the fact that complex k-roots always occur in pairs of the form $\pm a - ib$, corresponding to pairs of unstable modes which are really identical. It can be seen from Fig. 5 that, as one proceeds along the stability boundaries in the direction of increasing k the side of the curve for increased stability is always to the right for the type A and C boundaries and to the left for the B and D boundaries.

Other Criteria for Instability.—A word of caution might be inserted concerning the applicability of two other techniques that are in current use for determining the stability of a given configuration. One method of widespread popularity in wing flutter analysis is to calculate the amount of artificial structural damping required to permit the existence of a neutrally stable mode; if the damping required is *positive*, the original configuration is considered to be unstable. However, to the authors' knowledge, it has not been proved that a decrease in structural damping always leads to decreased stability. Indeed, an example will be given later where this is not necessarily the case for the present problem.

Another technique that has been applied to wing flutter[5] and was used by Shen for panel flutter[2] is to calculate the energy per cycle required to vibrate the structure harmonically by means of an external force; the structure is considered unstable if this energy is negative (i.e., if the external agency absorbs energy). Unfortunately, this concept is not always valid, as was shown by Frazer[6] in 1939, and, according to Frazer, before him by Southwell in 1927; Frazer showed that the total work per cycle done by an exciting force may well be negative even when the structure is stable.

Results for a Particular Altitude and Material

The results embodied in Figs. 4 and 5 may be more clearly visualized by considering their implication for a particular plate material and a particular flight altitude. The parameters ϵ and k_1 may be written as

$$\epsilon = (1/\pi)(\rho/\gamma)(a/t)$$

$$k_1 = \frac{\pi}{c}\frac{t}{a}\sqrt{\frac{E}{12(1-\mu^2)\gamma}}$$

Thus, the product

$$\epsilon k_1 = \frac{\rho}{\gamma c}\sqrt{\frac{E}{12(1-\mu^2)\gamma}}$$

depends only on ρ and c (determined by altitude) and on E and γ (determined by the plate material). Consequently, for altitude and material fixed, the points of interest in the k_1-ϵ plane lie along a hyperbola. Fig. 7 shows, in the k_1-ϵ plane, the region of practical interest; the stability boundaries for $M = 1.4$, and 2 are shown for comparison purposes. The bounding hyperbola of the cross-hatched practical region corresponds to magnesium at sea level; as altitude and material density are increased, hyperbolas further inside this region are obtained. Once altitude and material are specified, both ϵ and k_1 depend only on the thickness ratio t/a; stable and unstable regions can then be shown in a chart of t/a versus Mach Number by cross-plotting the data of Fig. 4 and using the information in Fig. 5 to specify the degree of instability. This has been done for the case of aluminum at sea level, with the results shown in Fig. 8.

The shaded regions in Fig. 8 correspond to unstable conditions, and the degree of instability has been noted in the various regions. (There is actually an extremely narrow region of degree 6 in the upper shaded region near $M = 2$ which cannot be shown with the scale used.) The implications of the results shown, as well as the significance of the dotted line and the sprinkling of symbols, are discussed in the next section.

Discussion

At first sight, Fig. 8 presents a discouraging picture indeed and one that is even less optimistic in many respects than the results of Miles and Shen. No stability at all appears possible, for any thickness, at supersonic Mach Numbers below approximately $M = 1.25$, and it appears that, even above this Mach Number, a sufficient increase in thickness can always render a stable panel unstable. The situation may be even worse than shown, for only three terms have been considered in the "even" flutter equation, Eq. (13). Furthermore, the flutter analysis of the panel is not complete without consideration of the "odd" solution, Eq. (14). In the subsonic range, the highest static stability boundary resulting from the odd solution is actually given by the dotted curve in Fig. 8 and corresponds to greater thicknesses than the even

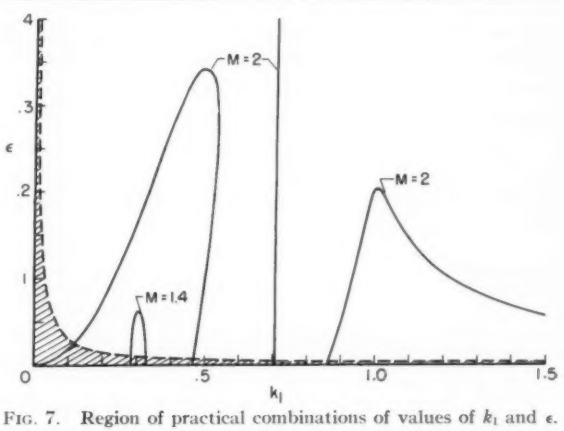

FIG. 7. Region of practical combinations of values of k_1 and ϵ.

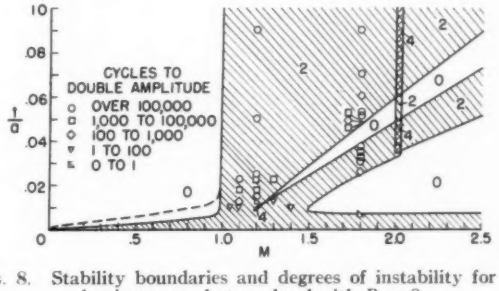

FIG. 8. Stability boundaries and degrees of instability for an aluminum panel at sea level with $R = 0$.

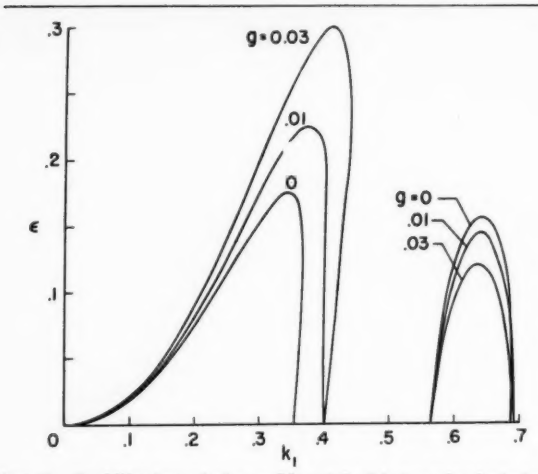

FIG. 9. Stability boundaries at $M = 1.8$ with damping included.

solution. No numerical results have been obtained for the predictions of the odd solution at supersonic speeds.

Even if we disregard this last consideration, the results of Fig. 8 obviously require modification or reinterpretation before they can be considered useful for design. It is easy to discount the subsonic results close to $M = 1$. At sonic velocity, linearized aerodynamic theory predicts infinite pressures in steady flow, and, since the points on the subsonic stability boundary correspond to zero flutter frequency, their validity breaks down close to $M = 1$. A reasonable empirical modification of the results in the subsonic range would be to assume a horizontal cutoff on the stability boundary at about $M = 0.95$.

Consider next the supersonic regions; the expression for the aerodynamic lift also becomes infinite at certain combinations of k and M. These singularities in the air forces actually appear only because the plate is infinitely long, and they correspond to a sort of resonance between the plate and the infinite field of flow; such singularities do not occur when the pressures on finite panels are calculated by linearized theory. It is significant that the flutter frequencies associated with most of the points on the higher stability boundaries are extremely close to these "resonant" frequencies; the infinities consequently may be partially responsible for the peculiarities of the solution. However, a simple rational procedure for removing the effects of these infinities is by no means as evident as it was in the subsonic region. Indeed, the infinities must not be entirely responsible for the unreasonable results, since they were not involved in Shen's results for a finite panel at $M = \sqrt{2}$. How, then, can the present results at supersonic speeds be rationalized? Two attempts to do so, one unsuccessful, the other promising, follow.

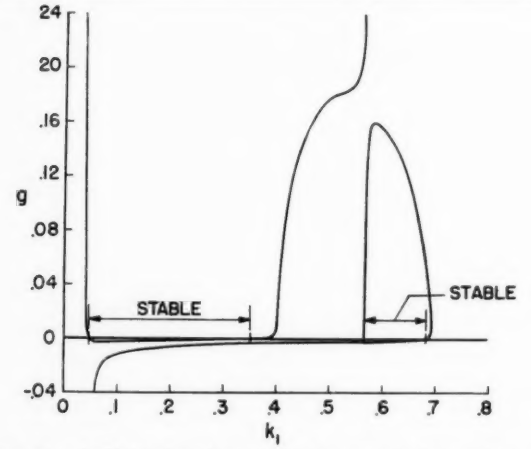

FIG. 10. Artificial damping required to sustain harmonic motion for $M = 1.8$, $\epsilon = 0.004$.

Effect of Structural Damping

The idea presented itself that perhaps the inclusion of a small amount of structural damping in the analysis might wipe out vast regions of instability in Fig. 8 and render the results more reasonable. Accordingly, the term $(Dg/\omega_1)w_{xxxx}$ representing viscous (Sezawa) damping was included in the differential equation of equilibrium, Eq. (7). [The addition of this type of damping term was chosen in preference to the more common use of a complex stiffness $D(1 + ig)$, because the latter is strictly applicable only to steady harmonic motion and leads to difficulties when complex frequencies are considered; the damping forces arising from both procedures are identical when $\omega = \omega_1$.]

Fig. 9 shows the stability boundaries for $M = 1.8$ obtained with values of g equal to 0.01 and 0.03, as well as the original stability boundaries for $g = 0$. As can be seen, not only are the stable regions inside the loops not greatly increased in extent by the addition of damping but the stable region in one of the loops is actually decreased in size.

An incidental outgrowth of this study is shown in Fig. 10, which, again for $M = 1.8$ and for $\epsilon = 0.004$, shows calculated values of g required to produce steady oscillation plotted against k_1. The curves pass through zero at the stability boundaries; but the remarkable fact to be noted is that, well within the second stable region, the *addition* of damping leads to a steady oscillation. Thus, the concept that removal of damping tends to destabilize is evidently not valid here, and, as was mentioned previously, doubt is cast on the use of the "artificial damping" concept for determining whether a given system is stable.

Rates of Growth of Unstable Oscillations

A more fruitful attempt to rationalize the results of Fig. 8 was made by actually calculating (approximately) the magnitude of the unstable roots at various points

in the unstable region. From the values of the real and imaginary parts of these roots, the number of cycles needed to double the amplitude of the oscillation was computed, and the results are shown by the symbols in Fig. 8. It is seen that, over a large portion of the region of instability, the flutter can be characterized as extremely mild. Indeed, the results, although they do not cover the entire range, tend to show that, above $M = 1.5$, only the lowest stability boundary need be taken seriously. Between $M = 1$ and $M = 1.5$, a transition between severe and mild flutter appears to take place at a value of t/a equal to about 0.015.

Concluding Remarks

On the basis of the results of the present investigation, it appears that a successful theoretical analysis of panel flutter which would provide useful data to designers must be carried several steps beyond the normal type of flutter analysis. Not only must a careful interpretation be given to the regions separated by stability boundaries but, in addition, it appears necessary to calculate the severity of flutter in order to avoid unduly conservative design requirements.

Appendix (A)—Solution to the Wavy Wall Problem

The Ackeret solution[3] for the pressure on a wavy wall is rederived here in a form appropriate to the present formulation of the problem. The wavy wall boundary (Fig. 2b) is

$$w = Re[a_n e^{in\pi x_1/a}]$$

The linearized equation for the potential of the velocity perturbation in a flow of Mach Number M_1 *above* the wall is

$$\varphi_{x_1x_1}(1 - M_1^2) + \varphi_{yy} = 0 \tag{A1}$$

For flow to the *right* (i.e., in the positive x_1-direction) the linearized boundary condition at the wall is

$$\varphi_y(x_1, 0) = M_1 c w_{x_1} \tag{A2}$$

and the linearized expression for the pressure perturbation at the wall is

$$\Delta p_u = -\rho M_1 c \varphi_{x_1}(x_1, 0) \tag{A3}$$

For flow to the *left*, the boundary condition is

$$\varphi_y(x_1, 0) = -M_1 c w_{x_1} \tag{A4}$$

and the pressure perturbation at the wall is

$$\Delta p_u = \rho M_1 c \varphi_{x_1}(x_1, 0) \tag{A5}$$

In all cases, the solution of Eq. (A1) is written as

$$\varphi = Re[h(y)e^{in\pi x_1/a}]$$

whence

$$h''(y) - \frac{n^2\pi^2}{a^2}(1 - M_1^2)h(y) = 0 \tag{A6}$$

For $M_1 < 1$, the solution of Eq. (A6) which is finite at infinity provides the following results:

$$\varphi = Re[B_n e^{-(n/|n|)\pi\lambda y/a} e^{in\pi x_1/a}]$$

where $\lambda = \sqrt{|M_1^2 - 1|}$, and, from Eq. (A2),

$$B_n = -[(iM_1c/\lambda)(n/|n|)]a_n$$

for flow to the right, while, from Eq. (A4),

$$B_n = +[(iM_1c/\lambda)(n/|n|)]a_n$$

for flow to the left. Using Eqs. (A3) and (A5) shows that, for flow to the left *or* right,

$$\Delta p_u = -\frac{\pi\rho c^2}{a} Re\left[|n|\frac{M_1^2}{\lambda} a_n e^{in\pi x_1/a}\right] \tag{A7}$$

For $M_1 > 1$, the solution of Eq. (A6) which satisfies the condition that there be no incoming disturbances from infinity[3] yields

$$\varphi = Re[C_n e^{(in\pi/a)(x_1 - \lambda y)}]$$

for flow to the right

$$\varphi = Re[C_n e^{(in\pi/a)(x_1 + \lambda y)}]$$

for flow to the left, where, from Eqs. (A2) and (A4),

$$C_n = -(M_1c/\lambda)a_n$$

The pressure perturbation, from Eq. (A3), is

$$\Delta p_u = \frac{\pi\rho c^2}{a} Re\left[in\frac{M_1^2}{\lambda} a_n e^{in\pi x_1/a}\right]$$

for flow to the right, while, from Eq. (A5),

$$\Delta p_u = \frac{-\pi\rho c^2}{a} Re\left[in\frac{M_1^2}{\lambda} a_n e^{in\pi x_1/a}\right]$$

for flow to the left.

Appendix (B)—Computation of Flutter Loci at Supersonic Speeds for the Three-Term Solution

The solution of Eq. (15) for k_1 and ϵ is, for $M > 1$ and $|k| < 2(M - 1)$,

$$\left.\begin{aligned} \epsilon &= \frac{k^2}{1 - (4k/\chi_{2I} + \chi_{-2I})}\sqrt{\frac{1 - (8k/\chi_{2I} + \chi_{-2I})}{2k(\chi_{2I} + \chi_{-2I}) - \chi_{2I}\chi_{-2I}}} \\ k_1 &= \frac{1}{4}\sqrt{k^2 + \frac{k^2}{1 - (4k/\chi_{2I} + \chi_{-2I})} + \epsilon\chi_R} \end{aligned}\right\} \tag{B1}$$

where the subscripts R and I refer to real and imaginary parts, respectively; for the range of k considered χ_{2R} equals χ_{-2R}, and both have been designated as χ_R. The signs of the square roots in Eq. (B1) have been selected so that only positive values of k_1 and ϵ result.

TABLE 1
Ranges of k Corresponding to Flutter Loci

M	Type A	Type B	Type C	Type D
1.1		0 , 0.2		
1.2		0.2698 , 0.4		
1.3		0.536 , 0.6		
1.4		0.7602 , 0.8		
1.5	0, 0.59236	0.9738 , 1.0		
1.6	0, 0.91080	1.1798 , 1.2		
1.7	0, 1.17643	1.3846 , 1.4		
1.8	0, 1.4194	1.5876 , 1.6		
1.9	0, 1.65000	1.79012, 1.8		
2.0	0, 1.87285	1.99184, 2.0	2.00000, 2.00000	
2.1	0, 2.00000		2.14712, 2.18670	2.19670, 2.2
2.2	0, 2.00000		2.32684, 2.3836	2.39664, 2.4
2.3	0, 2.00000		2.52189, 2.5832	2.59697, 2.6
2.4	0, 2.00000		2.72396, 2.78365	2.79726, 2.8
2.5	0, 2.00000		2.9288 , 2.9854	2.99746, 3.0

When $|k| > 2(M - 1)$, no solution exists because of the fact that all three β_n's always have negative imaginary parts (for $\epsilon > 0$). All of the real solutions to Eq. (15) are therefore given by Eq. (B1).

Examination of the χ_n's reveals that χ_R and $\chi_{2l}\chi_{-2l}$ are *even* functions of k and that $\chi_{2l} + \chi_{-2l}$ is an *odd* function of k; hence, the values of ϵ and k_1 for $k < 0$ are the same as those for $k > 0$, and our attention can be confined to the range $0 < k < 2(M - 1)$. Results for many values of M obtained by varying k in this range are shown in the form of plots of ϵ against k_1 in Fig. 4. At any one Mach Number, there are seen to be as many as four types of flutter loci; each locus arises from a different range of k, and the distinct ranges result from the fact that the quantity inside the square-root symbol in the expression for ϵ, Eq. (B1), changes sign as many as three times as k is increased from zero to $2(M - 1)$. The ranges of k for which this expression is positive (and, hence, for which real values of k_1 and ϵ result) are given in Table 1 for Mach Numbers between 1.1 and 2.5, in increments of 0.1. At each Mach Number, each range and the corresponding k_1-ϵ curves in Fig. 4 are designated as types A, B, C, or D, in order of increasing k.

It should be noted that many of the k-ranges in Table 1 are extremely small and could be easily overlooked if care is not taken. In addition, the values of k in the ranges often are extremely close to those values of k where one or another of the χ_n's becomes infinite; these critical values are $k = 2$ and $2(M - 1)$, the latter value coinciding with the upper limit of possible k's.

In connection with Fig. 4, it should be pointed out that, at some Mach Numbers not listed in Table 1, some curves undergoing rapid transition with change in Mach Number have been shown. In one instance, $M = 2.058171$, only a short segment of the type A curve is shown to illustrate the start of the rapid transition that occurs just below $M = \sqrt{2} + \sqrt{5} = 2.058171027$.

REFERENCES

[1] Miles, J. W., *Dynamic Chordwise Stability at Supersonic Speeds*, North American Aviation Report AL-1140, 1950.

[2] Shen, S. F., *Flutter of a Two-Dimensional Simply-Supported Uniform Panel in a Supersonic Stream*, Massachusetts Institute of Technology, Contract No. N5ori-07833, Office Naval Res. (Project NR-064-259), August 6, 1952.

[3] Liepmann, H. W., and Puckett, A. E., *Aerodynamics of a Compressible Fluid*, pp. 126–136; John Wiley & Sons, Inc., New York, 1947.

[4] Dugundji, J., *A Nyquist Approach to Flutter*, Readers' Forum, Journal of the Aeronautical Sciences, Vol. 19, No. 6, pp. 422–423, June, 1952.

[5] Myklestad, N. O., *Vibration Analysis*, pp. 250–255; McGraw-Hill Book Company, Inc., New York, 1944.

[6] Frazer, R. A., *On the Power Input Required to Maintain Forced Oscillations of an Aeroplane Wing in Flight*, British R. and M. No. 1872, July 21, 1939.

On the Approximate Solution of the Laminar Boundary-Layer Equations*

ITIRO TANI†
Cornell University

SUMMARY

A simple method is developed for solving approximately the equations of the laminar boundary layer. The velocity profile is assumed as a member of a one-parameter family of curves, the parameter being different from the usual Pohlhausen parameter. The Pohlhausen parameter is calculated by a simple quadrature formula, which is derived from the energy-integral relation. The relation between the profile parameter and Pohlhausen parameter is determined from the combination of both momentum-integral and energy-integral relations. The accuracy of the method is examined by comparing the results with those of exact solutions for the flow of incompressible fluid. Satisfactory agreement is obtained. The method of solution is then extended to the flow of compressible fluid along a heat-insulated wall, assuming the Prandtl Number slightly different from unity and the Sutherland formula for the variation of viscosity with temperature. As an example of the application, the effect of compressibility on separation point is discussed.

LIST OF SYMBOLS

x	= distance measured along the wall
y	= distance measured normal to the wall
u	= velocity component in the direction x
v	= velocity component in the direction y
T	= absolute temperature
c	= speed of sound
ρ	= density
μ	= viscosity
ν	= kinematic viscosity
k	= thermal conductivity
c_p	= specific heat at constant pressure
γ	= ratio of specific heats
σ	= Prandtl number, Eq. (42)
ξ	= $1 - \sqrt{\sigma}$, Eq. (46)
δ	= boundary layer thickness
δ^*	= displacement thickness, Eq. (5)
θ	= momentum thickness, Eq. (6)
θ^*	= energy thickness, Eq. (7)
λ	= Pohlhausen parameter, Eq. (24)
a	= velocity profile parameter, Eqs. (11), (64)
X, Y	= coordinate in the transformed flow, Eq. (54)
U, V	= velocity component in the transformed flow
Δ	= boundary layer thickness in the transformed flow
Δ^*	= displacement thickness in the transformed flow, Eq. (61)
Θ	= momentum thickness in the transformed flow, Eq. (62)
Θ^*	= energy thickness in the transformed flow, Eq. (63)
Λ	= Pohlhausen parameter in the transformed flow, Eq. (77)
A	= a constant, Eq. (23)
B	= a function of x, Eq. (56)
C	= a function of T, Eq. (48)
D, E, F	= functions of a, Eqs. (17), (18), (19)
G, H	= functions of a, Eq. (13)
P, Q	= functions of a, Eqs. (20), (21)
K, J	= functions of a, Eqs. (73), (74)
S	= a constant, Eq. (48)
Φ	= a function of u/u_1, Eq. (50)
Re	= Reynolds Number, $u_1 x/\nu_1$
M	= Mach Number, u_1/c_1
C_f	= coefficient of skin friction, Eq. (80)

Subscripts

1	= condition at the outer edge of the boundary layer
0	= reference condition, Eq. (69)
m	= mean value

Superscript

0	= condition at $x = 0$.

INTRODUCTION

IT HAS BEEN SHOWN by Stewartson[1] that the momentum equation for a compressible laminar boundary layer is transformed into that for an incompressible laminar boundary layer, assuming that the wall is thermally insulated, that the Prandtl Number is unity, and that the viscosity is proportional to the absolute temperature. If any one of the assumptions is dropped, the transformed equation is no longer of the same form as that for an incompressible flow, but it is still easy to solve because of the disappearance of variable density. Therefore it seems adequate to consider first the laminar boundary layer in incompressible fluids.

The most frequently used method of solving the boundary layer equations approximately is the momentum-integral method, in which the momentum equation is integrated over the boundary layer thickness, and is hence satisfied only in average. By assuming a definite form for the velocity profile as a function of the normal distance, an ordinary differential equation is obtained, with the distance along the wall as the independent variable. In the original method due to von Kármán and Pohlhausen,[2] a fourth-degree velocity profile is assumed, whose coefficients are determined by the

Received September 14, 1953.

* This research, carried out at the Graduate School of Aeronautical Engineering, Cornell University, was supported by the United States Air Force under Contract No. AF 33 (038)-21406, monitored by the Office of Scientific Research, Air Research and Development Command. The writer wishes to take this opportunity to acknowledge helpful discussions with Professors W. R. Sears and Nicholas Rott of the Cornell University during the course of the work.

† Professor, University of Tokyo, Japan. On leave from the University of Tokyo.

boundary conditions at the wall as well as at the outer edge of the boundary layer. Consequently, the velocity profile is expressed as a member of a one-parameter family of curves, with

$$\lambda = (\theta^2/\nu)(du_1/dx)$$

as the parameter, which makes its appearance through the condition that the momentum equation should be satisfied at the wall.

This method gives a reasonably accurate solution in a region of accelerated flow, but its adequacy in a region of retarded flow has been questioned. Separation of flow may actually occur where the method fails to give it. Various attempts have been made to increase the accuracy of the method. For example, Howarth[3] used the velocity profile obtained from the exact solution for the case when the velocity outside the boundary layer decreases linearly with the distance; Schlichting and Ulrich[4] assumed a sixth-degree polynomial for the velocity profile, so that it could satisfy additional conditions at the wall as well as at the outer edge of the boundary layer. These refinements generally yield fairly good results when compared with the original method due to Pohlhausen. Strictly speaking, however, none of the methods is sufficiently accurate because the velocity profile is expressed as a member of the family of curves with the Pohlhausen parameter λ, whereas the results of certain exact solutions suggest that λ cannot fix the velocity profile. In particular, λ should have a certain definite value at the separation point according to the assumption, but this is not the case according to the exact solutions, the value of λ at separation depending considerably on the velocity distribution outside the boundary layer.[5]

It is reasonable to suppose that the difficulty may be reduced by using a velocity profile with two parameters, one of which is λ and the other new. This has actually been done by Wieghardt,[6] who assumed an eleventh-degree velocity profile and determined the parameters by using the momentum-integral as well as the energy-integral relations, the latter of which is obtained by multiplying the momentum equation by velocity and integrating across the boundary layer thickness. Satisfactory results can be obtained, but the method appears quite tedious for practical application. An interesting modification has been proposed by Walz,[7] who used a one-parameter family of curves again but gave up the fulfillment of the condition that the momentum equation should hold at the wall. The procedure is thus considerably simplified, but results of comparatively high accuracy can still be obtained. Truckenbrodt[8] has recently extended the method so that the laminar and turbulent boundary layers may be treated along similar lines.

It is to be pointed out that the improvement of accuracy is attained by dropping one of the boundary conditions at the wall and satisfying the energy-integral relation instead. Since the Pohlhausen parameter λ enters only through the boundary condition, this is equivalent to saying that better results may be obtained by abandoning λ for use as the profile parameter and by adopting another profile parameter that should be determined such that the momentum-integral and energy-integral relations are both satisfied. The conclusion seems to be quite natural; because λ cannot fix the velocity profile, as mentioned above.

This method of approach is adopted in the present investigation. A simple fourth-degree polynomial is used as the velocity profile, quite the same as the original Pohlhausen scheme, but dropping one of the boundary conditions at the wall. Consequently, one of the coefficients of the polynomial remains undetermined, and it is used as the parameter for the velocity profile. Both the momentum-integral and energy-integral relations are considered, from which the relation between the profile parameter and the distance along the wall is determined. The analysis is given in the first part of the paper, and it is shown that satisfactory results are obtained when compared with the exact solutions.

In the second part of the paper, the analysis is extended to the laminar boundary layer in compressible fluids. The wall is assumed to be thermally insulated, but the other restrictions imposed by Stewartson are removed. The Prandtl Number may be different from unity, but the difference from unity is assumed small. The so-called Sutherland formula is adopted for the variation of viscosity with temperature, because it is considered desirable to use as accurate a formula as possible at high Mach Numbers where the variations in temperature are considerable. In order to simplify the analysis, however, a simple relation between temperature and velocity is assumed, the effect of Prandtl Number being taken into account approximately. The momentum equation is then transformed by the method proposed by Rott,[9] which is a useful extension of the original Stewartson transformation. The resulting equation is no longer of the same form as that for the incompressible flow, but it is still amenable to solution by a similar technique as mentioned above. The accuracy of the solution is checked in the case of a flat plate by comparing with Crocco's results,[10] and it is found to be satisfactory. The method of solution is then applied for estimating the separation point when the velocity outside the boundary layer decreases linearly with the distance.

(I) Laminar Boundary Layer in Incompressible Fluids

Basic Equations

Consider first the steady two-dimensional laminar boundary layer flow of an incompressible fluid. The continuity equation is

$$\partial u/\partial x + \partial v/\partial y = 0 \qquad (1)$$

and the momentum equation is

$$u\frac{\partial u}{\partial x} + v\frac{\partial u}{\partial y} = u_1\frac{du_1}{dx} + \nu\frac{\partial^2 u}{\partial y^2} \tag{2}$$

where x and y are the distances measured along and normal to the wall respectively, u and v are the velocity components in the directions x and y, respectively, u_1 is the velocity outside the boundary layer, and ν is the kinematic viscosity. Integrating Eq. (2) with respect to y from $y = 0$ to $y = \delta$, where δ is the thickness of the boundary layer, and taking account of Eq. (1), we have the momentum-integral relation:

$$\frac{u_1}{\nu}\frac{d\theta^2}{dx} + 2\frac{\theta^2}{\nu}\frac{du_1}{dx}\left(2 + \frac{\delta^*}{\theta}\right) = \frac{2\theta}{u_1}\left(\frac{\partial u}{\partial y}\right)_{y=0} \tag{3}$$

Multiplying Eq. (2) by u and integrating with respect to y from $y = 0$ to $y = \delta$, we have the energy-integral relation:

$$\frac{u_1}{\nu}\frac{d\theta^{*2}}{dx} + 6\frac{\theta^{*2}}{\nu}\frac{du_1}{dx} = \frac{4\theta^*}{u_1^2}\int_0^\delta \left(\frac{\partial u}{\partial y}\right)^2 dy \tag{4}$$

Here, δ^*, θ, and θ^* are the displacement thickness, momentum thickness, and energy thickness, respectively,

$$\delta^* = \int_0^\delta \left(1 - \frac{u}{u_1}\right) dy \tag{5}$$

$$\theta = \int_0^\delta \frac{u}{u_1}\left(1 - \frac{u}{u_1}\right) dy \tag{6}$$

$$\theta^* = \int_0^\delta \frac{u}{u_1}\left(1 - \frac{u^2}{u_1^2}\right) dy \tag{7}$$

Velocity Profile

Following Pohlhausen,[2] we assume the velocity profile in the form

$$\frac{u}{u_1} = a_0 + a\frac{y}{\delta} + b\frac{y^2}{\delta^2} + c\frac{y^3}{\delta^3} + d\frac{y^4}{\delta^4} \tag{8}$$

and determine the coefficients a_0, a, b, c, and d, which are functions of x, from the conditions

$$\left.\begin{aligned} y = 0: &\quad u = 0 \\ y = \delta: &\quad u = u_1,\quad \partial u/\partial y = 0,\quad \partial^2 u/\partial y^2 = 0 \end{aligned}\right\} \tag{9}$$

The usual condition

$$y = 0: \qquad \partial^2 u/\partial y^2 = -(u_1/\nu)(du_1/dx) \tag{10}$$

which states that Eq. (2) should be satisfied at the wall, is now dropped, so that one of the coefficients, say a, remains undetermined. This coefficient a is simply adopted as the parameter for the velocity profile, because it possesses a clear physical meaning in that it is proportional to the shearing stress at the wall. We thus obtain

$$\frac{u}{u_1} = \frac{y^2}{\delta^2}\left(6 - 8\frac{y}{\delta} + 3\frac{y^2}{\delta^2}\right) + a\frac{y}{\delta}\left(1 - \frac{y}{\delta}\right)^3 \tag{11}$$

Introducing the nondimensional quantities

$$\delta^*/\delta = D, \qquad \theta/\delta = E, \qquad \theta^*/\delta = F \tag{12}$$

$$H = \delta^*/\theta = D/E, \qquad G = \theta^*/\theta = F/E \tag{13}$$

$$\frac{2\theta}{u_1}\left(\frac{\partial u}{\partial y}\right)_{y=0} = P, \qquad \frac{4\theta^*}{u_1^2}\int_0^\delta \left(\frac{\partial u}{\partial y}\right)^2 dy = Q \tag{14}$$

we can write Eqs. (3) and (4) in the form

$$\frac{u_1}{\nu}\frac{d\theta^2}{dx} + 2(2 + H)\frac{\theta^2}{\nu}\frac{du_1}{dx} = P \tag{15}$$

$$\frac{u_1}{\nu}\frac{dG^2\theta^2}{dx} + 6\frac{G^2\theta^2}{\nu}\frac{du_1}{dx} = Q \tag{16}$$

where

$$D = 2/5 - a/20 \tag{17}$$

$$E = 4/35 + a/105 - a^2/252 \tag{18}$$

$$F = \frac{876}{5005} + \frac{73}{5005}a - \frac{23}{5460}a^2 - \frac{a^3}{2860} \tag{19}$$

$$P = 2aE \tag{20}$$

$$Q = [(4/35)F](48 - 4a + 3a^2) \tag{21}$$

The quantities D, E, F, G, H, P, and Q are functions of a only, and their numerical values are tabulated in Table 1.

Quadrature Formula for Momentum Thickness

It is readily shown that Eq. (15) may be integrated in the quadrature formula

$$\frac{\theta^2}{\nu} = Au_1^{-(n+1)}\int_0^x u_1^n\, dx \tag{22}$$

provided that the distance x is measured from the point where $\theta = 0$, and that $P - (3 + 2H)\lambda$ can be replaced by a linear function of λ such that

$$P - (3 + 2H)\lambda = A - n\lambda \tag{23}$$

where A and n are constants and

$$\lambda = (\theta^2/\nu)(du_1/dx) \tag{24}$$

is the so-called Pohlhausen parameter. This method of approximate integration was put forward independently by Hudimoto[11] and the present writer[12] early in 1941. The values $A = 0.44$ and $n = 5$ proposed by the present writer were obtained by evaluating the left side of Eq. (23) from Howarth's solution for the case when the velocity outside the boundary layer decreases linearly with the distance.[3] Formulas of a similar type have also been found by Young and Winterbottom,[13] Walz,[14] and Thwaites,[15] independently.

It is not possible, however, to proceed similarly in the present calculation, because λ is no longer used as the profile parameter. Instead, Q is a slowly changing function of a, so that it may be replaced by a constant value Q_m. Eq. (16) is then integrated in the form

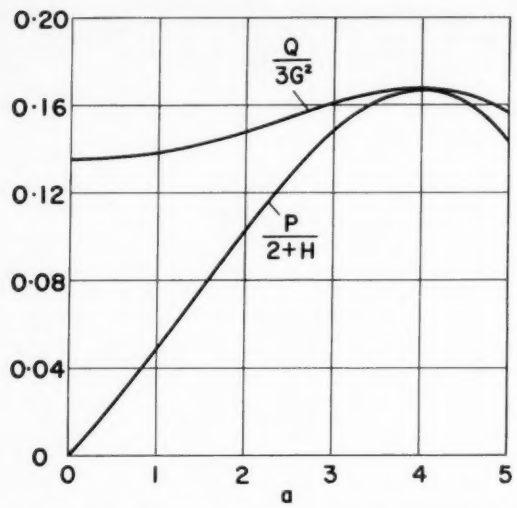

FIG. 1. Both sides of Eq. (35) are plotted as functions of a. Both curves have a local maximum at $a = 4$ but do not exactly coincide with each other.

$$G^2 \frac{\theta^2}{\nu} = Q_m u_1^{-6} \int_0^x u_1^5 \, dx \tag{25}$$

Replacing, moreover, the function G by a constant value G_m, we have

$$\frac{\theta^2}{\nu} = \frac{Q_m}{G_m^2} u_1^{-6} \int_0^x u_1^5 \, dx \tag{26}$$

As will be seen later, $Q = 1.079$ and $G = 1.567$ for the flow along a flat plate. Using these values for Q_m and G_m, we get

$$\frac{\theta^2}{\nu} = 0.44 \, u_1^{-6} \int_0^x u_1^5 \, dx \tag{27}$$

which is exactly the same as previously obtained from the momentum-integral. It was Truckenbrodt[8] who first found that the quadrature formula for the momentum thickness may also be deduced from the energy-integral, although he used the velocity profile obtained from the exact solution for the case when the velocity outside the boundary layer is proportional to the power of distance.

We now consider Eq. (27) as the first approximate solution for θ^2/ν. We then calculate λ by Eq. (24). Therefore, we determine λ as the function of x. But, since it is a, and not λ, that is used as the parameter for the velocity profile, it is necessary to obtain a relation that relates λ and a.

Determination of the Parameter

Eliminating $d\theta^2/dx$ from Eqs. (15) and (16), we have

$$\lambda(H - 1) = \frac{1}{2}\left(P - \frac{Q}{G^2}\right) + \lambda \frac{d \ln G}{d \ln u_1} \tag{28}$$

from which we can determine the relation between λ and a. First, we neglect the second term on the right side, and we obtain the first approximation to the relation between λ and a. Then we estimate the neglected term, and proceed to the second approximation, and so on.

After determining the relation between λ and a, we are in a position to check the accuracy of the quadrature formula (27). The function Q may now be plotted against λ and replaced by a linear function

$$Q = Q_m + r\lambda \tag{29}$$

where Q_m and r are constants, so that Eq. (16) is again integrated in the form

$$\frac{\theta^2}{\nu} = \frac{Q_m}{G^2} u_1^{-(6-r)} \int_0^x u_1^{5-r} \, dx \tag{30}$$

where G is treated as dependent on λ. Thus we get the second approximate solution for θ^2/ν. In most cases, however, the effects due to the variability of Q and G cancel each other, and the result obtained from Eq. (30) remains almost the same as that from Eq. (27). It turns out therefore that the simple quadrature formula (27) is a sufficient approximation.

It is to be noticed that Truckenbrodt[8] derived from Eqs. (15) and (16) a differential equation for the quantity $L = \int (H - 1)^{-1} d \ln G$, and solved it by an approximate method. L is also a function of a, and the advantage of using such a quantity may be readily seen from the Eq. (28) which, as a matter of fact, is essentially the same as the differential equation of Truckenbrodt. However, there is a difference in the treatment of this equation: it is used by Truckenbrodt to determine L as a function of x, while in the present analysis it is used to obtain the relation between λ and a. Another difference is that in Truckenbrodt's solution the velocity profile is adopted which is obtained from the exact solution for the special case when the velocity outside the boundary layer is proportional to the power of the distance, while in the present analysis the velocity profile is assumed as a simple polynomial, which is more convenient to be extended to the case of compressible fluids.

Particular Values of the Parameter

As clearly indicated by Eq. (28), the relation between λ and a is not universal, but depends on the velocity distribution outside the boundary layer. However, there are a couple of particular values of a corresponding to certain definite conditions. For example, the separation point is characterized by the particular value $a = 0$. Other particular cases are the flow along a flat plate and the flow at the stagnation point.

For the flow along a flat plate, $\lambda = 0$ and $G =$ constant.† Therefore we have the condition

† At the minimum pressure point of a flow with pressure gradient λ vanishes but G is not necessarily stationary.

$$P = \frac{Q}{G^2} \tag{31}$$

from which we obtain

$$a = 1.857 \tag{32}$$

as the particular value of the parameter for the flat plate. We have also

$$P = 0.439, \quad Q = 1.079, \quad G = 1.567, \quad H = 2.60 \tag{33}$$

while the Blasius solution for the flat plate gives

$$P = 0.441, \quad Q = 1.090, \quad G = 1.572, \quad H = 2.59 \tag{34}$$

It appears therefore that the present approximate method predicts the flat plate characteristics with satisfactory accuracy.

In order to find the condition at the stagnation point, we put $u_1 = 0$ in Eqs. (15) and (16) and eliminate du_1/dx from them. We then have

$$P/(2 + H) = Q/3G^2 \tag{35}$$

as the equation for determining the value of a. Unfortunately, however, it is found that there is no root of the equation in the physically significant range of a. Similar difficulties have already been experienced in connection with the refinement of the Pohlhausen solution.[4] It will be found, however, that the curves of $P/(2 + H)$ and $Q/3G^2$ plotted against a come very close to each other in the neighborhood of the point where both curves have a local maximum, as shown in Fig. 1. We tentatively take the value of a at this point

$$a = 4.00 \tag{36}$$

as the value corresponding to the stagnation point. We then have

$$P = 0.711, \qquad \lambda = 0.084 \tag{37}$$

On the other hand, the exact solution for the flow $u_1 = x$ gives[16]

$$P = 0.721, \qquad \lambda = 0.085 \tag{38}$$

It is seen from this comparison that the approximate determination (36) is sufficiently accurate for practical purposes.

Comparison with the Exact Solutions

In order to check the accuracy of the solution as a whole, calculations are made for the case when the velocity outside the boundary layer is given by $u_1 = u_1^0 \times (1 - x^n)$, where u_1^0 is the velocity at $x = 0$. Exact solutions have been obtained by Howarth[3] for the case $n = 1$, and by the present writer[5] for the cases $n = 2$, 4, and 8. Results are shown in Fig. 2, where the Pohlhausen parameter λ is plotted against the nondimensional shearing stress P, instead of against the profile parameter a. This method of representation is preferable, because there is no analogue to a in the exact solution, and P/a is a slowly changing function of a. It will be seen that the accuracy is satisfactory except for the case $n = 8$. Although it is difficult to extend the calculation right up to the separation point because of the considerable change in the value of $(d \ln G)/(d \ln u_1)$, it is still possible to arrive at a point so near to the separation point that the latter point may be extrapolated with sufficient accuracy. The result seems to be encouraging, since the method can predict fairly accurately how the relation between λ and P (hence λ and a) changes in accordance with the velocity distribution outside the boundary layer. Such a change was demonstrated by the present writer,[5] but until now there has been proposed no satisfactory solution which takes this effect into account.

(II) Laminar Boundary Layer in Compressible Fluids

Basic Equations

For the steady two-dimensional laminar boundary layer in compressible fluids, we have the continuity equation

$$(\partial/\partial x)(\rho u) + (\partial/\partial y)(\rho v) = 0 \tag{39}$$

the momentum equation

$$\rho u \frac{\partial u}{\partial x} + \rho v \frac{\partial u}{\partial y} = \rho_1 u_1 \frac{du_1}{dx} + \frac{\partial}{\partial y}\left(\mu \frac{\partial u}{\partial y}\right) \tag{40}$$

and the energy equation

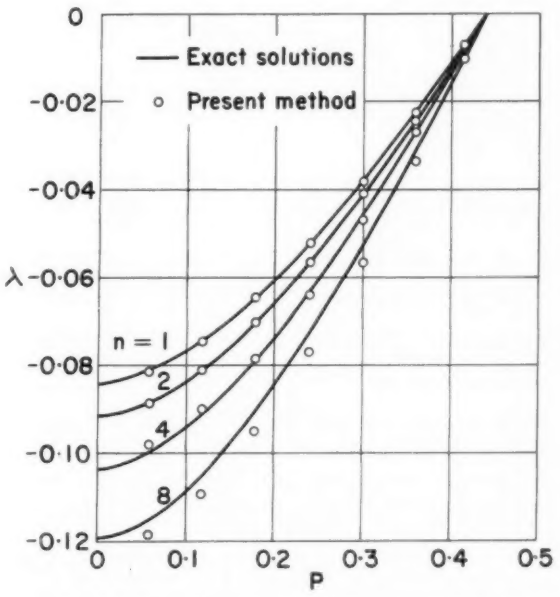

FIG. 2. Relation between the Pohlhausen parameter λ and the nondimensional shearing stress P for the velocity distribution $u_1 = u_1^0(1 - x^n)$, $n = 1$, 2, 4, and 8.

$$\rho u c_p \frac{\partial T}{\partial x} + \rho v c_p \frac{\partial T}{\partial y} = -\rho_1 u u_1 \frac{du_1}{dx} + \frac{\partial}{\partial y}\left(k \frac{\partial T}{\partial y}\right) + \mu \left(\frac{\partial u}{\partial y}\right)^2 \quad (41)$$

where ρ is the density, μ is the viscosity, k is the thermal conductivity, c_p is the specific heat at constant pressure, T is the absolute temperature, suffix 1 denotes the condition at the outer edge of the boundary layer, and other symbols have the same meaning as defined in Part I. μ and k are considered as functions of T, while c_p and the Prandtl Number

$$\sigma = \mu c_p / k \quad (42)$$

are assumed constant. Since the pressure remains constant across the boundary layer, we have

$$\rho / \rho_1 = T_1 / T \quad (43)$$

Outside the boundary layer we have the isentropic relationship

$$\left(\frac{\rho_1}{\rho_0}\right)^{\gamma - 1} = \frac{T_1}{T_0} \quad (44)$$

where γ is the ratio of specific heats, and the suffix 0 denotes a certain reference condition.

It is assumed that there is no heat transfer through the wall. Therefore we have the condition

$$y = 0: \qquad \partial T / \partial y = 0 \quad (45)$$

The Prandtl Number σ is assumed to be slightly different from unity such that the square of the quantity

$$\xi = 1 - \sqrt{\sigma} \quad (46)$$

may be neglected compared to unity. Finally, the viscosity is assumed to be given by the Sutherland formula

$$\mu = \mu_0 C (T / T_0) \quad (47)$$

where

$$C = (T/T_0)^{1/2}[(T_0 + S)/(T + S)] \quad (48)$$

and S is a constant which for air has the value 216°R.

C is not assumed constant, as usually done, but treated as a function of the temperature, because it seems highly desirable to use as accurate a formula as possible for the variation of viscosity with temperature.

Temperature Profile

For a Prandtl Number of unity and zero heat transfer at the wall, the analysis can be considerably simplified because the energy equation (41) is replaced by a simple relation between temperature and velocity, viz.,

$$\frac{T}{T_1} = 1 + \frac{\gamma - 1}{2} \frac{u_1^2}{c_1^2}\left(1 - \frac{u^2}{u_1^2}\right) \quad (49)$$

where c_1 is the local sound speed at the outer edge of the boundary layer. Assuming the Prandtl Number slightly different from unity, we write

$$\frac{T}{T_1} = 1 + \frac{\gamma - 1}{2} \frac{u_1^2}{c_1^2}\left[\sqrt{\sigma}\left(1 - \frac{u^2}{u_1^2}\right) + \xi \Phi\right] \quad (50)$$

where Φ is an undetermined function of u/u_1 such that $\Phi = 0$ when $u/u_1 = 0$. This approximate expression is exact when $\sigma = 1$, and, moreover, it gives the temperature at the wall

$$T_{\text{wall}} = T_1\left(1 + \sqrt{\sigma} \frac{\gamma - 1}{2} \frac{u_1^2}{c_1^2}\right) \quad (51)$$

which seems to be supported by the results of calculation due to Tifford and Chu[17] even in the presence of a pressure gradient.

Assuming the temperature boundary layer has the same thickness as the velocity boundary layer,† and integrating Eq. (41) with respect to y from $y = 0$ to $y = \delta$, we have

$$\int_0^\delta \rho u c_p (T - T_1)\, dy = \frac{1}{2}\int_0^\delta \rho u (u_1^2 - u^2)\, dy \quad (52)$$

Substituting Eq. (50) we obtain

$$\int_0^\delta \rho u \Phi\, dy = \int_0^\delta \rho u \left(1 - \frac{u^2}{u_1^2}\right) dy \quad (53)$$

which yields an integral condition to be satisfied by the function Φ.

Stewartson-Rott Transformation

It was shown by Stewartson[1] that the momentum equation (40) may be transformed into that for an incompressible fluid, provided that there is no heat transfer, the Prandtl Number is unity, and the viscosity is proportional to the absolute temperature. The transformation was modified by Rott[9] such that the effect of Prandtl Number is taken into account, by assuming the temperature profile in a form similar to Eq. (50) where the term $\xi\Phi$ is omitted. The transformation is given by

$$\left.\begin{aligned} X &= \int_0^x \left(\frac{T_1}{T_0}\right)^{\gamma/(\gamma - 1) + (1/2)\sqrt{\sigma}} dx \\ Y &= \left(\frac{T_1}{T_0}\right)^{(1/2)\sqrt{\sigma}} \int_0^y \frac{\rho}{\rho_0}\, dy \end{aligned}\right\} \quad (54)$$

where x and y are the coordinates of the original flow, and X and Y are the coordinates of the transformed flow.

Applying the transformation (54) to the momentum equation (40), and making use of the temperature profile (50) we obtain

$$U(\partial U/\partial X) + V(\partial U/\partial Y) = (1 + \xi B \Phi)[U_1(dU_1/dX)] + \nu_0(\partial/\partial Y)[C(\partial U/\partial Y)] \quad (55)$$

† See also the subsequent footnote.

where U and V are the velocity components in the directions X and Y, U_1 is the velocity outside the boundary layer in the transformed flow, and

$$B = \frac{[(\gamma - 1)/2](u_1^2/c_1^2)}{1 + \sqrt{\sigma}[(\gamma - 1)/2](u_1^2/c_1^2)} \tag{56}$$

There exists a relation between U_1 and u_1 such that

$$U_1 = (T_0/T_1)^{(1/2)\sqrt{\sigma}}\, u_1 \tag{57}$$

and, moreover

$$U/U_1 = u/u_1 \tag{58}$$

Eq. (55) is no longer of the same form as Eq. (2) for the incompressible flow, because the restrictions imposed on the Prandtl Number and the viscosity-temperature relation have been removed. It is still easy to solve, however, since the variable density has disappeared.

Integrating Eq. (55) with respect to Y from $Y = 0$ to $Y = \Delta$ where Δ is the thickness of the boundary layer in the transformed flow, we have

$$\frac{U_1}{\nu_0}\frac{d\Theta^2}{dX} + 2\frac{\Theta^2}{\nu_0}\frac{dU_1}{dX}\left(2 + \frac{\Delta^*}{\Theta} + \frac{\xi B}{\Theta}\int_0^\Delta \Phi\, dY\right) = \frac{2\Theta}{U_1}\left(\frac{\partial U}{\partial Y}\right)_{Y=0} \tag{59}$$

Multiplying Eq. (55) by U and integrating with respect to Y from $Y = 0$ to $Y = \Delta$, we have

$$\frac{U_1}{\nu_0}\frac{d\Theta^{*2}}{dX} + 6\frac{\Theta^{*2}}{\nu_0}\frac{dU_1}{dX}\left(1 + \frac{2}{3}\frac{\xi B}{\Theta^*}\int_0^\Delta \Phi\frac{U}{U_1}\, dY\right) = \frac{4\Theta^*}{U_1^2}\int_0^\Delta C\left(\frac{\partial U}{\partial Y}\right)^2 dY \tag{60}$$

These equations are the analogues of the momentum-integral relation (3) and energy-integral relation (4) respectively, and Δ^*, Θ, and Θ^* are the displacement thickness, momentum thickness, and energy thickness in the transformed flow, respectively,

$$\Delta^* = \int_0^\Delta \left(1 - \frac{U}{U_1}\right) dY \tag{61}$$

$$\Theta = \int_0^\Delta \frac{U}{U_1}\left(1 - \frac{U}{U_1}\right) dY \tag{62}$$

$$\Theta^* = \int_0^\Delta \frac{U}{U_1}\left(1 - \frac{U^2}{U_1^2}\right) dY \tag{63}$$

Velocity Profile

We now assume the velocity profile in the form

$$\frac{U}{U_1} = \frac{Y^2}{\Delta^2}\left(6 - 8\frac{Y}{\Delta} + 3\frac{Y^2}{\Delta^2}\right) + a\frac{Y}{\Delta}\left(1 - \frac{Y}{\Delta}\right)^3 \tag{64}$$

where a is the profile parameter. This is exactly the same as used in incompressible flow, Eq. (11).

Since C and Φ are functions of u/u_1, or of U/U_1 by virtue of Eq. (58), they may be considered as functions of Y/Δ. We assume therefore

$$C = \alpha_0 + \alpha_1(Y/\Delta) + \alpha_2(Y^2/\Delta^2) + \alpha_3(Y^3/\Delta^3) \tag{65}$$

$$\Phi = \beta_0 + \beta_1(Y/\Delta) + \beta_2(Y^2/\Delta^2) + \beta_3(Y^3/\Delta^3) + \beta_4(Y^4/\Delta^4) \tag{66}$$

where the coefficients, α's and β's, are determined by the conditions†

$$\left.\begin{aligned} Y = 0\text{:}\quad & C = C_0,\quad \partial C/\partial Y = 0,\\ & \Phi = 0,\quad \partial\Phi/\partial Y = 0\\ Y = \Delta\text{:}\quad & C = C_1,\quad \partial C/\partial Y = 0,\\ & \Phi = 0,\quad \partial\Phi/\partial Y = 0 \end{aligned}\right\} \tag{67}$$

and

† These boundary conditions are based on the assumption that the temperature boundary layer has the same thickness as the velocity boundary layer. This is not correct except when the Prandtl Number is unity. However, the error due to this assumption is considered small, because the function C is multiplied by $(\partial U/\partial Y)^2$ which is small near the outer edge of the boundary layer, and also the function Φ is multiplied by ξ which is assumed small in the present analysis.

TABLE 1

a	D	E	F	G	ln G	H	P	Q	Q/G^2	J	K
0	0.4000	0.1143	0.1750	1.531	0.4262	3.500	0	0.960	0.4094	0.333	2.382
0.25	0.3875	0.1164	0.1784	1.532	0.4268	3.328	0.0582	0.962	0.4098	0.317	2.330
0.50	0.3750	0.1181	0.1812	1.535	0.4285	3.176	0.1181	0.968	0.4109	0.298	2.282
0.75	0.3625	0.1192	0.1834	1.539	0.4311	3.041	0.1788	0.979	0.4133	0.278	2.238
1.00	0.3500	0.1198	0.1850	1.544	0.4345	2.921	0.2397	0.994	0.4169	0.257	2.198
1.25	0.3375	0.1200	0.1860	1.550	0.4383	2.813	0.3000	1.014	0.4219	0.236	2.161
1.50	0.3250	0.1196	0.1862	1.557	0.4425	2.716	0.3589	1.038	0.4282	0.214	2.125
1.75	0.3125	0.1188	0.1858	1.564	0.4471	2.630	0.4158	1.066	0.4357	0.193	2.092
2.00	0.3000	0.1175	0.1845	1.571	0.4518	2.554	0.4698	1.097	0.4443	0.173	2.060
2.25	0.2875	0.1156	0.1825	1.579	0.4566	2.486	0.5203	1.130	0.4536	0.154	2.029
2.50	0.2750	0.1133	0.1797	1.586	0.4613	2.427	0.5665	1.165	0.4632	0.137	1.999
3.00	0.2500	0.1071	0.1714	1.600	0.4700	2.333	0.6429	1.234	0.4821	0.107	1.940
3.50	0.2250	0.0990	0.1595	1.611	0.4767	2.273	0.6931	1.290	0.4970	0.084	1.879
4.00	0.2000	0.0889	0.1436	1.615	0.4796	2.250	0.7111	1.313	0.5031	0.067	1.812
4.50	0.1750	0.0768	0.1235	1.608	0.4752	2.279	0.6911	1.281	0.4952	0.054	1.731
5.00	0.1500	0.0627	0.0989	1.578	0.4561	2.392	0.6270	1.165	0.4678	0.046	1.622

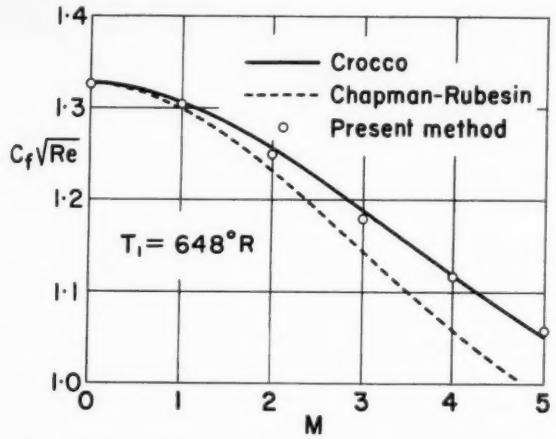

FIG. 3. Skin-friction coefficient of a flat plate plotted against the Mach Number. Free-stream temperature 648°R., Prandtl Number 0.72.

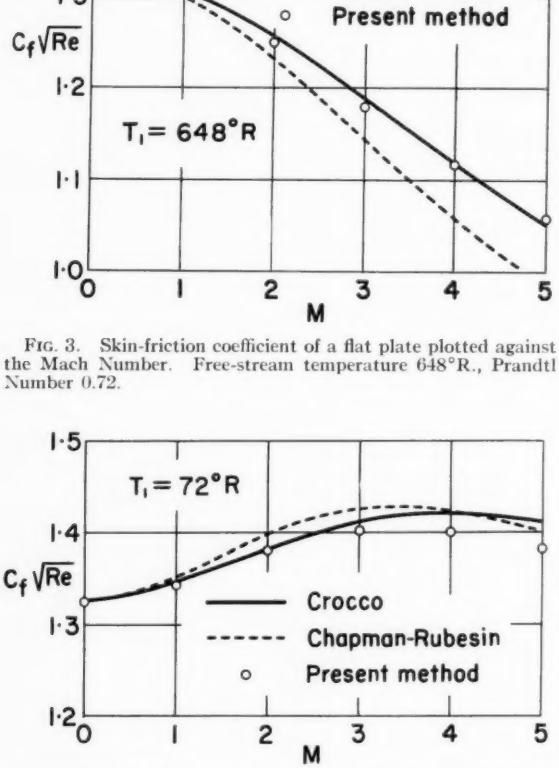

FIG. 4. Skin-friction coefficient of a flat plate plotted against the Mach Number. Free-stream temperature 72°R., Prandtl Number 0.72.

$$\int_0^{\Delta} \Phi \frac{U}{U_1}\, dY = \Theta^* \tag{68}$$

the last condition being obtained from Eqs. (53) and (63).

The reference condition 0 is now chosen such that the temperature T_0 is given by the relation

$$T_0 = T_1\{1 + \sqrt{\sigma}[(\gamma - 1)/2](u_1^2/c_1^2)\} \tag{69}$$

In other words, T_0 is equal to the wall temperature [Eq. (51)]. With this definition we have

$$C_0 = 1,\ C_1 = (T_1/T_0)^{1/2}[(T_0 + S)/(T_1 + S)] \tag{70}$$

Eqs. (59) and (60) are then written in the form

$$\frac{U_1}{\nu_0}\frac{d\Theta^2}{dX} + 2(2 + H + \xi BK)\frac{\Theta^2}{\nu_0}\frac{dU_1}{dX} = P \tag{71}$$

$$\frac{U_1}{\nu_0}\frac{dG^2\Theta^2}{dX} + 6\left(1 + \frac{2}{3}\xi B\right)\frac{G^2\Theta^2}{\nu_0}\frac{dU_1}{dX} = Q[1 + J(C_1 - 1)] \tag{72}$$

respectively, where G, H, P, and Q are given by Eqs. (13), (17), (18), (19), (20), and (21), and

$$K = \frac{1}{E}\left(\frac{584}{2145} - \frac{146}{57915}a - \frac{19763}{3127410}a^2\right) \tag{73}$$

$$J = (1/Q)\{16/35 - (13/105)a + a^2/84\} \tag{74}$$

K and J are also dependent only on a, and their numerical values are given in Table 1.

Eqs. (71) and (72) are almost identical with Eqs. (15) and (16) for incompressible flow, the only difference being in the term proportional to ξB and the term proportional to $(C_1 - 1)$. These additional terms represent the effect of Prandtl Number different from unity, and the effect of viscosity-temperature relation different from a simple proportionality, respectively.

Approximate Method of Solution

Eqs. (71) and (72) may be solved in exactly the same way as in incompressible flow. The quadrature formula for the momentum thickness in the transformed flow is

$$\frac{\Theta^2}{\nu_0} = \frac{Q_m}{G_m^2}\, U_1^{-6}\int_0^X U_1^5\,[1 + J_m(C_1 - 1)]\, dX \tag{75}$$

which is obtained from Eq. (72) by neglecting the term $(2/3)\xi B$ and replacing Q, G, and J by constant values corresponding to the flow along a flat plate.† Then, eliminating $d\Theta^2/dX$ from Eqs. (71) and (72), we obtain

$$\Lambda[H - 1 + \xi B(K - 2)] = (1/2)P - (Q/2G^2)[1 + J(C_1 - 1)] + \Lambda[(d\ln G)/(d\ln U_1)] \tag{76}$$

which yields the relation between the profile parameter a and the Pohlhausen parameter in the transformed flow

$$\Lambda = (\Theta^2/\nu_0)(dU_1/dX) \tag{77}$$

Eqs. (75), (76), and (77) correspond to Eqs. (26), (28), and (24), respectively.

Skin Friction on a Flat Plate

In order to check the accuracy of the method, the skin friction on a flat plate is calculated and compared with that given by other solutions. First, the parameter a is determined from the condition

$$P = (Q/G^2)[1 + J(C_1 - 1)] \tag{78}$$

which is obtained by putting $\Lambda = 0$ and $G =$ constant in Eq. (76). Next, the momentum thickness Θ in the transformed flow is determined by integrating Eq. (71) in the form

$$\Theta^2 = P(\nu_0 X/U_1) \tag{79}$$

Then the coefficient of skin friction based on the free-stream characteristics is given by

$$C_f = \frac{4}{\rho_1 u_1^2}\left(\mu\frac{\partial u}{\partial y}\right)_{y=0} = \frac{2\sqrt{P}}{\sqrt{C_1}\sqrt{Re}} \tag{80}$$

† For most practical purposes, values corresponding to incompressible flow ($a = 1.857$, $Q_m/G_m^2 = 0.44$, $J_m = 0.184$) may be used with sufficient accuracy.

where $Re = u_1 x/\nu_1$ is the Reynolds Number based on the distance from the leading edge.

Values of $C_f\sqrt{Re}$ are calculated for various values of Mach Number $M = u_1/c_1$ assuming $\gamma = 1.4$ and $\sigma = 0.72$ ($\xi = 0.15$). Results for the free-stream temperature $T_1 = 648°$R. and $T_1 = 72°$R. are represented in Figs. 3 and 4, respectively. Included for comparison are results calculated by Crocco[10] and by Chapman and Rubesin.[18] Crocco's results are considered to be most reliable because he used the Sutherland formula (47), while Chapman and Rubesin replaced C by a constant value. It is seen from this comparison that the present method gives results which are sufficiently accurate for practical purposes. It is also to be noted that the effect of Prandtl Number is rather small compared with the effect of viscosity-temperature relation different from a simple proportionality.

Compressibility Effect on Separation

Transforming back to the original flow, we obtain from Eqs. (75) and (77)

$$\Lambda = \frac{Q_m}{G_m^2}\left(\frac{T_0}{T_1}\right)^{\frac{2\gamma-1}{\gamma-1}-2\sqrt{\sigma}}\frac{du_1}{dx}\,u_1^{-6}\int_0^x\left\{1+J_m(C_1-1)\right\}\left(\frac{T_1}{T_0}\right)^{\frac{\gamma}{\gamma-1}-2\sqrt{\sigma}}u_1^5\,dx \quad (81)$$

where T_0/T_1 is given by Eq. (69). This formula enables us to calculate Λ directly from the velocity distribution in the original flow. The relation between Λ and a may be determined from Eq. (76), where $\ln U_1$ should preferably be replaced by $\ln u_1 - (\sqrt{\sigma}/2)\ln(T_1/T_0)$.

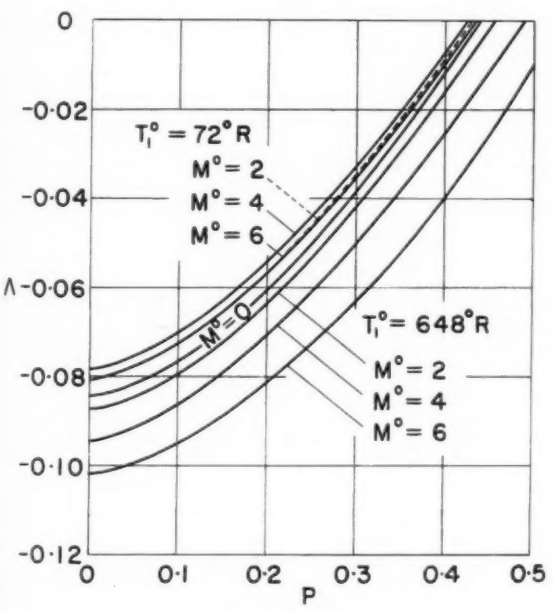

FIG. 5. Relation between the Pohlhausen parameter Λ in the transformed flow and the nondimensional shearing stress P for the velocity distribution $u_1 = u_1^0(1 - x)$.

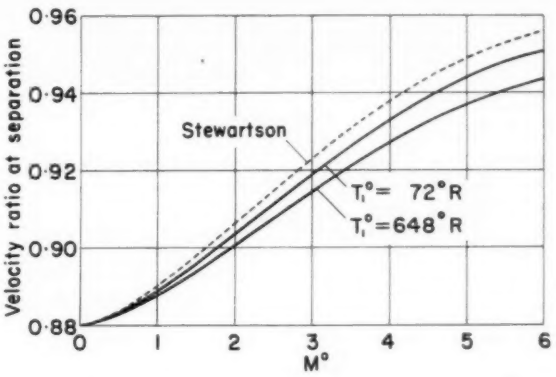

FIG. 6. Effect of compressibility on separation for the velocity distribution $u_1 = u_1^0(1 - x)$. The velocity ratio at the separation point is plotted against the Mach Number.

As an example of the application of the method, the calculation was made for the boundary layer when the velocity outside the boundary layer is given by

$$u_1 = u_1^0(1 - x) \quad (82)$$

where u_1^0 is the value of u_1 at $x = 0$. It is assumed that $\gamma = 1.4$, $\sigma = 0.72$ ($\xi = 0.15$), and the free-stream temperature at $x = 0$ is $T_1^0 = 648°$R. and $T_1^0 = 72°$R., respectively. Results are shown in Fig. 5, where the Pohlhausen parameter Λ is plotted against the nondimensional shearing stress P for various values of the Mach Number $M^0 = u_1^0/c_1^0$. As in the skin friction on a flat plate, the effect of compressibility is greater for the case $T_1^0 = 648°$R. than for the case $T_1^0 = 72°$R.

The separation point is determined by locating the value of x for which Λ attains the value corresponding to $P = 0$. Results of this calculation are shown in Fig. 6, where the velocity ratio u_1/u_1^0 at the separation point is plotted against the Mach Number M^0. Included also is the result calculated by Stewartson[1] by assuming that the Prandtl Number is unity, the viscosity is proportional to temperature, and the value of Λ at separation is the same as for incompressible flow. In spite of these assumptions, Stewartson's results appear to be comparatively good; this is because of the fortunate circumstances that the separation is delayed by the effect of viscosity-temperature relation different from a simple proportionality, while it is hastened by the effect of distortion of velocity distribution in the transformation (54) and (57).

REFERENCES

[1] Stewartson, K., *Correlated Incompressible and Compressible Boundary Layers*, Proc. Roy. Soc., London, Vol. 200, pp. 84–100, 1949.

[2] Pohlhausen, K., *Zur näherungsweisen Integration der Differentialgleichung der laminaren Grenzschicht*, Zeitschr. f. angew. Math. u. Mech., Vol. 1, pp. 252–268, 1921.

[3] Howarth, L., *On the Solution of the Laminar Boundary Layer Equations*, Proc. Roy. Soc., London, Vol. 164, pp. 547–579, 1938.

(*Continued on page 504*)

Readers' Forum

BRIEF REPORTS of investigations in the aeronautical sciences and discussions of papers published in the JOURNAL are presented in this special department. The publication will be completed as soon as possible after receipt of the material. The Editorial Committee does not hold itself responsible for the opinions expressed by the correspondents.

A Note About the Effects of Product of Inertia on Lateral Stability

C. N. Tsu
Design Specialist, Northrop Aircraft, Inc., Hawthorne, Calif.
February 18, 1954

IN REFERENCES 1–3, the importance of the products of inertia on lateral stability of aircraft has been shown. This note points out a step in evaluating the effects of the product of inertia on aircraft dynamic lateral stability which may simplify to some extent this evaluation.

The lateral equations of motion from reference 1 are repeated below for convenience.

$$(I_xD^2 - C_{l_{\dot\phi}}D)\phi - (I_{xz}D^2 + C_{l_{\dot\psi}}D)\psi - C_{l_\beta}\beta = 0 \quad (1)$$

$$(I_zD^2 - C_{n_{\dot\psi}}D)\psi - (I_{xz}D^2 + C_{n_{\dot\phi}}D)\phi - C_{n_\beta}\beta = 0 \quad (2)$$

$$[(2b\mu/V)(D\psi + D\beta)] - (C_L + C_{y_{\dot\phi}}D)\phi - (C_L \tan\gamma + C_{y_{\dot\psi}}D)\psi - C_{y_\beta}\beta = 0 \quad (3)$$

It is observed from the above equations that the product of inertia terms $I_{xz}D^2\psi$ and $I_{xz}D^2\phi$ are only in Eqs. (1) and (2). By the manipulations of $[I_x(1) + I_{xz}(2)]$ and $[I_z(2) + I_{xz}(1)]$ Eqs. (1) and (2) now may be rewritten as (1′) and (2′).

$$(I_xD^2 - C_{l_{\dot\phi}}'D)\phi - C_{l_{\dot\psi}}'D\psi - C_{l_\beta}'\beta = 0 \quad (1')$$

$$(I_zD^2 - C_{n_{\dot\psi}}'D)\psi - C_{n_{\dot\phi}}'D\phi - C_{n_\beta}'\beta = 0 \quad (2')$$

where

$$C_{l_{\dot\phi}}' = [C_{l_{\dot\phi}} + (I_{xz}/I_z)C_{n_{\dot\phi}}]/\{1 - [(I_{xz}/I_x)(I_{xz}/I_z)]\} \quad (4)$$

$$C_{l_{\dot\psi}}' = [C_{l_{\dot\psi}} + (I_{xz}/I_z)C_{n_{\dot\psi}}]/\{1 - [(I_{xz}/I_x)(I_{xz}/I_z)]\} \quad (5)$$

$$C_{l_\beta}' = [C_{l_\beta} + (I_{xz}/I_z)C_{n_\beta}]/\{1 - [(I_{xz}/I_x)(I_{xz}/I_z)]\} \quad (6)$$

$$C_{n_{\dot\psi}}' = [C_{n_{\dot\psi}} + (I_{xz}/I_x)C_{l_{\dot\psi}}]/\{1 - [(I_{xz}/I_x)(I_{xz}/I_z)]\} \quad (7)$$

$$C_{n_{\dot\phi}}' = [C_{n_{\dot\phi}} + (I_{xz}/I_x)C_{l_{\dot\phi}}]/\{1 - [(I_{xz}/I_x)(I_{xz}/I_z)]\} \quad (8)$$

$$C_{n_\beta}' = [C_{n_\beta} + (I_{xz}/I_x)C_{l_\beta}]/\{1 - [(I_{xz}/I_x)(I_{xz}/I_z)]\} \quad (9)$$

Thus the form of Eqs. (1′) and (2′) become identical to that of Eqs. (1) and (2) with I_{xz}, the product of inertia, made zero. Consequently, the effects of product of inertia on dynamic lateral stability may now be evaluated both qualitatively and quantitatively through the use of equivalent lateral stability derivatives as defined in relationships (4) through (9). Known effects of stability derivatives on dynamic stability may now be utilized to anticipate the effects of product of inertia. Stability boundary plots such as contained in the references may now be plotted in terms of these equivalent rolling moment and yawing moment derivatives with side force derivatives remaining unaltered.

When rudder and aileron controls are involved, it can be shown that the resulting equivalent yawing and rolling moment control derivatives are related to the natural derivatives in the same way as the stability derivatives.

REFERENCES

[1] Sternfield, L., *Some Considerations of the Lateral Stability of High Speed Aircraft*, NACA TN No. 1282, 1947.

[2] McKinney, M. O., Jr., and Drake, H. M., *Correlation of Experimental and Calculated Effects of Products of Inertia on Lateral Stability*, NACA TN No. 1370, 1947.

[3] Sternfield, L., *Effects of Product of Inertia on Lateral Stability*, NACA TN No. 1193, 1947.

Concluding Remarks on Detached Shock Waves

Robert Wesley Truitt
Professor of Aeronautical Engineering, Virginia Polytechnic Institute, Blacksburg, Va.
February 18, 1954

IN REFERENCE 1, I took issue with Laitone's statement that Moeckel's result[2] for shock detachment distance was not valid for thin wedges near Mach Number one. It was shown quite clearly in Fig. 1,[1] that Moeckel's values for semiangle $\theta = 4.5°$ at Mach Numbers near unity are in excellent agreement with experiment, whereas Laitone's formula showed extremely poor agreement.

Laitone is correct when later,[3] in explaining his poor agreement with experiment, he concludes that his own formula [Eq. (3)[4]: " . . . rightly may be restricted to Mach Numbers less than 1.01! For Mach Numbers greater than this—i.e., when the results [Laitone's Eq. (3)[4]] do *not* apply—there cannot be any important effect of nose shape, . . . "

It should be pointed out, however, that earlier in Fig. 7,[5] Laitone *does* apply and compare his Eq. (3),[4] with Moeckel's result[2] in the free-stream Mach Number range $(1.1 \leq M_0 \leq 1.5)$ and concludes: " . . . Fig. 7[5] proves there is a considerable effect for *slender* wedges ($\theta = 5°, 10°, 15°$) *near* Mach Number of unity." It is clear that, at that time, Laitone considered Mach Numbers, $(1.1 \leq M_0 \leq 1.5)$, sufficiently near Mach Number one to compare his results with Moeckel's. Laitone also shows *his* experimental results in Fig. 7[5] to be in accord with his Eq. (3)[4] for the same Mach Number range.

In view of reliable experimental results shown in Fig. (1),[1] it must be concluded that Laitone's theoretical and experimental results shown in Fig. 7,[5] are not only incorrect but misleading.

REFERENCES

[1] Truitt, R. W., *Comments on Location of Detached Shock Waves Ahead of Plane Bodies*, Readers' Forum, Journal of the Aeronautical Sciences, Vol. 20, No. 9, p. 651, September, 1953.

[2] Moeckel, W. E., *Approximate Method for Predicting the Form and Location of Detached Shock Waves Ahead of Plane and Axially Symmetric Bodies*, NACA TN No. 1921, July, 1949.

[3] Laitone, E. V., *Comments on Location of Detached Shocks and Truitt's Dilemma*, Readers' Forum, Journal of the Aeronautical Sciences, Vol. 21, No. 1, pp. 64–65, January, 1954.

[4] Laitone, E. V., *Comments on a Method for Location of Detached Shock Waves Ahead of Plane Bodies*, Readers' Forum, Journal of the Aeronautical Sciences, Vol. 20, No. 5, p. 360, May, 1953.

[5] Laitone, E. V., *A Study of Transonic Gas Dynamics by the Hydraulic Analogy*, Journal of the Aeronautical Sciences, Vol. 19, No. 4, pp. 265–272, April, 1952.

Factors Affecting Transition Reynolds Numbers on Models in Supersonic Wind Tunnels

John Laufer
Senior Research Engineer, Jet Propulsion Laboratory, California Institute of Technology, Pasadena, Calif.
February 19, 1954

RECENT PUBLICATIONS[1, 2] have indicated that the transition Reynolds Number of boundary layers on the same 10° cone in different wind tunnels varied greatly in no obviously predictable fashion. The great scatter of the experimental data was believed to be caused by disturbances of various degrees present in the tunnels.

These investigations indicate clearly that if a quantitative study of the mechanism of the transition phenomenon is to be undertaken in a wind tunnel, the elimination or understanding of perturbation fields of the flow in wind tunnels is essential.

In general, these disturbances found in supersonic wind tunnel nozzle flows may be of three different types[3]: (a) vorticity fluctuations (or transverse waves); (b) sound, or longitudinal waves—including weak compression waves emanating from the imperfect nozzle walls; and (c) temperature fluctuations. Although these disturbances are coupled especially at higher Mach Numbers, one can make some statement as to their possible origin in wind tunnels. For instance, a considerable amount of vorticity fluctuations is generated by blowers, turning vanes, honey combs, etc. Longitudinal wave type disturbances can originate from poorly fabricated nozzle walls or possibly from turbulent shear layers.[4] Finally, temperature fluctuations might be caused by inadequate mixing of air in coolers or by large local turbulent dissipation. Unfortunately, at the present time no adequate experimental method is available that would permit a direct study of these effects.

The method of approach to this problem adopted at the Jet Propulsion Laboratory of the California Institute of Technology is an indirect one. It is proposed to attempt a successive elimination of the above mentioned three contributions to the perturbation field in the supersonic tunnel. Strictly speaking, of course, this is not possible because of the interaction existing between them. However, since one has some physical picture of the origin of the largest part of these disturbances, one might artificially change the conditions under which they are generated. Specifically, the variation, if any, of the boundary layer transition Reynolds Number could be observed on a wind tunnel model under two conditions; first, when disturbances of type (a) are reduced by installing damping screens in the tunnel settling chamber; second, when they are greatly increased by the installation of a grid before the contraction. Similar experiments can be carried out involving disturbances of types (b) and (c).

At present only the first set of experiments, as described above, has been carried out at this Laboratory in the 18 in. by 20 in. supersonic wind tunnel. The turbulence levels in the settling chamber under the two conditions were 0.6 per cent and 7 per cent. These values were approximately constant for the Mach Number range 1.4 to 4.0, and nearly independent of the tunnel stagnation pressure. The temperature fluctuations were negligibly small.

A 5° included angle cone, 100 cm. in length, was used as the wind tunnel model. The method of detecting transition was similar to that reported in reference 1. Thermocouples were placed 2 cm. apart and surface temperatures were recorded. The sudden rise in temperature indicated transition.

Some typical results are given in Figs. 1, 2, and 3. The values of the ordinate are proportional to the difference of the model surface temperature, T_s and the temperature at the outer edge of the boundary layer, T. The Reynolds Number is defined in terms of free stream conditions and wetted length on the cone surface. The results were normalized by the factor A, to yield identical values of temperature difference for the laminar portion of the boundary layer.

The results may be summarized as follows: In the low Mach Number flows ($M < 2.5$) the turbulence level of the settling chamber had a strong effect on the boundary layer transition Reynolds Number. However, no such effect could be detected for flows at $M > 2.5$. This result was further substantiated by similar experiments conducted in the JPL 12- by 12-in. supersonic tunnel. The working section of this tunnel has a much different entrance condition and a contraction ratio only one-third as large as the 18- by 20-in. tunnel. Some experiments on the transition Reynolds Number of a flat plate boundary layer

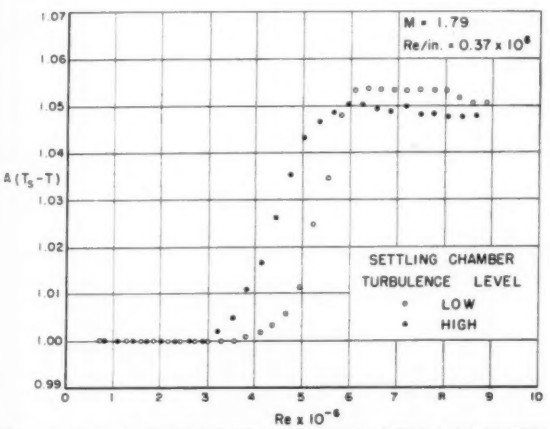

Figure 1. SURFACE TEMPERATURE DISTRIBUTION ALONG CONE SURFACE

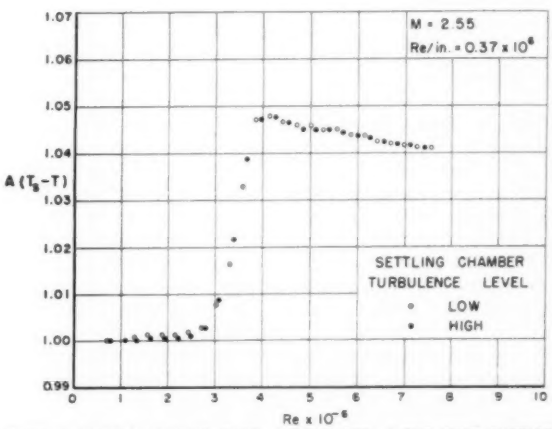

Figure 2. SURFACE TEMPERATURE DISTRIBUTION ALONG CONE SURFACE

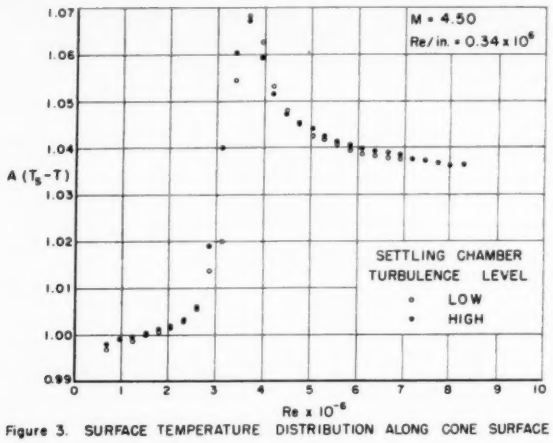

Figure 3. SURFACE TEMPERATURE DISTRIBUTION ALONG CONE SURFACE

conducted in the 18- by 20-in. tunnel were also consistent with the above conclusion.

It is interesting to note that in the Mach Number range $1.4 < M < 4$ the transition Reynolds Number decreased monotonically with increasing Mach Number for constant Reynolds Number per inch, a trend also reported in reference 5.

References

[1] Ross, Albert O., *Determination of Boundary Layer Transition Reynolds Numbers by Surface Temperature Measurement of a 10° Cone in Various NACA Supersonic Wind Tunnels*, NACA TN No. 3020, Oct., 1953.

[2] Czarnecki, K. R., and Sinclair, A. R., *Factors Affecting Transition at Supersonic Speeds*, NACA RM L53I 18a, Nov., 1953.

[3] Kovásznay, L. S. G., *Turbulence in Supersonic Flow*, Journal of the Aeronautical Sciences, Vol. 20, No. 10, pp. 657–674, Oct., 1953.

[4] Liepmann, H. W., *Aspects of the Turbulence Problem*, Zeitschrift für Angewandte Mathematik und Physik, Vol. 3, Part I, pp. 321–342, 1952.

[5] Lange, A. H., Gieseler, L. P., and Lee, R. E., *Variation of Transition Reynolds Number with Mach Number*, Readers' Forum, Journal of the Aeronautical Sciences, Vol. 20, No. 10, p. 718, Oct., 1953.

Transonic Flow Past Wedge Profiles by Hydraulic Analogy

E. V. Laitone* and Helmer Nielsen†
University of California, Berkeley, and Ames Aeronautical Laboratory, NACA, Moffett Field, Calif., Respectively
February 19, 1954

BY UTILIZING the analogy existing between the gravity waves propagated in shallow water and the two-dimensional flow of a perfect gas with a specific heat ratio of 2, an experimental study was made of the transonic flow about symmetrical slender wedge profiles.

In the hydraulic analogy the local water depth corresponds to both the density and the temperature of the transonic gas flow. This permits direct evaluation of the equivalent gas flow velocity distribution by simply measuring the variation of the water depth. However, since the tests were made by towing the model through $^1/_4$-in. deep water (the best conditions for the analogy[1]), it was practically impossible to measure the surrounding water depths by pressure measurements or simple depth gages. Consequently, the water heights were evaluated by measuring the variation in the electrical resistance of 0.004-in. diameter piano wire probes.

* Associate Professor.
† Aeronautical Research Scientist.

These water height measurements were used to compute the velocity distribution along the stagnation streamline from the detached shock wave to the nose of the wedge. The experimental data shown in Fig. 1 were thus obtained by Nielsen,[2] and are presented in terms of the standard pressure coefficient defined as

$$C_p = (p - p_1)/[(1/2)\rho_1 V_1^2] = (2/\gamma M_1^2)\,[(p/p_1) - 1] \quad (1)$$

or corresponding to the hydraulic analogy with a specific heat ratio of $\gamma = 2$ as

$$C_p = (1/M_1^2)\,[(h/h_1)^2 - 1] = (gh_1/V_1^2)\,[(h/h_1)^2 - 1] \quad (2)$$

The data presented in Fig. 1 were those obtained with a wedge base width of $^3/_4$ in. (Y_s = One-half base width = $^3/_8$ in.) and with semivertex angles (θ) of 5° and 20°. The distance X was measured along the stagnation streamline ahead of the wedge as shown in Fig. 1.

Fig. 2 summarizes the experimental data of reference 2 in terms of the detachment distance ($X = L$) measured to the foremost position (normal shock portion) of the detached bow shock wave.

The principal aim of these tests was to check the validity of the simplifying assumptions of the small perturbation theory presented in reference 3 for determining the location of the detached bow shock wave as the Mach Number approached unity. The theory developed in reference 3 was based on the observation that in the limiting case as the Mach Number approached unity, the detached bow shock wave and the sonic line became nearly parallel lines, far apart, and both extending an unlimited distance from the body. Then the interaction between the sonic line and the detached shock would be negligible, so the velocity variation along the stagnation streamline should be practically the same as that produced in a subsonic flow having $M_\infty \equiv M_2 = (2 -$

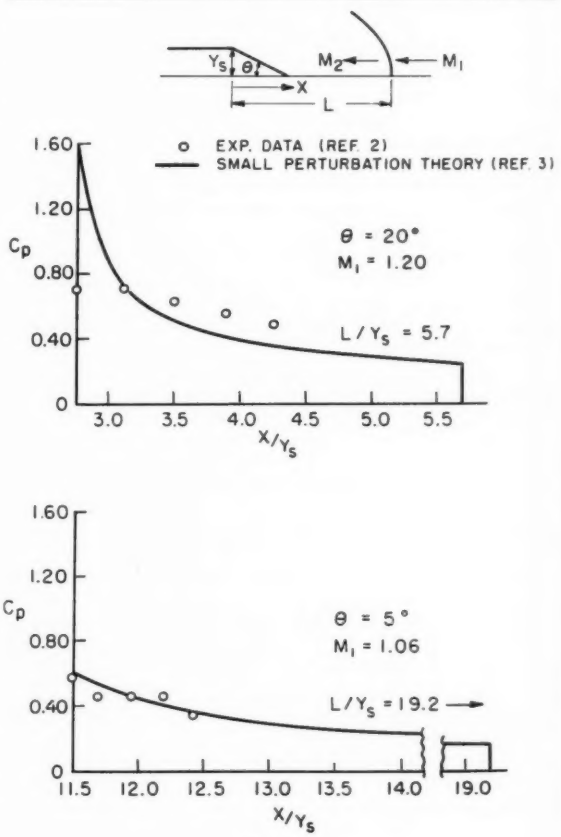

FIG. 1.

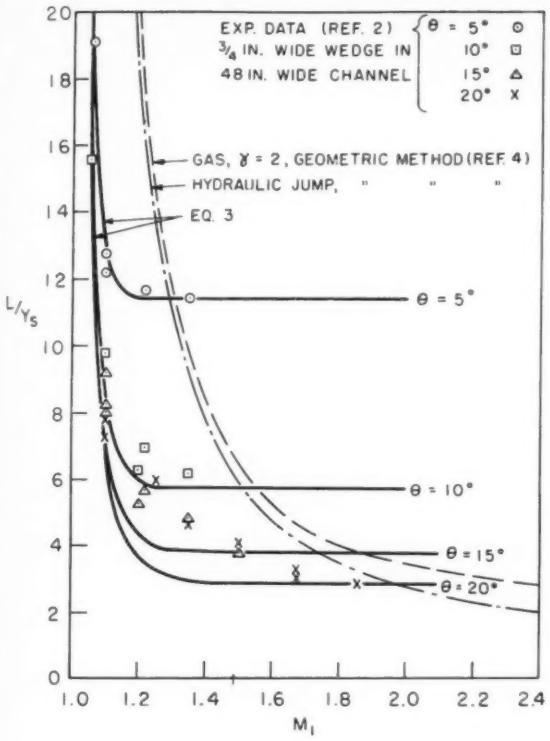

FIG. 2.

M_1). Then it was shown that the shock wave detachment distance would be determined as the distance ahead on the stagnation streamline where the velocity drop through the normal shock portion (with M_1 ahead and M_2 behind) produced the required velocity ratio corresponding to the subsonic flow velocity variation along the stagnation streamline. This yields the expression for the detachment distance L from the shoulder of the wedge as

$$\ln [1 - (Y_s/\theta L)]^{-1} = [(4\sqrt{2}\,\pi)/(\gamma + 1)\theta]\,(M_1 - 1)^{3/2} \quad (3)$$

which agrees with the transonic similarity relation. The experimental data on the detachment distance for the slenderest wedge tested in reference 2 compared favorably with this theory, as shown in Fig. 2, but, as would be expected, only for Mach Numbers approaching unity.

Fig. 1 compares the velocity or pressure coefficient variation used in the small perturbation theory of reference 3 with the experimental values calculated from the measured local water depths. It is seen that there is some justification in assuming that the flow variation behind the detached shock is similar to that in subsonic flow, but in agreement with the basic assumption, only for the slenderest wedge at Mach Numbers near unity. At the higher Mach Numbers or larger nose angles the velocity gradient became radically different from the subsonic variation assumed in reference 3, as would be expected.

It is interesting to note that the experimental work being conducted at the present time indicates that as the channel walls are moved nearer to the model, the detached shock moves farther ahead of the nose, especially for Mach Numbers near unity. The measured distance, just before choking or a strong Mach-reflection occurs, tends to approach Moeckel's[4] result, which predicts a detachment distance independent of the wedge angle.

REFERENCES

[1] Laitone, E. V., *A Study of Transonic Gas Dynamics by the Hydraulic Analogy*, Journal of the Aeronautical Sciences, Vol. 19, No. 4, pp. 265–272, April, 1952.

[2] Nielsen, Helmer, *Study of the Flow Field Behind Detached Shock Waves at Transonic Velocities by the Surface Wave Analogy*, M.S. Thesis, University of California, Berkeley, 1951.

[3] Laitone, E. V., *A Note on Detached Shock Waves*, Journal of the Aeronautical Sciences, Vol. 16, No. 7, pp. 441–442, July, 1949.

[4] Moeckel, W. E., *Approximate Method for Predicting Form and Location of Detached Shock Waves Ahead of Plane or Axially Symmetric Bodies*, NACA TN No. 1921, July, 1949.

Errata to "The Calculation of Wall Shearing Stress from Heat-Transfer Measurements in Compressible Flows"[1]

Nick S. Diaconis
Lewis Flight Propulsion Laboratory, NACA, Cleveland, Ohio
May 6, 1954

EQS. (9), (12), AND (13) are incorrect. The correct solution of Eq. (6) results in the following

$$T_1 = T_{ad} - [(\gamma - 1)/2] M_\infty^2 K\eta^2$$

$$T_2 = (T_w - T_{ad}) + \left[(T_{ad} - T_w)/\int_0^\infty e^{-\omega^2}\,d\omega\right]\int_0^u e^{-\omega^2}\,d\omega$$

This correction in the temperature distribution has no effect on the expression for the Nusselt Number, Eq. (16), or the conclusions.

REFERENCE

[1] Diaconis, N. S., Journal of the Aeronautical Sciences, Readers' Forum, Vol. 21, No. 3, p. 201, March, 1954.

Aerodynamic Coefficients of an Oscillating Airfoil in Two-Dimensional Subsonic Flow

R. Timman, A. I. van de Vooren, and J. H. Greidanus
National Aeronautical Research Institute, Amsterdam-W, Holland
February 7, 1954

NUMERICAL VALUES for the aerodynamic coefficients of an oscillating wing in two-dimensional subsonic flow, calculated by aid of an analytical solution in terms of Mathieu functions, have been published by the authors in THIS JOURNAL.[1, 2] Considerable question regarding the accuracy of these values was put forward by Fettis[3] and Jordan[4] with the argument that the reciprocity relation, which was not known at the time that the authors published their data, was not satisfied. Consequently it was investigated whether the formulas giving the final solution were in agreement with the reciprocity relation. This appeared to be the case as has been shown by Timman,[5] who also simplified the formula used for calculating the strength of the pressure singularity at the leading edge. The reason that the numerical values did not satisfy the reciprocity relation was that in spite of numerous checks one small error had been made in the numerical evaluation. Meanwhile, this error has been eliminated by the Mathematical Centre and revised values satisfying the reciprocity relation up to a few units in the fifth decimal figure, are now available. The values for the wing alone are given subsequently, but values for the wing with control surface and for the same parameter values as in reference 2 may be applied for at the above mentioned address.

Table of Aerodynamic Coefficients for an Oscillating Wing Without Control Surface in a Subsonic Compressible Flow

	ω	k_a'	k_a''	m_a'	m_a''	k_b'	k_b''	m_b'	m_b''
$\beta = 0.35$	0.12526	−0.03780	−0.20708	0.02305	0.10310	−1.63901	0.19841	0.83864	−0.23938
	0.25071	−0.04504	−0.35479	0.05835	0.17531	−1.47348	0.00434	0.73659	−0.28036
	0.37607	−0.00721	−0.48870	0.08358	0.23923	−1.38307	−0.22005	0.69553	−0.30712
	0.50143	0.07066	−0.62280	0.10669	0.30135	−1.34873	−0.44226	0.68462	−0.33724
	0.62679	0.18513	−0.76311	0.13000	0.36391	−1.34751	−0.65928	0.69158	−0.37303
	0.75214	0.33416	−0.91357	0.15526	0.42783	−1.36988	−0.87210	0.71078	−0.41456
	1.00286	0.73149	−1.25889	0.21672	0.56101	−1.47202	−1.29041	0.77549	−0.51389
	1.25357	1.25435	−1.68831	0.30040	0.70093	−1.64720	−1.70144	0.86627	−0.63487
	1.88036	2.98984	−3.35837	0.66249	1.04848	−2.44851	−2.63852	1.16267	−1.04038
	3.25929	5.65269	−10.76088	2.26230	0.94136	−5.56393	−2.67570	1.74483	−2.33706
$\beta = 0.50$	0.150	−0.05383	−0.24597	0.04232	0.12124	−1.68214	0.23763	0.83270	−0.30922
	0.300	−0.05380	−0.41753	0.08578	0.20097	−1.47756	−0.02165	0.72370	−0.36423
	0.450	0.00624	−0.58574	0.12756	0.27335	−1.42920	−0.28722	0.69241	−0.42089
	0.600	0.11518	−0.76998	0.17467	0.34475	−1.45797	−0.53672	0.69439	−0.49342
	0.750	0.26531	−0.98147	0.23215	0.41567	−1.54078	−0.76941	0.71295	−0.58283
	0.900	0.44865	−1.22993	0.30397	0.48419	−1.67055	−0.98266	0.73908	−0.68912
	1.125	0.76270	−1.69025	0.44459	0.57369	−1.94698	−1.25161	0.77776	−0.87868
	1.650	1.40780	−3.20087	0.91373	0.61429	−2.85365	−1.46749	0.77221	−1.40931
	3.000	1.59994	−6.94061	1.45510	−0.56677	−3.76865	0.03345	0.36345	−2.24191
$\beta = 0.60$	0.10667	−0.04943	−0.19575	0.03421	0.09633	−1.86936	0.36713	0.92205	−0.34021
	0.21333	−0.07629	−0.32752	0.07321	0.15689	−1.60844	0.20071	0.77758	−0.40274
	0.32000	−0.06854	−0.44809	0.11022	0.20770	−1.51052	0.00648	0.71360	−0.45219
	0.42667	−0.03375	−0.57275	0.14944	0.25486	−1.49181	−0.17577	0.68429	−0.51160
	0.53333	0.02225	−0.70847	0.19407	0.29938	−1.52246	−0.34110	0.67083	−0.58393
	0.64000	0.09424	−0.85986	0.24636	0.34027	−1.58989	−0.48751	0.66319	−0.66899
	0.80000	0.22008	−1.12305	0.34174	0.38986	−1.74558	−0.66495	0.64819	−0.81726
	0.96000	0.34792	−1.43253	0.45668	0.41609	−1.94892	−0.77849	0.61444	−0.98228
	1.17333	0.48458	−1.90226	0.62640	0.39739	−2.24764	−0.81037	0.52431	−1.20300
	1.70667	0.60559	−3.05676	0.92567	0.08932	−2.71678	−0.44410	0.15748	−1.55086
	3.20000	1.39471	−6.71096	0.66588	−0.47911	−2.76302	0.04326	0.14946	−1.68445
$\beta = 0.70$	0.10929	−0.06374	−0.20732	0.04436	0.10039	−1.94140	0.48289	0.94266	−0.43431
	0.21857	−0.09728	−0.34027	0.09261	0.15628	−1.64938	0.28887	0.76434	−0.50798
	0.36429	−0.09030	−0.50905	0.15803	0.21277	−1.55542	0.03511	0.65995	−0.60981
	0.54643	−0.03728	−0.74659	0.25654	0.26037	−1.62288	−0.19215	0.56929	−0.78017
	0.65571	0.00165	−0.90813	0.32502	0.27047	−1.71004	−0.27299	0.50157	−0.89374
	0.80143	0.04668	−1.13908	0.41820	0.25499	−1.83952	−0.31322	0.38165	−1.03431
	0.94714	0.07896	−1.37216	0.49782	0.20710	−1.94657	−0.29046	0.23596	−1.13722
	1.16571	0.12721	−1.69741	0.56441	0.10281	−2.02057	−0.21190	0.02337	−1.19746
	1.74857	0.49529	−2.64753	0.54909	−0.06614	−2.06328	−0.21709	−0.16975	−1.12835
$\beta = 0.80$	0.1125	−0.08660	−0.21965	0.06102	0.10194	−2.01344	0.66787	0.93719	−0.59020
	0.2250	−0.12970	−0.35128	0.12165	0.14414	−1.68292	0.43232	0.69110	−0.67578
	0.3375	−0.14245	−0.47812	0.18204	0.16501	−1.59870	0.25706	0.53640	−0.77544
	0.4950	−0.14150	−0.66100	0.26228	0.15755	−1.59763	0.12830	0.31465	−0.90164
	0.5850	−0.13596	−0.76387	0.29605	0.13686	−1.60182	0.09553	0.18194	−0.93528
	0.7200	−0.11381	−0.91241	0.32198	0.10109	−1.58923	0.05702	0.01564	−0.92375
	0.9000	−0.04437	−1.12005	0.33094	0.07604	−1.57545	−0.02672	−0.09456	−0.86194
	1.0800	0.04905	−1.37509	0.35439	0.07442	−1.62762	−0.11982	−0.11059	−0.84291
	1.8000	0.31751	−2.51642	0.43858	−0.09528	−1.83661	−0.08111	−0.20169	−0.97367

Definition of Coefficients:

$$K = \pi\rho_0 l v^2 e^{i\nu t}(Ak_a + Bk_b)$$

$$M = \pi\rho_0 l^2 v^2 e^{i\nu t}(Am_a + Bm_b)$$

K = aerodynamic force, positive downward

M = aerodynamic moment about mid-chord point, positive tail-heavy

ρ_0 = air density (in undisturbed state)

l = semichord

v = speed of flight

β = Mach Number, v/c

ν = frequency of the vibration

ω = reduced frequency, $\nu l/v$

t = time

Al = amplitude of translation in mid-chord point, positive downward

B = amplitude of rotation, positive if trailing edge downward

k_a', k_a'' = real and imaginary part of k_a, etc.

All data contained in the table should be accurate within a few units of the last digit.

References

[1] Timman, R., van de Vooren, A. I., and Greidanus, J. H., *Aerodynamic Coefficients of an Oscillating Airfoil in Two-Dimensional Subsonic Flow*, Journal of the Aeronautical Sciences, Vol. 18, No. 12, pp. 797–802, December, 1951.

[2] van de Vooren, A. I., *Aerodynamic Coefficients of an Oscillating Airfoil with Control Surface in Two-Dimensional Subsonic Flow*, Journal of the Aeronautical Sciences, Vol. 20, No. 3, pp. 153–159, March, 1953.

[3] Fettis, H. E., *Comments on "Aerodynamic Coefficients of an Oscillating Airfoil in Two-Dimensional Subsonic Flow,"* Journal of the Aeronautical Sciences, Vol. 19, No. 5, pp. 353–354, May, 1952.

[4] Jordan, P. F., *Further Comments on Aerodynamic Coefficients of an Oscillating Aerofoil in Two-Dimensional Subsonic Flow*, Journal of the Aeronautical Sciences, Vol. 20, No. 5, pp. 362–363, May, 1953.

[5] Timman, R., *Linearized Theory of the Oscillating Airfoil in Compressible Subsonic Flow*, Journal of the Aeronautical Sciences, Vol. 21, No. 4, pp. 230–236, April, 1954.

Characteristic Solution for Axially Symmetric Transonic Flow

Erik Mollø-Christensen
Research Engineer, Department of Aeronautical Engineering, Massachusetts Institute of Technology, Cambridge, Mass.
February 26, 1954

Introduction

J. D. Cole has given the expression for simple waves in slightly perturbed two-dimensional transonic flow.[1] It can be shown that the potential corresponding to Cole's solution is of the form

$$\varphi(x, y) = X(x)Y(y)$$

where $X(x)$ and $Y(y)$ are functions of x only and y only, respectively.

Supposing that the potential equation for axially symmetric flow has a similar separated solution, and proceeding to seek it, one finds that such a solution exists, and is a characteristic solution.

Both the characteristic solutions correspond to expansion around a bend, and the flows are explicitly given in the physical plane.

(1) Two-Dimensional Transonic Characteristics

The equation for the perturbation potential φ is [2]:

$$\frac{\gamma + 1}{a^*}\varphi_x\varphi_{xx} = \varphi_{yy} \tag{1}$$

Set

$$\varphi(x, y) = X(x)Y(y) \tag{2}$$

where $X(x)$ and $Y(y)$ are functions of, respectively, x and y alone.

Substituting in Eq. (1), one obtains:

$$\frac{\gamma + 1}{a^*}\frac{X'(x)X''(x)}{X(x)} = \frac{Y''(y)}{[Y(y)]^2} \tag{3}$$

Solving the two equations

$$\varphi(x, y) = \frac{a^*}{3(\gamma + 1)}\frac{(x + c_1)^3}{(y + c_2)^2} \tag{4}$$

where c_1 and c_2 are arbitrary constants. To this solution can be added the obvious solution of Eq. (1):

$$\varphi_1(x, y) = A_1 y \tag{5}$$

A_1 being a constant.

The components of perturbation velocity are:

$$u = \varphi_x = \frac{a^*}{\gamma + 1}\left(\frac{x + c_1}{y + c_2}\right)^2 \tag{6}$$

and

$$v = \varphi_y = -\frac{2}{3}\frac{a^*}{\gamma + 1}\left(\frac{x + c_1}{y + c_2}\right)^3 \tag{7}$$

and v can be expressed as a function of u alone, viz.,

$$v = A_1 \pm \frac{2}{3}\sqrt{\frac{\gamma + 1}{a^*}}\,u^{3/2} \tag{8}$$

which is the expression given by Cole for the transonic characteristics. We note that the potential given by Eq. (4) vanishes at $x = -c_1$, as do its first derivatives, which correspond to uniform sonic flow. It will also be noted from Eq. (8), that when u is negative, v is imaginary, so the solution is only valid for supersonic local Mach Numbers.

(2) Axially Symmetric Flow

Let r be the radial distance. The potential equation for axially symmetric flow over a slender body of rotation is

$$\frac{\gamma + 1}{a^*}\varphi_x\varphi_{xx} = \frac{1}{r}\varphi_r + \varphi_{rr} \tag{9}$$

Trying a solution of the form

$$\varphi(x, r) = X(x)R(r) \tag{10}$$

yields, upon substitution,

$$\frac{\gamma + 1}{a^*}\frac{X'(x)X''(x)}{X(x)} = \frac{1}{r}R'(r) + R''(r)/[R(r)]^2 \tag{11}$$

Solving the two ordinary differential equations yields

$$\varphi(x, r) = \frac{2}{9}\frac{a^*}{\gamma + 1}\frac{(x + c_1)^3}{r^2} \tag{12}$$

The velocity components are

$$\left.\begin{aligned} u &= \varphi_x = \frac{2}{3}\frac{a^*}{\gamma + 1}\left(\frac{x + c_1}{r}\right)^2 \\ v &= \varphi_r = -\frac{4}{9}\frac{a^*}{\gamma + 1}\left(\frac{x + c_1}{r}\right)^3 \end{aligned}\right\} \tag{13}$$

And they are interrelated as follows:

$$v = \pm\sqrt{2/3}\sqrt{\frac{\gamma + 1}{a^*}}\,u^{3/2} \tag{14}$$

The solution found is therefore a characteristic solution.

The solution is not valid when r vanishes since then there can be no further opportunity for the flow to expand. The solution is also restricted to supersonic flow, because of the square root in Eq. (14), which makes v imaginary for negative u.

References

[1] Cole, J. D., *Problems in Transonic Flow*, Sc.D. Thesis, C.I.T. (1949), Pasadena.

[2] Lin, C. C., Reissner, E., and Tsien, H. S., *On Two-dimensional Non-Steady Motion of a Slender Body in a Compressible Fluid*, Journal of Mathematics and Physics, Vol. XXVII, No. 3, pp. 220–231, Oct., 1948.

On the Interaction of a Plane Shock Wave with a Wedge

Ken-iti Munakata
Physical Institute, University of Kyoto, Kyoto, Japan
January 17, 1954

(1) Introduction

Let a plane shock wave of any strength traveling horizontally into a still air, encounter a corner formed by two plane solid walls. It is known by experiments that the reflection process takes either of two qualitatively different forms: regular reflection or Mach reflection. Unsteady flow takes place within the region bounded by reflected shock (and Mach shock) and the walls.

When the viscosity and heat conductivity of the air are neglected there is no intrinsic length in the problem; the flow pattern remains similar to itself (i.e., is pseudo-stationary) and may be described in terms of the variables R/t and α alone. Here, R and α are the plane polar coordinates with the corner as origin and t is the time measured from an instant the incident shock struck the corner.

Extensive studies of the problem have been carried out experimentally.[1] However, theoretical investigations of the field of flow have so far been confined to cases when the vertex angle 2δ of the wedge is small or when it does not differ much from π. This paper provides a preliminary account of an attempt to solve

approximately the pseudo-stationary flow field for the cases of arbitrary values of δ and shock strength.

Solutions of the linearized equations for velocity components and pressure are obtained which enable us to solve the boundary value problem. It is shown that a singularity of rapid expansion takes place on the line bounding the region of influence of the corner on the flow field. This effect is clearly verified† by the experimental results of White.[2]

(2) Equations for Pseudo-Stationary Flow

Let the velocity components in R and α directions, pressure, density, and velocity of sound at any point be U, V, P, Ω, and C, respectively, and let the quantities at a certain standard point be denoted with suffix 2 which is moving uniformly in such a way that the state is constant in time. If now the transformations

$$R/C_2t = r, \qquad U/C_2 = M + u, \qquad V/C_2 = N + v,$$
$$U_2/C_2 = M, \qquad V_2/C_2 = N, \qquad C/C_2 = c,$$
$$P/(\Omega_2 C_2^2) = p, \qquad \Omega/\Omega_2 = \rho$$

be made, and if the fact that u, v, c, p, ρ depend on r and α be used, the equations of conservation of mass, momentum, and entropy become as follows:

$$(M + u - r)\frac{\partial \rho}{\partial r} + \frac{N + v}{r}\frac{\partial \rho}{\partial \alpha} + \rho\left[\frac{\partial u}{\partial r} + \frac{M + u}{r} + \frac{1}{r}\frac{\partial v}{\partial \alpha}\right] = 0 \quad (1)$$

$$(M + u - r)\frac{\partial u}{\partial r} + \frac{N + v}{r}\frac{\partial u}{\partial \alpha} - \frac{(N + v)^2}{r} + \frac{1}{\rho}\frac{\partial p}{\partial r} = 0 \quad (2)$$

$$(M + u - r)\frac{\partial v}{\partial r} + \frac{N + v}{r}\frac{\partial v}{\partial \alpha} + \frac{(M + u)(N + v)}{r} + \frac{1}{\rho r}\frac{\partial p}{\partial \alpha} = 0 \quad (3)$$

$$(M + u - r)\frac{\partial p}{\partial r} + \frac{N + v}{r}\frac{\partial p}{\partial \alpha} - c^2\left[(M + u - r)\frac{\partial \rho}{\partial r} + \frac{N + v}{r}\frac{\partial \rho}{\partial \alpha}\right] = 0 \quad (4)$$

Eliminating ρ and p between these equations one obtains

$$[(M + u - r)^2 - c^2]\frac{\partial u}{\partial r} + \frac{(M + u - r)(N + v)}{r}\frac{\partial u}{\partial \alpha} - c^2\frac{M + u}{r} + (M + u - r)(N + v)\frac{\partial v}{\partial r} + \frac{(N + v)^2 - c^2}{r}\frac{\partial v}{\partial \alpha} + (N + v)^2 = 0 \quad (5)$$

It can be shown that the system of Eqs. (1)–(4) with $c^2 = \gamma p/\rho$ is hyperbolic for $(M + u - r)^2 + (N + v)^2 > c^2$ and elliptic for $(M + u - r)^2 + (N + v)^2 < c^2$.

Considering that the whole field suffers a uniform expansion in time about the corner, one may regard r to represent the "phase velocity" of a point having fixed property. Then it is convenient to think of the "local field velocity" having components $M + u - r$ and $N + v$. It is the flow velocity relative to an observer traveling with the point in question. The flow field changes its character when the local field velocity exceeds the local speed of sound.

From now on we consider the case when $N = 0$ and u, v are small as compared with M. Then Eqs. (1)–(4) can be approximated as

$$[(M - r)(\partial u/\partial r)] + (\partial p/\partial r) = 0 \quad (6)$$

$$\{[r(M - r)](\partial v/\partial r)\} + Mv + (\partial p/\partial \alpha) = 0 \quad (7)$$

$$\{[r(M - r)](\partial p/\partial r)\} + r(\partial u/\partial r) + M + u + (\partial v/\partial \alpha) = 0 \quad (8)$$

Elimination of p between Eqs. (6) and (7) results in

$$(M - r)\frac{\partial^2 u}{\partial r \partial \alpha} - 2(M - r)\frac{\partial v}{\partial r} - r(M - r)\frac{\partial^2 v}{\partial r^2} = 0$$

For $r \neq M$, this equation can be integrated once with respect to r to give

$$\partial u/\partial \alpha - r\partial v/\partial r - v = f(\alpha) \quad (9)$$

Here $f(\alpha)$ is an arbitrary function of α, and it is to be noted that the vorticity is given by $-f(\alpha)/r$. Elimination of p and u from Eqs. (6), (8), and (9) gives a second-order equation in v:

$$[1 - (M - r)^2]r^2\frac{\partial^2 v}{\partial r^2} + [3 - 2(M - r)^2]r\frac{\partial v}{\partial r} + \frac{\partial^2 v}{\partial \alpha^2} + v + f(\alpha) = 0 \quad (10)$$

If we put $v = v^* + g(\alpha)$ and let $g''(\alpha) + g(\alpha) + f(\alpha) = 0$, then the equation for v^* becomes

$$[1 - (M - r)^2]r^2\frac{\partial^2 v^*}{\partial r^2} + [3 - 2(M - r)^2]r\frac{\partial v^*}{\partial r} + \frac{\partial^2 v^*}{\partial \alpha^2} + v^* = 0 \quad (11)$$

Integrating Eqs. (9) and (7) with respect to α it will be seen after some considerations that the solutions are given in terms of v^* and an arbitrary function $g(\alpha)$ as follows:

$$u = \int [r(\partial v^*/\partial r) + v^*]d\alpha - g'(\alpha) - M \quad (12)$$

$$v = v^* + g(\alpha) \quad (13)$$

$$p = -\int \{[r(M - r)(\partial v^*/\partial r)] + Mv^*\}\, d\alpha - M\int g(\alpha)\, d\alpha \quad (14)$$

In this approximation the equation becomes elliptic in the circle: $r < M + 1$ for $M \leq 1$ or in the ring region: $M - 1 < r < M + 1$ for $M > 1$. It may be noted that all the characteristics touch the circles $r = M + 1$ or $r = M - 1$.

(3) Solutions for the Case of Regular Reflection

To solve Eq. (11), we assume v^* in the form:

$$v^* = Z(r)\sin(k\pi\alpha/\alpha_0) \quad (15)$$

and make use of a substitution

$$z = (M^2 - 1)/2r - (M - 1)/2 \quad (16)$$

Then we get the following equation:

$$z(1 - z)\frac{d^2 Z}{dz^2} + \left(-\frac{1}{2M + 2} - \frac{1}{M^2 - 1}z\right)\frac{dZ}{dz} - \frac{k^2\pi^2/\alpha_0^2 - 1}{M^2 - 1}Z = 0 \quad (17)$$

Thus, we find that Z is given in terms of hypergeometric functions as follows:

$$Z = B_1 F(a_k, b_k, c_k; z) + B_2(-z)^{1-c_k}F(a_k - c_k + 1, b_k - c_k + 1, 2 - c_k; z) \quad (18)$$

$$= B_3(-z)^{-a_k}F(a_k, a_k - c_k + 1, a_k - b_k + 1; 1/z) + B_4(-z)^{-b_k}F(b_k, b_k - c_k + 1, b_k - a_k + 1; 1/z) \quad (19)$$

where $B_1 - B_4$ are constants and

† The author is indebted to Professor Walker Bleakney of Princeton University for valuable discussions and for sending him several papers.

$$\left.\begin{matrix} a_k \\ b_k \end{matrix}\right\} = \frac{M^2 - 2 \pm \sqrt{M^4 + 4k^2\pi^2(1 - M^2)/\alpha_0^2}}{2(1 - M^2)}$$
$$c_k = -1/(2M + 2) \qquad (20)$$

To settle the problem, we consider hereafter the case of regular reflection as shown in Fig. 1, in which the reflected shock is divided into two parts: a straight part AB after which a region ABD of uniform flow follows, and a curved part BC which bounds the region BCOD of pseudo-stationary flow. If we choose the point D as the standard point, the various quantities with suffix 2 are equal to those immediately behind the reflected shock at A and can be obtained by the simple theory of regular reflection. Then M is less than unity except for strong incident shocks with $P_0/P_1 \lesssim 0.2$. The line BD must coincide with the circle $r = M + 1$. If one takes the line OA as $\alpha = 0$, the constant α_0 should be taken as $\pi - \delta$ so as to make $v = 0$ on OA and on OC. Then, for any integer k, $a_k > 0$ and $b_k < 0$ for $M < 1$. Since v must vanish at the origin, the second term in Eq. (19) must be discarded; $g(\alpha) = 0$ by the same reason.

Consequently, by superposition we find that

$$v = \sum_k A_k(-z)^{-a_k} F\left(a_k, a_k - c_k + 1, a_k - b_k + 1; \frac{1}{z}\right) \times \sin\frac{k\pi\alpha}{\pi - \delta} \qquad (21)$$

and the expression valid near $r = M + 1$ is seen to be

$$v = \sum A_k \sin\frac{k\pi\alpha}{\pi - \delta}\left[\frac{\Gamma(1 - c)\Gamma(a - b + 1)}{\Gamma(1 - b)\Gamma(a - c + 1)} F(a, b, c; z) + \frac{\Gamma(c - 1)\Gamma(a - b + 1)}{\Gamma(a)\Gamma(c - b)}(-z)^{1-c} F(a - c + 1,\ b - c + 1, 2 - c; z)\right] \qquad (22)$$

Note that in this and in the following equations the suffixes k of a_k, b_k, and c_k are omitted for convenience. By use of Eqs. (12) and (14) u and p are obtained as follows:

$$u + M = \sum A_k \frac{\pi - \delta}{k\pi}\cos\frac{k\pi\alpha}{\pi - \delta}\left\{-(-z)^{-a}F\left(a, a - c + 1, a - b + 1; \frac{1}{z}\right) + \left(z - \frac{1 - M}{2}\right)\left[a(-z)^{-a-1} F\left(a, a - c + 1, a - b + 1; \frac{1}{z}\right) - \frac{a(a - c + 1)}{a - b + 1} \times (-z)^{-a-2} F\left(a + 1, a - c + 2, a - b + 2; \frac{1}{z}\right)\right]\right\} \qquad (23)$$

$$= \sum A_k \frac{\pi - \delta}{k\pi}\cos\frac{k\pi\alpha}{\pi - \delta}\left\{-\frac{\Gamma(1 - c)\Gamma(a - b + 1)}{\Gamma(1 - b)\Gamma(a - c + 1)} F(a, b, c; z) - \frac{\Gamma(c - 1)\Gamma(a - b + 1)}{\Gamma(a)\Gamma(c - b)}(-z)^{1-c} F(a - c + 1, b - c + 1, 2 - c; z) + \left(z - \frac{1 - M}{2}\right)\left[\frac{\Gamma(1 - c)\Gamma(a - b + 1)}{\Gamma(1 - b)\Gamma(a - c + 1)}\frac{ab}{c} \times F(a + 1, b + 1, c + 1; z) + \frac{\Gamma(c - 1)\Gamma(a - b + 1)}{\Gamma(a)\Gamma(c - b)}(c - 1)(-z)^{-c} F(a - c + 1, b - c + 1, 2 - c; z) + \frac{\Gamma(c - 1)\Gamma(a - b + 1)}{\Gamma(a)\Gamma(c - b)}\frac{(a - c + 1)(b - c + 1)}{2 - c}(-z)^{1-c} F(a - c + 2, b - c + 2, 3 - c; z)\right]\right\} \qquad (24)$$

$$p + \text{const.} = \sum A_k \frac{\pi - \delta}{k\pi}\cos\frac{k\pi\alpha}{\pi - \delta}\left\{M(-z)^{-a}F\left(a, a - c + 1, a - b + 1; \frac{1}{z}\right) - \left(\frac{1 - M}{2} + Mz\right)\left[a(-z)^{-a-1} F\left(a, a - c + 1, a - b + 1; \frac{1}{z}\right) - \frac{a(a - c + 1)}{a - b + 1} \times (-z)^{-a-2} F\left(a + 1, a - c + 2, a - b + 2; \frac{1}{z}\right)\right]\right\} \qquad (25)$$

$$= \sum A_k \frac{\pi - \delta}{k\pi}\cos\frac{k\pi\alpha}{\pi - \delta}\left\{M\frac{\Gamma(1 - c)\Gamma(a - b + 1)}{\Gamma(1 - b)\Gamma(a - c + 1)} F(a, b, c; z) + M\frac{\Gamma(c - 1)\Gamma(a - b + 1)}{\Gamma(a)\Gamma(c - b)}(-z)^{1-c} F(a - c + 1, b - c + 1, 2 - c; z) - \left(\frac{1 - M}{2} + Mz\right) \times \left[\frac{\Gamma(1 - c)\Gamma(a - b + 1)}{\Gamma(1 - b)\Gamma(a - c + 1)}\frac{ab}{c} F(a + 1, b + 1, c + 1; z) + \frac{\Gamma(c - 1)\Gamma(a - b + 1)}{\Gamma(a)\Gamma(c - b)} \times (c - 1)(-z)^{-c} F(a - c + 1, b - c + 1, 2 - c; z) + \frac{\Gamma(c - 1)\Gamma(a - b + 1)}{\Gamma(a)\Gamma(c - b)}\frac{(a - c + 1)(b - c + 1)}{2 - c} \times (-z)^{1-c} F(a - c + 2, b - c + 2, 3 - c; z)\right]\right\} \qquad (26)$$

The constants A_k are to be determined so as to make u, v, and p assume the values on BC which are given by the shock relations. Considerable difficulties arise, however, inasmuch as the form of the reflected shock is not known beforehand. One will have to rely upon some methods of trial and error, or make use of experimental results when available. Considering the fact that entropy is constant along a line which is tangential at any point to the local field velocity, we can find density from the distributions of velocity and pressure.

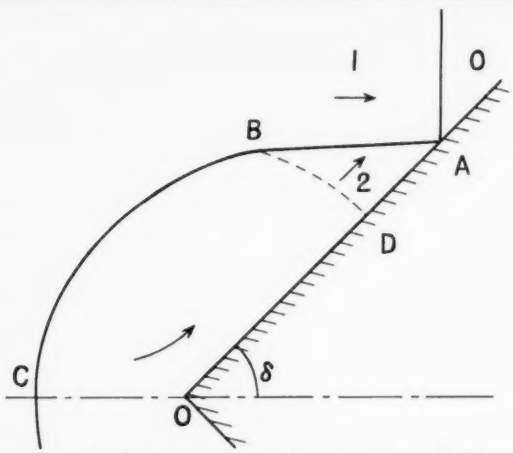

FIG. 1. Configuration and notation of regular reflection.

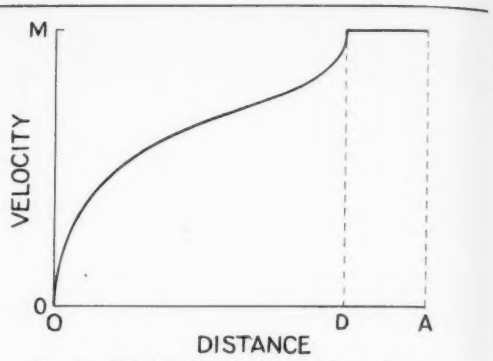

FIG. 2. Velocity distribution on the wedge.

(4) SINGULARITY OF RAPID EXPANSION

A few qualitative descriptions of the features of the flow field were obtained from preliminary computations making use of three terms in the expressions (21)–(26) for a case of $P_0/P_1 = 0.8$ and $\delta = 45°$. The velocity distribution on the wedge is shown schematically in Fig. 2. The tangent of the curve is vertical at D. It is due to terms $(-z)^{-c_k} = (-z)^{1/(2M+2)}$ in the expression (24), the exponent of which is independent of k.

The corresponding singularity appears in the pressure distribution on the wedge which has a similar character as the curve in Fig. 2 near the point D.† It can be considered as representing approximately a rapid expansion due to disturbance originating from the corner that is receding from an observer traveling, for example, with the point of intersection of the shocks and the wall. The disturbance is reaching up to the point D, where the material speed + the sound speed = the phase speed, but not further; it is accumulating so to speak there.

† It can also be seen in the results of Lighthill[3] for the special case of δ near $\pi/2$.

The singularity of rapid expansion, though it is unfamiliar in the stationary flow, has its verification in the curves of pressure distribution on the wedge which were obtained by White[2] making use of wedges with $\delta = 30°$ and $38°$.

If one reduces the vertex angle of the corner for fixed intensity of the incident shock the triangular region ABD of uniform flow reduces and finally to a point. Then, the singularity of rapid expansion occurs immediately behind the compression by reflected shock at point A. It may well be possible that the singularity gives influence on the ordinary relations of regular reflection. It might further be responsible, at least partly, for the well-known discrepancies between theory and experiment for Mach reflection.

Lastly, the writer wishes to express his sincere thanks to Professor S. Tomotika for his kind inspection of the paper.

REFERENCES

[1] Fletcher, C. H., Taub, A. H., and Bleakney, Walker, *The Mach Reflection of Shock Waves at Nearly Glancing Incidence*, Reviews of Modern Physics, Vol. 23, No. 3, pp. 271–286, July (1951).

[2] White, Donald R., *An Experimental Survey of the Mach Reflection of Shock Waves*, Technical Report II-10, Department of Physics, Princeton University, August, 1951.

[3] Lighthill, M. J., *The Diffraction of Blast, II*, Proc. Roy. Soc. A., Vol. 200, pp. 554–565, 1950.

On the Approximate Solution of the Laminar Boundary-Layer Equations

(*Continued from page 495*)

[4] Schlichting, H., and Ulrich, A., *Zur Berechnung des Umschlages laminar-turbulent*, Jahrbuch der deutschen Luftfahrtforschung, I8, pp. 8–36, 1942.

[5] Tani, I., *On the Solution of the Laminar Boundary Layer Equations*, J. Phys. Soc., Japan, Vol. 4, pp. 149–154, 1949.

[6] Wieghardt, K., *Ueber einen Energiesatz zur Berechnung laminarer Grenzschichten*, Ingenieur-Archiv, Vol. 16, pp. 231–242, 1948.

[7] Walz, A., *Anwendung des Energiesatzes von Wieghardt auf einparametrige Geschwindigkeitsprofile in laminarer Grenzschichten*, Ingenieur-Archiv, Vol. 16, pp. 243–248, 1948.

[8] Truckenbrodt, E., *Ein Quadraturverfahren zur Berechnung der laminaren und turbulenten Reibungsschicht bei ebener und rotationssymmetrischer Strömung*, Ingenieur-Archiv, Vol. 20, pp. 211–228, 1952.

[9] Rott, N., *Compressible Laminar Boundary Layer on a Heat-Insulated Body*, Journal of the Aeronautical Sciences, Vol. 20, pp. 67–68, 1953.

[10] Crocco, L., *Lo strato limite laminare nei gas*, Monographie Scientifiche di Aeronautica, No. 3, 1946.

[11] Hudimoto, B., *An Approximate Method for Calculating the Laminar Boundary Layer* (in Japanese), Jour. Soc. Aero. Sci., Japan, Vol. 8, pp. 279–282, 1941.

[12] Tani, I., *A Simple Method for Determining the Laminar Separation Point* (in Japanese), Jour. Aero. Res. Inst., Tokyo Imp. Univ., No. 199, 1941.

[13] Young, A. D., and Winterbottom, N. E., *Note on the Effect of Compressibility on the Profile Drag of Aerofoils in the Absence of Shock Waves*, A.R.C. Report No. 4697, 1940.

[14] Walz, A., *Ein neuer Ansatz für das Geschwindigkeitsprofil der laminaren Grenzschicht*, Lilienthal-Bericht No. 141, 1941.

[15] Thwaites, B., *Approximate Calculation of the Laminar Boundary Layer*, Aero. Quart., Vol. 1, pp. 245–280, 1949.

[16] Hartree, D. R., *On the Equation Occurring in Falkner and Skan's Approximate Treatment of the Equations of the Boundary Layer*, Proc. Cambr. Phil. Soc., Vol. 33, pp. 223–239, 1937.

[17] Tifford, A. N., and Chu, S. T., *On Heat Transfer, Recovery Factors, and Spin for Laminar Flows*, Journal of the Aeronautical Sciences, Vol. 19, pp. 787–789, 1952.

[18] Chapman, D. R., and Rubesin, M. W., *Temperature and Velocity Profiles in the Compressible Laminar Boundary Layer with Arbitrary Distribution of Surface Temperature*, Journal of the Aeronautical Sciences, Vol. 16, pp. 547–565, 1949.